

DISSERTATION

L. Stanger



TECHNISCHE
UNIVERSITÄT
WIEN

INSTITUT FÜR
MECHANIK UND
MECHATRONIK
Mechanics & Mechatronics



DISSERTATION

Model-Based Multivariable Control of Dual Fluidized Bed Gasification

carried out for the purpose of obtaining the degree of
Doctor technicae (Dr. techn.)

submitted at TU Wien
Faculty of Mechanical and Industrial Engineering

by

Lukas STANGER

Mat.No.: 01425851

under the supervision of

Ao.Univ.Prof. Dipl.-Ing. Dr.techn. Martin Kozek
and

Privatdoz. Dipl.-Ing. Dr.techn. Alexander Schirrer
Institute of Mechanics and Mechatronics

Wien, 2025

Meiner Familie.

Acknowledgment

This work was supported by the project ADORe-SNG, which is funded by the Austrian Climate and Energy Fund (FFG, No. 881135).

Supervisors

Ao.Univ.Prof. Dipl.-Ing. Dr.techn. Martin Kozek
Institut für Mechanik und Mechatronik
Technische Universität Wien

Privatdoz. Dipl.-Ing. Dr.techn. Alexander Schirrer
Institut für Mechanik und Mechatronik
Technische Universität Wien

Reviewers

Univ.-Prof. Dipl.-Ing. Dr.techn. Martin Horn
Institut für Regelungs- und Automatisierungstechnik
Technische Universität Graz

Univ.Prof. Dipl.-Ing. Dr.techn. Stefan Jakubek
Institut für Mechanik und Mechatronik
Technische Universität Wien

Going to press

I confirm, that the printing of this thesis requires the approval of the examination board.

Affidavit

I declare in lieu of oath, that I wrote this thesis and carried out the associated research myself, using only the literature cited in this volume. If text passages from sources are used literally, they are marked as such. I confirm that this work is original and has not been submitted for examination elsewhere, nor is it currently under consideration for a thesis elsewhere. I acknowledge that the submitted work will be checked electronically-technically using suitable and state-of-the-art means (plagiarism detection software). On the one hand, this ensures that the submitted work was prepared according to the high-quality standards within the applicable rules to ensure good scientific practice *Code of Conduct* at the TU Wien. On the other hand, a comparison with other student theses avoids violations of my personal copyright.

Wien, 16. März 2025

Lukas Stanger

Danksagung

Am Ende dieser Reise ist es mir ein besonderes Anliegen, all jenen zu danken, die mich auf diesem Weg begleitet, inspiriert und unterstützt haben.

Herzlichen Dank meinen Betreuern Martin Kozek und Alexander Schirrer, die mir nicht nur fachlich zur Seite standen, sondern mir auch den nötigen Freiraum gegeben haben, meine Ideen zu entwickeln. Eure Unterstützung und euer Vertrauen waren essenziell für diese Arbeit.

Ein großes Dankeschön auch an unsere Projektpartner, insbesondere an die Kollegen vom Institut für Verfahrenstechnik Alex, Stefan, Martin und Florian. Ihr habt mir geholfen, in die Welt des DFB-Prozesses einzutauchen und viel zu lernen. Die gemeinsamen Versuchstage waren zweifellos die spannendsten Tage meines Doktorats.

Ebenso danke ich meinen Kollegen am Institut für Mechanik und Mechatronik – allen voran Lukas und Markus – für die bereichernden und unterhaltsamen Gespräche in unseren Kaffeepausen, die jeden Arbeitstag aufgelockert haben.

Ein herzliches Dankeschön auch an meine Studienfreunde aus dem Bachelor- und Masterstudium a.k.a. „TU Connect“. Ich schätze es sehr, dass unser Kontakt über die Jahre lebendig geblieben ist, sei es bei Segeltörns, Hochzeiten oder Geburtstagsfeiern.

Ganz besonders danke ich meinen Eltern, die mich immer und bei jeder meiner Entscheidungen unterstützt haben – ohne euch wäre dieser Weg selbstverständlich nicht möglich gewesen. Und meiner lieben Su, dafür, dass du immer für mich da bist, und mir mit deiner Liebe und Unterstützung immer die nötige Kraft gibst.

Kurzfassung

Die Zweibett-Wirbelschicht (engl. *Dual Fluidized Bed*, DFB) Gaserzeugung ist ein vielversprechendes Verfahren zur Erzeugung wertvoller Energieträger aus biogenen Rohstoffen als Ersatz für fossile Brennstoffe. Der Betrieb von DFB-Gaserzeugungsanlagen erfolgt derzeit überwiegend manuell oder durch einfache Eingrößenregelkreise, während umfassende wissenschaftliche Ansätze zur Regelung zentraler Prozessgrößen fehlen.

Ziel dieser Dissertation ist es, diese Forschungslücke zu schließen, indem innovative Regelungskonzepte entwickelt, implementiert und experimentell validiert werden. Der Fokus liegt auf der Regelung entscheidender Prozessgrößen wie Gaserzeugungstemperatur, Produktgasmassenstrom und Bettmaterialzirkulation. Dadurch soll der Automatisierungsgrad deutlich gesteigert und die Wettbewerbsfähigkeit der Technologie verbessert werden. Die entwickelten Regelungskonzepte wurden an einer 100-kW-Pilotanlage der TU Wien getestet.

Die Grundlage für die Entwicklung fortschrittlicher Regelungsmethoden bilden mathematische Modelle, die die Zusammenhänge zwischen Stellgrößen, Störgrößen und Regelgrößen beschreiben. Der erste Teil der Arbeit widmet sich der Identifikation dieser Modelle. Hierbei kamen sowohl physikalische als auch datengetriebene Ansätze zum Einsatz. Wo möglich, wurden die Zusammenhänge durch physikalische Gleichungen, wie Massen- und Energiebilanzen oder thermodynamische Gleichgewichte, abgebildet. Ergänzend wurden datengetriebene Methoden, etwa künstliche neuronale Netze oder Gaußprozess-Regressionen, für spezifische Teilaspekte wie den Umlauf des Bettmaterials genutzt. Die Parametrierung der Modelle basierte auf Messdaten der 100-kW-Anlage, sowohl aus früheren Versuchen als auch aus eigens durchgeführten Identifikationsexperimenten.

Ein zentraler Beitrag der Arbeit ist die Entwicklung eines modellprädiktiven Reglers (MPC), der wesentliche Prozessgrößen wie die Gaserzeugungstemperatur und den Produktgasmassenstrom regelt. Der MPC berücksichtigt dabei zahlreiche Beschränkungen, wie ein notwendiger Restsauerstoffgehalt im Abgas oder Mindestanforderungen an die Gasströme zur Fluidisierung der Reaktoren. Ergänzend regelt ein untergeordneter Regler die Bettmaterialzirkulationsrate durch Anpassung der Lufttrimmung im Verbrennungsreaktor.

Im letzten Teil dieser Arbeit wird die Regelung der Bettmaterialzirkulationsrate vertiefend untersucht, und alternative Ansätze zur Regelung dieser Größe werden vorgestellt: Ein linearer Minimum-Varianz-MPC sowie ein nichtlinearer Regler auf Basis der Gaußprozess-Regression. Da datenbasierte Modelle in bestimmten Betriebsbereichen unterschiedlich präzise Vorhersagen liefern, nutzen die entwickelten Regelungsstrategien gezielt Informationen zur Modellgenauigkeit und redundante Aktuatoren des Systems. Dies ermöglicht eine gezielte Prozessführung in Bereichen mit hoher Modellgenauigkeit. Der nichtlineare Ansatz bietet eine Methode, die flexibel und anlagenunabhängig einsetzbar ist. Er wurde in Simulationen an der 100-kW-Pilotanlage sowie an einer 1-MW-Demonstrationsanlage getestet und anschließend an der

100-kW-Pilotanlage erfolgreich implementiert.

Sowohl die Simulations- als auch die Experimentergebnisse zeigen, dass die vorgestellten Methoden erfolgreich zur Regelung wichtiger Prozessvariablen im DFB-Gaserzeugungsprozess eingesetzt werden können und somit die Forschungslücke in Bezug auf Regelungsstrategien für derartige Anlagen adressieren.

Abstract

The dual fluidized bed (DFB) gasification process is a promising technology for producing valuable energy carriers from biogenic raw materials as a substitute for fossil fuels. Currently, DFB gasification plants are predominantly operated manually or with basic single-input control loops, while comprehensive scientific approaches for controlling key process variables are lacking.

This dissertation aims to address this research gap by developing, implementing, and experimentally validating innovative control strategies. The focus is on controlling critical process variables, such as the gasification temperature, product gas mass flow, and solids circulation rate. This is intended to significantly increase the level of automation and enhance the competitiveness of the technology. The control concepts developed were tested on a 100 kW pilot plant at TU Wien.

The development of advanced control methods is based on mathematical models that describe the relationships between control inputs, disturbances, and output variables. The first part of the work focuses on identifying these models, employing both physical and data-driven approaches. Where feasible, relationships were represented by physical equations, such as mass and energy balances or thermodynamic equilibria. Complementary to this, data-driven methods like artificial neural networks or Gaussian process regression were applied to specific aspects, such as solids circulation rate. Model parameters were derived from measurement data gathered from both previous experiments and dedicated identification tests conducted on the 100 kW pilot plant.

A central contribution of the dissertation is the development of a model predictive controller (MPC) to control key process variables like gasification temperature and product gas mass flow. The MPC accounts for numerous constraints, including a required residual oxygen concentration in the exhaust gas and minimum gas flow rates necessary for reactor fluidization. Additionally, a subordinate controller controls the solids circulation rate by adjusting airflow in the combustion reactor.

The final part of the dissertation examines the control of solids circulation rate in greater detail, presenting alternative approaches for controlling this variable. These include a linear minimum variance MPC and a nonlinear controller based on Gaussian process regression. Since data-driven models provide varying prediction accuracy across different operating conditions, the developed control strategies leverage information on model accuracy and redundant actuators to guide the process in areas with higher model reliability. The nonlinear approach offers a flexible and plant-independent solution, validated through simulations on the 100 kW pilot plant and a 1 MW demonstration facility. It was subsequently implemented and successfully tested on the 100 kW pilot plant.

Both the simulation and experimental results demonstrate that the presented methods

can successfully control key variables in the DFB gasification process, thereby addressing the research gap in control strategies for such plants.

Contents

Overview	1
1 Motivation	1
2 Problem statement	2
2.1 Dual fluidized bed gasification	2
2.2 Objectives and challenges in operating dual fluidized bed gasification plants	6
2.3 State-of-the-art and open issues in modeling and control	7
3 Key objectives of this thesis	7
4 Scientific approach	8
4.1 Dynamic modeling	9
4.2 Model predictive control	13
4.3 Gaussian process regression-based control of solids circulation rate	16
4.4 Experimental investigation	19
5 Scientific contribution	21
6 Outlook	24
Bibliography	27
Publications	31
Publication A	33
<i>Dynamic modeling of dual fluidized bed steam gasification for control design</i>	
Publication B	45
<i>Model predictive control of a dual fluidized bed gasification plant</i>	
Publication C	63
<i>Minimum-Variance Model Predictive Control for Dual Fluidized Bed Circulation Control</i>	
Publication D	71
<i>Gaussian Process Regression-Based Control of Solids Circulation Rate in Dual Fluidized Bed Gasification</i>	
About the author	85

Nomenclature

Acronyms

bm	Biomass
CR	Combustion reactor
DFB	Dual fluidized bed
FG	Flue gas
GP	Gaussian process
GR	Gasification reactor
ILS	Internal loop seal
LLS	Lower loop seal
MPC	Model predictive control(ler)
PG	Product gas
ULS	Upper loop seal

Mathematical notation

\bar{x}	Steady-state target value for x
\mathbf{x}^T	Transpose of \mathbf{x}
\hat{x}	Estimate of x
$\ \mathbf{x}\ $	Euclidean norm of \mathbf{x}

Subscripts

i	Time step within prediction horizon
k	Time step
c	Solids circulation

Symbols

β_0, β_1	Heat transport (bed material) parameters (kW/°C and kW/(mbar·°C))
\mathbf{A}	System matrix
\mathbf{B}	Control input matrix
\mathbf{B}_d	Disturbance state input matrix
\mathbf{C}	Output matrix
\mathbf{C}_d	Disturbance state output matrix
\mathbf{d}	Disturbance state vector
\mathbf{E}	Disturbance input matrix
\mathbf{H}	Controlled output matrix
\mathbf{I}	Identity matrix

\mathbf{K}	Covariance matrix
\mathbf{Q}	State deviation weighting matrix
\mathbf{R}	Input deviation weighting matrix
\mathbf{r}	Reference vector
\mathbf{R}_Δ	Input rate weighting matrix
\mathbf{R}_∞	Weighting matrix for steady-state control inputs
\mathbf{u}	Control input vector
\mathbf{u}^*	Desired input vector
\mathbf{v}	Output noise
\mathbf{w}	Process noise
\mathbf{x}	State vector
\mathbf{y}	Output vector
\mathbf{y}^*	Controlled output vector
\mathbf{z}	Disturbance input vector
Δp	Pressure difference in the upper part of the combustion reactor (mbar)
\dot{H}	Enthalpy flow rate (kW)
\dot{m}	Mass flow rate (kg/h)
\dot{n}	Molar flow rate (mol/h)
\dot{Q}	Heat flow rate (kW)
\dot{V}	Volumetric flow rate (Nm ³ /h)
η	Slack variable
μ	Mean
σ	Standard deviation
τ	Time constant (s)
C	Heat capacity (kJ/°C)
N_c	Length of control horizon
N_p	Total length of prediction horizon
T	Temperature (°C)
t	Time (s)
w_η	Slack variable weight
w_{ash}	Ash content in biomass (weight fraction)
y_{O_2}	Oxygen concentration in the dry flue gas (Vol.-%)

Overview

The introductory chapter of this dissertation provides the foundation for understanding the context and significance of the research presented in the subsequent publications. It begins by outlining the motivation for developing a multivariable controller for dual fluidized bed (DFB) gasification systems, followed by a detailed problem statement that examines the process, the associated operational challenges, and the state-of-the-art in modeling and control. Key objectives of this research are then defined, guiding the scientific approach, which integrates dynamic modeling, model predictive control (MPC), Gaussian process (GP) regression, and experimental investigations. The chapter is concluded by summarizing the scientific contributions of this work, establishing its relevance and significance in the broader field of renewable energy systems.

1 Motivation

The ongoing threat of global warming and environmental degradation has underscored the urgent need to transition from fossil fuels to renewable energy sources [1]. Fossil fuels, which currently dominate global energy consumption, contribute significantly to greenhouse gas emissions, and their depletion is inevitable. To mitigate climate change, it is essential to diversify energy systems and replace fossil fuels with renewable alternatives.

Although solar and wind power have gained popularity in recent years, with the leveled cost of electricity significantly decreasing, biomass remains an important component of the global primary energy supply. Biomass is not only a renewable and sustainable energy source, it also has the advantage of being storable and dispatchable, which means that it can provide continuous, reliable energy [2].

A promising pathway for utilizing biomass is through gasification, which is a thermochemical process that converts solid materials, such as biomass, into a gas, commonly called product gas, through interaction with a gasification agent. An effective method is DFB steam gasification. By using steam as the gasification agent and through a specialized process design, this method produces a product gas primarily composed of hydrogen, carbon monoxide, carbon dioxide, and methane [3]. DFB gasification is versatile in terms of feedstock, allowing not only the use of traditional biomass sources like wood but also waste materials such as agricultural and forestry residues, municipal solid waste, or sewage sludge [4]. This flexibility makes it an attractive option for renewable energy production.

The product gas from DFB steam gasification offers different utilization pathways due to its composition. In the past, the main focus of using product gas from DFB steam gasification was to generate electricity through combined heat and power processes. In recent years, product gas has also gained attention as a key feedstock for synthetic fuel production through

Fischer-Tropsch synthesis [5] or methanation [6], enabling the creation of synthetic natural gas, methanol, or other hydrocarbons. In addition, the gas can be upgraded to hydrogen [7], supporting hydrogen economy initiatives, or used directly in industrial processes that require a renewable, high-energy gas. This flexibility makes DFB gasification an attractive option to integrate renewable energy sources into various sectors.

DFB gasification plants have been developed on both the laboratory and industrial scales over the past decades. Industrial-scale plants have been put into operation in Austria, Germany, Sweden, Thailand, and Japan [8]. A comprehensive overview of their historical development can be found in [9].

Currently, DFB gasification plants are predominantly operated manually or utilize multiple single-input single-output (SISO) controllers. These controllers regulate key process variables such as product gas flow rate, gasification temperature, and oxygen concentration in the flue gas. Despite their utility, SISO control loops can lead to unexpected interactions and can even cause instability in multivariable coupled systems [10]. The absence of comprehensive multivariate control approaches in the literature indicates a significant opportunity to improve process efficiency and reduce operational costs through the implementation of advanced control concepts that consider the couplings of different process parameters.

Model-based control strategies, in particular MPC, have emerged as a promising solution to control complex multivariable systems in the process industry [11]. MPC allows the prediction of future system behavior and the optimization of control actions accordingly, providing a method that can effectively handle the multivariable nature of gasification systems, explicitly consider constraints, and achieve decoupling of process variables.

Successful application of MPC requires a dynamic model of the process to be controlled that is capable of predicting the variables and their dynamic coupling that should be controlled in dependence on the input variables that can be manipulated, such as fuel, steam, and airflows into the plant.

2 Problem statement

2.1 Dual fluidized bed gasification

This section provides a brief introduction to DFB steam gasification, to the extent that it is relevant for the control of such systems. DFB gasification is one method for generating syngas from solid fuels, particularly biomass. For alternative methods of gas generation, please refer to [12]. More detailed descriptions of DFB gasification can be found in [9, 3].

In DFB gasification, syngas is produced from biomass by dividing the process into two main parts: gasification and combustion (Figure 1). The gasification stage occurs in the gasification reactor (GR), where the biomass undergoes drying, pyrolysis, and gasification in the presence of steam. Some of the biomass remains ungasified and is transported in the form of char to the combustion reactor (CR), where it is combusted in the presence of air. Both reactors are operated as fluidized bed reactors. Since air is only introduced into the CR, the syngas generated in the GR is almost nitrogen-free, enhancing its quality by avoiding dilution. This syngas has thus a higher energy content, making it more suitable for downstream processes such as chemical synthesis or biofuel production.

Bed material is constantly circulating between the two reactors, serving two critical

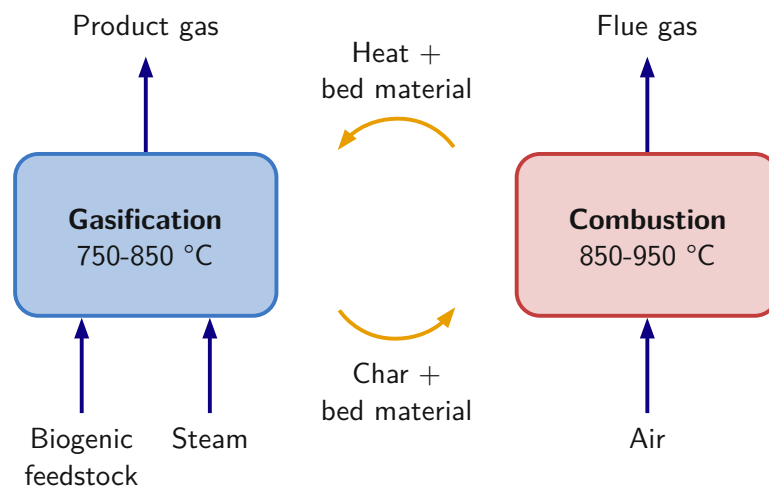


Figure 1: Principle of DFB steam gasification. Figure adapted from [13].

functions. First, it transports the ungasified char from the GR to the CR for combustion. Second, it transfers heat generated in the CR to the GR, where it maintains the overall endothermic gasification reactions. This efficient heat transfer is essential for maintaining the gasification process.

100 kW advanced DFB steam gasification pilot plant at TU Wien

Figure 2 illustrates the design of the DFB gasification pilot plant at TU Wien. The lower GR utilizes steam for fluidization and is operated as a bubbling fluidized bed reactor. The CR is fluidized by air and is operated as a fast fluidized bed reactor. The two reactors are connected by a lower loop seal (LLS) at the bottom and an upper loop seal (ULS) at the top. The internal loop seal (ILS) is necessary for the internal bed material circulation of the GR. All loop seals are fluidized with steam.

Biomass is fed to the fluidized bed of the GR. The ungasified char is transported via the LLS to the CR. There, the char is combusted in the presence of air, thereby heating up the bed material. Heating oil is used as an auxiliary fuel in the CR, which is required to compensate for the relatively high heat loss of the pilot plant. Industrial plants typically avoid using heating oil as an auxiliary fuel. Instead, product gas can be recirculated to the CR.

The air necessary for combustion is fed into the reactor in three stages. These airflows are referred to as primary air (air 1), secondary air (air 2), and tertiary air (air 3), whereby the primary air is the lowermost airflow and the secondary and tertiary air are fed above it. A larger volume flow of air at a lower entry point leads to increased circulation of the bed material and vice versa. Thus, this air staging can be used to control the mass flow of bed material circulating between the two reactors.

To improve gas-solid interaction in the GR, a reactor design featuring a countercurrent column above the GR's freeboard was proposed in [14]. This design aims to enhance gas-solid contact, resulting in a lower tar content in the product gas and greater fuel flexibility. It enables the gasification of low-cost feedstocks, such as plastic waste.

Figure 3 depicts the TU Wien pilot plant. More comprehensive descriptions of this plant

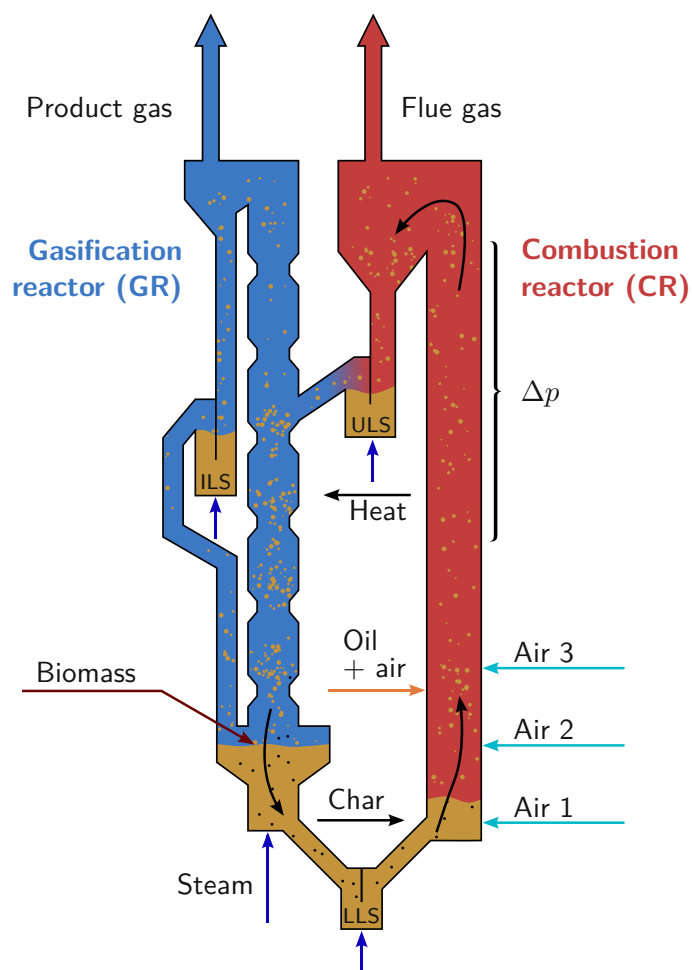


Figure 2: DFB gasification pilot plant at TU Wien. Figure adapted from [Publication A](#).

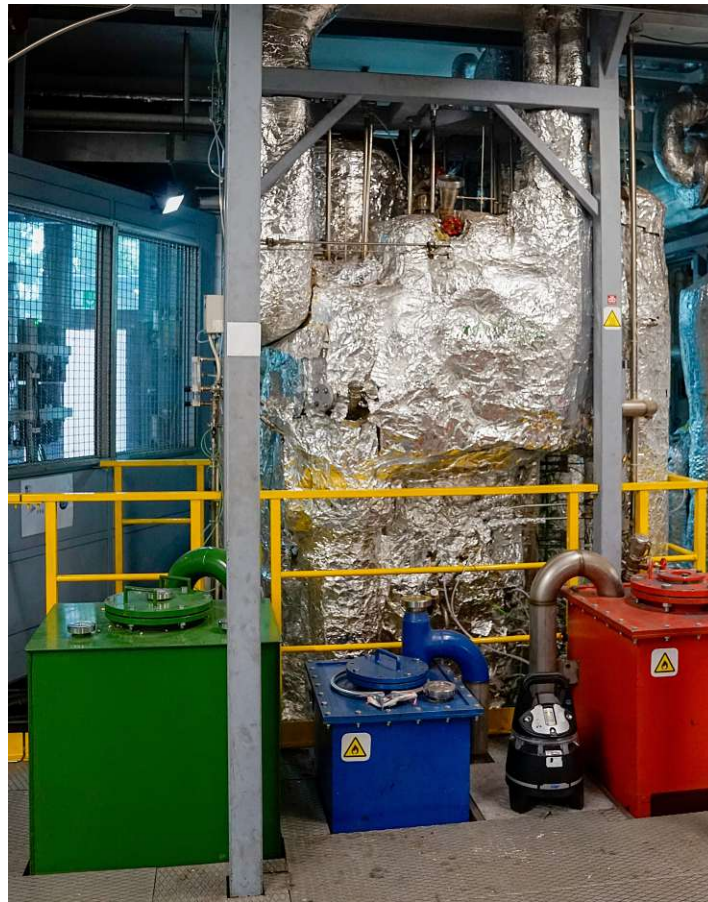


Figure 3: Upper part of the 100 kW pilot plant at TU Wien. From [Publication B](#).

are given in [15, 4].

The role of the solids circulation rate in DFB gasification

In DFB gasification, the solids circulation rate is critical as it determines the amount of char and heat transported between the interconnected reactors. Therefore, it affects the reactor temperatures as well as product gas composition and tar content in the product gas [16].

To control the solids circulation rate, the CR is typically equipped with multiple air inlets positioned at different heights. With this design, the total volume of air needed for full combustion in the CR may be maintained while adjusting the solids circulation rate. Air introduced at lower levels of the reactor tends to lift the bed material upward, thereby increasing the circulation rate. In contrast, air introduced at higher levels has less of an effect on circulation or may even reduce it.

Measuring the solids circulation rate in circulating fluidized bed systems is a challenging task, and various techniques have been proposed to address this challenge. Different approaches are reviewed in [17]. Some approaches involve disrupting the particle flow and measuring the resulting accumulation of bed material, as demonstrated in studies like [18, 19]. Other

techniques rely on optical sensors to track particle movement [20] or place obstacles in the particle flow and measure the impact on the obstacle [21]. Another widely adopted method involves measuring the pressure drop at the top of the CR, as presented in [22, 23, 24]. This pressure-based technique is particularly suitable for industrial-scale plants and remains effective during hot operations, making it a practical choice for real-time monitoring in operational environments.

2.2 Objectives and challenges in operating dual fluidized bed gasification plants

The operation of DFB gasification plants involves several key objectives and challenges due to the complex nature of the system. These plants are characterized by strong couplings between GR and CR, different time constants for the processes involved, and the need to control multiple interdependent variables. DFB gasification plants are typically operated at a steady-state operating point. Occasionally, however, it may be necessary to switch between different operating points, and unmeasured disturbances must be compensated for in order to maintain the steady-state point.

Key control objectives include maintaining the temperature in the GR and ensuring a constant product gas flow rate. The temperature in the GR is crucial because it directly affects the quality of the syngas, particularly its composition and the amount of tars. Higher temperatures generally reduce the tar content, improving the quality of the product gas for applications such as chemical synthesis or energy production, however, can decrease the process efficiency. The flow rate of product gas needs to be constant, as it is critical for downstream processes such as Fischer-Tropsch synthesis, or synthetic natural gas production.

There are several operational constraints that must be considered when controlling a DFB gasification plant. One important factor is the oxygen content in the flue gas from the CR. A certain level of residual oxygen is desired to ensure complete combustion of the fuel in the CR. Another important parameter is the steam-to-fuel ratio in the GR, which has a significant impact on the product gas composition. Additionally, the fluidization of the reactors must be maintained within specific limits to ensure the desired fluidization regime. Furthermore, each control input, such as fuel feed and air supply, has physical minimum and maximum limits that must be respected.

Several control inputs are available for process control. The biomass and steam fed to the GR primarily influence the product gas mass flow, its composition, and the gasification temperature. In addition, the biomass feed influences the amount of char transported to the CR and thus the oxygen concentration in the flue gas. In the CR, air is supplied through several stages. Adjustment of the airflow in these stages determines the overall oxygen supply to the CR and influences the solids circulation rate, which in turn affects the heat transferred to the GR. For the 100 kW pilot plant, three air stages are available in the CR, resulting in redundant control actuators. Fuel oil can be used as a supplementary fuel in the CR to provide sufficient heat for the gasification reactions.

The adjustment of the steam used to fluidize the loop seals relies on manual valves for the pilot plant and can thus not be manipulated by an automatic controller. However, these adjustments can be treated as measured disturbances in the control system. Additionally, the temperatures of both the incoming air and steam supplied to the plant vary slowly over time, but these variations are monitored and can also be accounted for in the control strategy.

2.3 State-of-the-art and open issues in modeling and control

Modeling of DFB gasification plants

Various modeling approaches for steam gasification are discussed in the literature. A brief overview is given below and a comprehensive review of DFB gasification models is available in [3].

Thermodynamic equilibrium models are commonly used to predict product gas composition. For instance, [25] presents a model to estimate gas composition at different gasification temperatures, while [26] examines the influence of the steam-to-fuel ratio at a fixed temperature, both based on Gibbs free energy minimization. Similarly, [27] predicts product gas composition in DFB steam gasification, incorporating variables such as temperature and fuel moisture content. In [28], pyrolysis is incorporated into the model and compared with pilot plant data, and a quasi-equilibrium model is used in [29] to study the effects of gasification temperature and steam-to-fuel ratios.

Experimental studies on product gas composition for different bed materials and fuels are found in [30], [31], and [13]. Process efficiency and fuel moisture content effects are simulated in [32]. Models incorporating mass and energy balances for the GR and the CR are provided in [33] and [34]. In these publications, each reactor is modeled separately and the incoming bed material from the other reactor is treated as model input.

A method to estimate solids circulation rate based on pressure gradients and airflows is introduced in [23], while [35] models solids circulation rate using computational fluid dynamics, though at high computational cost.

Despite these advancements, no DFB gasification plant model in the literature fully accounts for the influence of manipulable inputs on critical process variables (e.g., gasification and combustion temperatures, solids circulation rate, and product gas composition) while considering all relevant couplings.

Control of DFB gasification plants

To the best of the author's knowledge, state-of-the-art DFB gasification plants are either operated manually or use multiple SISO controllers to control key process variables, such as product gas quantity, gasification temperature, and flue gas oxygen content, as described in [36]. In [37], a PID control strategy is introduced that effectively controls product gas quantity and reduces fuel consumption. Beyond this, control strategies for DFB gasification have received limited attention in the literature.

Notably, no multivariable control strategies have been documented for DFB gasification plants that can simultaneously control all critical process variables. Moreover, the automatic control of solids circulation rate - an essential parameter in DFB gasification - remains an unexplored area in the literature. Implementing such control systems could improve process efficiency and reduce operational costs.

3 Key objectives of this thesis

To address the research gaps outlined in the previous section, the following overarching objective is formulated:

Key objective:

Develop a multivariable control strategy for a DFB gasification pilot plant, with a focus on real-world implementation and potential transferability to other plants.

To achieve this goal, research questions will be formulated. These questions will guide the investigations:

- RQ-1.** *How can a dynamic model of the DFB gasification process be developed to support model-based control design, and which approaches (e.g., first-principles, data-driven) are suitable for accurately capturing key dynamics?*
- RQ-2.** *How can model predictive control be employed to control key variables such as gasification temperature, product gas flow rate, ensuring offset-free tracking of constant references in the presence of system disturbances, model uncertainties, and process constraints?*
- RQ-3.** *How can model uncertainties and actuator redundancy be effectively addressed in the control strategy for the solids circulation rate in DFB gasification plants?*

By achieving these objectives, this work aims to provide an initial contribution toward closing the research gap in control strategies for DFB gasification plants and thus contribute to advancing the technology of DFB gasification.

Out of scope

This thesis does not include investigations into process efficiency or optimization beyond the development of the control strategy. Additionally, it does not cover the comparison of different control methods or paradigms outside the proposed approach.

4 Scientific approach

To implement advanced multivariable control methods such as MPC, a dynamic model of the process is required. This model provides a mathematical description of how the process behaves and how it can be influenced. The model is then used either for control design or directly by the controller, as in the case of MPC, where the model predicts future process behavior. [Publication A](#) focuses on developing this model of DFB gasification. It presents a gray-box modeling approach that combines first-principles with data-driven methods to capture the key dynamics of the most relevant variables in the DFB gasification process, and is thus addressing [RQ-1](#).

[Publication B](#), [C](#), and [D](#) focus on control methods for DFB gasification. [Publication B](#) addresses [RQ-2](#) by applying linear MPC to control the 100 kW DFB gasification pilot plant using a hierarchical structure. At the high level, a linear MPC regulates the product gas flow rate and gasification temperature, while considering constraints, such as maintaining a minimum oxygen content in the flue gas. At the lower level, a second linear MPC controls the solids circulation rate according to the high-level MPC's targets by adjusting air staging in

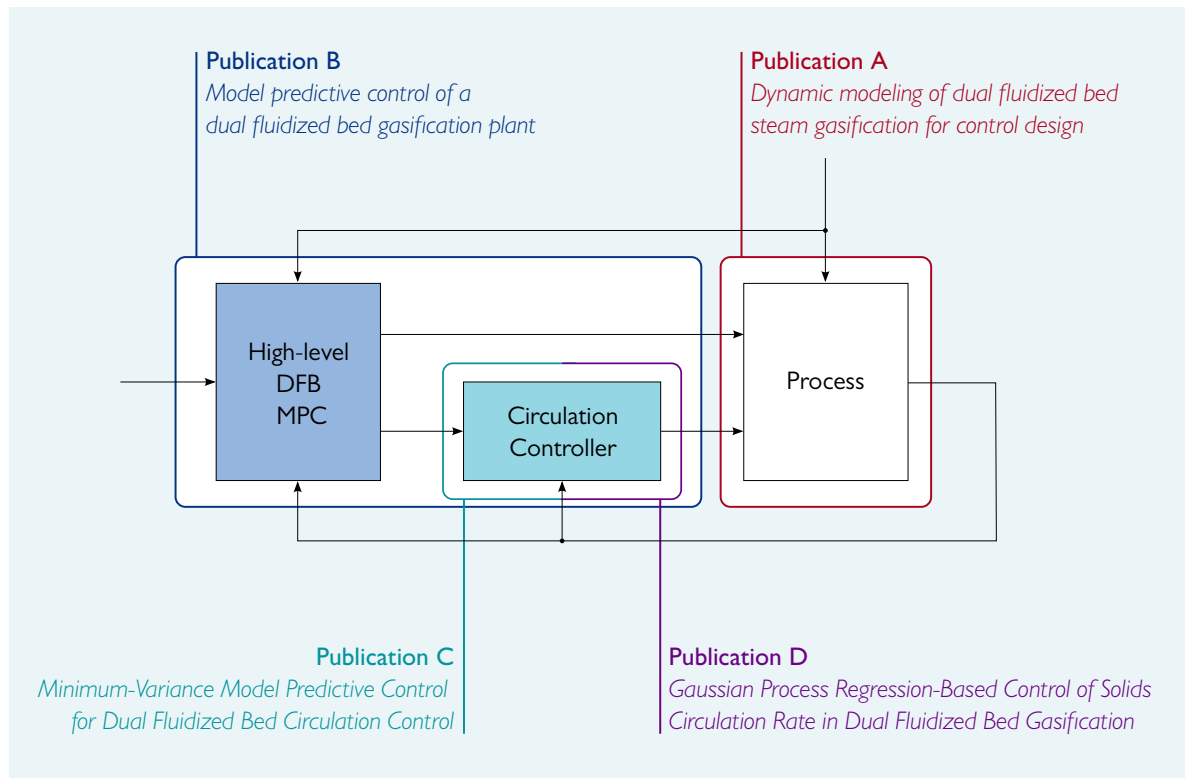


Figure 4: Overview of the control concept for DFB gasification and corresponding publications in this thesis.

the CR. The circulation rate is represented by the pressure difference in the upper CR, as this serves as a reliable measure of the circulation rate.

The solids circulation rate control is explored in greater depth in Publications C and D to address RQ-3. In Publication C, a linear minimum-variance MPC approach is introduced, useful when only limited measurement data is available for modeling the solids circulation rate. Here, MPC explicitly accounts for model uncertainties. Publication D presents an alternative approach using GP regression to control the solids circulation rate. This nonlinear method offers flexibility and improved scalability across different plants. Applied to both the 100 kW pilot plant and a 1 MW demonstration plant, this approach demonstrates the ease of implementation across plants without extensive modeling efforts.

Figure 4 illustrates the control concept and provides an overview of the publications included in this thesis.

4.1 Dynamic modeling

The dynamic behavior of process variables crucial for control is modeled, focusing on variables that should be controlled, such as the gasification temperature, along with important internal states like the combustion temperature. The model considers how these process variables are influenced by plant inputs, which include control inputs like fuel feed as well as measured

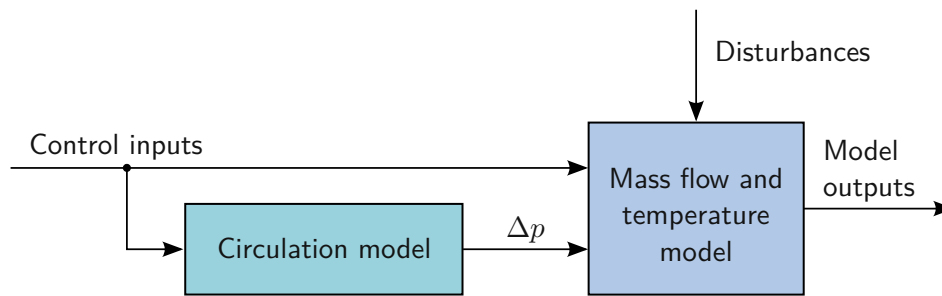


Figure 5: Structure of the dynamic DFB model. Figure adapted from [Publication A](#).

disturbances such as the temperature of air supplied to the CR.

The approach combines a first-principle model, based on mass and energy balances, with data-driven submodels where necessary. Where feasible, first-principle models based on mass and energy balances form the foundation of the model. This approach should enhance transferability to other DFB gasification plants, allowing the model structure to be reused while specific parameters can be adjusted for different plant configurations. Parameters that are unknown in the first place, such as the heat capacities of the reactors, are estimated using measurement data. Data-driven submodels address parts of the process that are challenging to model by first-principle approaches, such as the heat transported by bed material from the CR to the GR based on solids circulation rate and temperature difference.

The primary variables selected for modeling align with the process objectives outlined in Section 2.2. A consistent product gas flow rate is essential for downstream synthesis, requiring precise control. Gasification temperature, which significantly influences the product gas composition, demands accurate regulation. Since both the flue gas flow rate and the CR top temperature are interdependent with product gas flow and gasification temperature, respectively, they are included in the model. Additionally, to ensure complete combustion in the CR, it is desirable to maintain a certain oxygen content in the flue gas. Therefore, the oxygen content is considered in the model so that it can later be considered by the MPC.

Given the importance of solids circulation in the process, a submodel is developed for it. In this work, the pressure difference in the upper part of the CR, denoted by Δp , is used as a direct measure of the solids circulation rate, which then serves as an input to the energy balance. This approach allows the model to account for heat transport from the CR to the GR, driven by solids circulation rate. The model structure is illustrated in Figure 5.

As part of this work, targeted identification tests were conducted at the 100 kW pilot plant to collect data for parameter identification of the grey-box model and for identifying the circulation models. During these tests, the system was excited using stepwise changes in the control inputs to capture its dynamic behavior.

Mass balance

A mass balance is formulated for the GR and the CR, to model the product gas mass flow rate and the flue gas mass flow rate, respectively.

A first-order differential equation is employed as a model for the mass flow of product gas

\dot{m}_{PG} leaving the GR:

$$\frac{d\dot{m}_{\text{PG}}}{dt} = \frac{1}{\tau_{\text{PG}}} (-\dot{m}_{\text{PG}} + \dot{m}_{\text{bm}}(1 - w_{\text{ash}}) + \dot{m}_{\text{steam,GR,total}} - \dot{m}_{\text{char}}), \quad (1)$$

with the time constant τ_{PG} , the mass of biomass fed to the GR \dot{m}_{bm} , the ash content of the biomass w_{ash} , the total amount of steam fed to the GR $\dot{m}_{\text{steam,GR,total}}$, and the char that is transported to the CR via the LLS \dot{m}_{char} . Therefore, it is assumed that at steady state, the product gas mass flow is equal to the mass of ash-free biomass, plus the total amount of steam fed to the GR, reduced by the mass of char leaving the GR. It is assumed that a constant fraction of the biomass remains ungasified and is transported to the CR as char.

The mass flow of flue gas \dot{m}_{FG} is modeled by a first-order differential equation as well, with

$$\frac{d\dot{m}_{\text{FG}}}{dt} = \frac{1}{\tau_{\text{FG}}} (-\dot{m}_{\text{FG}} + \dot{m}_{\text{char}} + \dot{m}_{\text{steam,CR}} + \dot{m}_{\text{air}} + \dot{m}_{\text{oil}}), \quad (2)$$

with the time constant τ_{FG} , the steam streaming to the CR $\dot{m}_{\text{steam,CR}}$, the air feed \dot{m}_{air} and the oil feed \dot{m}_{oil} .

Energy balance

The reactor temperatures are modeled through energy balances for each reactor, incorporating two temperature state variables per reactor: one for the temperature inside the reactor and another for the temperature of the reactor wall. For the GR, the energy balance

$$C_{\text{GR}} \frac{dT_{\text{GR}}}{dt} = \dot{H}_{\text{bm}} + \dot{H}_{\text{steam,GR,total}} - \dot{H}_{\text{char}} - \dot{H}_{\text{PG}} + \dot{Q}_{\text{bed}} - \dot{Q}_{\text{wall,GR}}, \quad (3)$$

models the gasification temperature T_{GR} , where C_{GR} is a heat capacity and \dot{H}_{bm} , $\dot{H}_{\text{steam,GR,total}}$, \dot{H}_{char} and \dot{H}_{PG} are the flows of conventional enthalpy of the biomass, steam, char, and product gas, respectively. Conventional enthalpies for biomass and char are computed based on their lower heating values, which are determined using Boie's formula and compositional analysis. The conventional enthalpy of the product gas is computed using a pseudo-equilibrium model of its composition. Heat transferred by the bed material from the CR to the GR is represented by \dot{Q}_{bed} , while $\dot{Q}_{\text{wall,GR}}$ describes the heat transfer from the gas within the reactor to the reactor wall, thereby coupling the internal reactor temperature state to the reactor wall temperature state. The heat balance for the reactor wall

$$C_{\text{GR,wall}} \frac{dT_{\text{GR,wall}}}{dt} = \dot{Q}_{\text{wall,GR}} - \dot{Q}_{\text{loss,GR}}, \quad (4)$$

models the temperature of the reactor wall $T_{\text{GR,wall}}$, with the heat capacity $C_{\text{GR,wall}}$ and the heat loss $\dot{Q}_{\text{loss,GR}}$. Heat loss $\dot{Q}_{\text{loss,GR}}$ is assumed to vary linearly with T_{GR} .

Similarly, for the CR, an energy balance is established for the top temperature T_{CR} :

$$C_{\text{CR}} \frac{dT_{\text{CR}}}{dt} = \dot{H}_{\text{char}} + \dot{H}_{\text{oil}} + \dot{H}_{\text{air}} + \dot{H}_{\text{steam,CR}} - \dot{H}_{\text{FG}} - \dot{Q}_{\text{bed}} - \dot{Q}_{\text{wall,CR}}, \quad (5)$$

incorporating the heat capacity C_{CR} and the flows of conventional enthalpies \dot{H}_{oil} , \dot{H}_{air} , $\dot{H}_{\text{steam,CR}}$, and \dot{H}_{FG} , corresponding to the oil, staged air, steam, and flue gas, respectively.

$\dot{Q}_{\text{wall,CR}}$ represents the coupling term linking the inside temperature state and the wall temperature state. The conventional enthalpy of the flue gas is calculated based on its composition, which is computed as described in Section 4.1.

A second energy balance describes the CR reactor wall temperature $T_{\text{CR,wall}}$

$$C_{\text{CR,wall}} \frac{dT_{\text{CR,wall}}}{dt} = \dot{Q}_{\text{wall,CR}} - \dot{Q}_{\text{loss,CR}}, \quad (6)$$

with the heat capacity $C_{\text{CR,wall}}$.

The bed material heat flow \dot{Q}_{bed} couples the temperature states T_{GR} and T_{CR} . This heat transport is assumed to depend on the temperature difference between the GR and the CR and on the solids circulation rate, indicated by the pressure drop in the upper CR Δp :

$$\dot{Q}_{\text{bed}} = (\beta_0 + \beta_1 \Delta p)(T_{\text{CR}} - T_{\text{GR}}), \quad (7)$$

where β_0 and β_1 are parameter identified using measurement data.

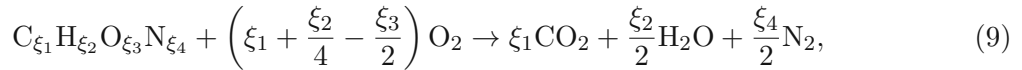
Combustion model

To model the oxygen content in the flue gas, it is assumed that a sufficient supply of air \dot{V}_{air} is always available, ensuring the complete combustion of both char \dot{m}_{char} and oil \dot{m}_{oil} . Assuming ideal gas behavior, the oxygen content in the dry flue gas can be determined using

$$y_{\text{O}_2} = \frac{\dot{n}_{\text{O}_2,\text{FG}}}{\dot{n}_{\text{CO}_2,\text{FG}} + \dot{n}_{\text{N}_2,\text{FG}} + \dot{n}_{\text{O}_2,\text{FG}}}, \quad (8)$$

where $\dot{n}_{\text{O}_2,\text{FG}}$, $\dot{n}_{\text{CO}_2,\text{FG}}$, and $\dot{n}_{\text{N}_2,\text{FG}}$ represent the molar flows of O_2 , CO_2 , and N_2 in the flue gas, respectively. Other minor components in the flue gas are neglected here.

Using the stoichiometric equation for combustion,



the steady-state oxygen content in the flue gas can be derived as

$$y_{\text{O}_2} = \frac{\dot{n}_{\text{O}_2,\text{in}} - 2\dot{n}_{\text{C},\text{in}} - 0.5\dot{n}_{\text{H},\text{in}}}{\dot{n}_{\text{N}_2,\text{in}} + \dot{n}_{\text{O}_2,\text{in}} - 0.5\dot{n}_{\text{H},\text{in}}}, \quad (10)$$

where $\dot{n}_{\text{O}_2,\text{in}}$, $\dot{n}_{\text{C},\text{in}}$, $\dot{n}_{\text{H},\text{in}}$, and $\dot{n}_{\text{N}_2,\text{in}}$ represent the input flows of oxygen, carbon, hydrogen, and nitrogen into the CR. These flows depend on the input rates of char, oil, and air, along with their respective compositions. The char composition is determined from sample analysis, while the compositions of the heating oil and air are known. It can be noted from this expression that the steam feed has no effect on the oxygen content in the dry flue gas, making the oxygen content a nonlinear function of the mass flows of char, oil, and air:

$$y_{\text{O}_2} = \phi(\dot{m}_{\text{char}}, \dot{m}_{\text{oil}}, \dot{V}_{\text{air}}). \quad (11)$$

Since variations in the fuel or air feed do not immediately alter the flue gas oxygen content, a first-order differential equation is used to capture this dynamic behavior:

$$\frac{dy_{\text{O}_2}}{dt} = \frac{1}{\tau_{\text{O}_2}} (-y_{\text{O}_2} + \phi(\dot{m}_{\text{char}}, \dot{m}_{\text{oil}}, \dot{V}_{\text{air}})), \quad (12)$$

where τ_{O_2} is the time constant. In accordance with the assumption of complete combustion, $y_{\text{O}_2} \geq 0$ must hold.

Solids circulation rate model

Different methods are employed to model the solids circulation rate in DFB gasification. Across all cases, a first-order dynamic model is used, given by

$$\frac{d(\Delta p)}{dt} = \frac{1}{\tau_c} (-\Delta p + \xi(\mathbf{u})), \quad (13)$$

where $\xi(\mathbf{u})$ represents the model's nonlinear input transformation and τ_c is a time constant. This configuration is often referred to as a Hammerstein model in the literature, particularly when the static part exhibits nonlinear behavior. Different approaches are applied for this static component, as discussed below. The solids circulation rate is modeled not only for the 100 kW pilot plant but also for a cold flow model, where it serves as the basis for the minimum-variance MPC circulation controller, as presented in [Publication C](#). Additionally, the model is extended to the 1 MW demonstration plant, as detailed in [Publication D](#).

Linear model. A linear model for the solids circulation rate is presented in [Publication B](#), structured as

$$\Delta p = b_0 + b_1 \dot{V}_{\text{air}1} + b_2 \dot{V}_{\text{air}2} + b_3 \dot{V}_{\text{air}3} + b_4 \dot{m}_{\text{bm}}, \quad (14)$$

where $\dot{V}_{\text{air}1}$, $\dot{V}_{\text{air}2}$, and $\dot{V}_{\text{air}3}$ are the airflows to the CR, and $b_0 - b_4$ are model parameters. In [Publication C](#), this approach is adapted for the cold flow model by omitting the biomass feed \dot{m}_{bm} and $\dot{V}_{\text{air}3}$, as only two air stages are available.

Artificial neural network. [Publication A](#) introduces an artificial neural network (ANN) for the solids circulation rate in the 100 kW pilot plant. [Publication D](#) further applies ANNs to both the 100 kW pilot plant and the 1 MW demonstration plant, where the ANN serves as a simulation model to validate the controller against simulated conditions. ANNs enable the modeling of nonlinear input-output relationships. For the 100 kW pilot plant, the biomass feed and three air streams are used as inputs, while for the 1 MW demonstration plant, the inputs include the biomass feed, the total air feed to the CR, and the valve positions for air streams 2 and 3.

Gaussian process regression. GP regression is employed in [Publication D](#) to predict the solids circulation rate for both the 100 kW pilot plant and the 1 MW demonstration plant. GP regression offers the advantage of providing confidence intervals for predictions, reflecting the model's uncertainty. The input variables for GP regression are the same as those used for the ANNs.

4.2 Model predictive control

Linear MPCs are employed in various parts of this work:

- High-level DFB MPC ([Publication B](#))
- MPC as circulation controller ([Publication B](#))
- Minimum-variance MPC as circulation controller for the cold flow model ([Publication C](#))

Each application uses a linear or linearized model (i.e., linear MPC) with the objective of achieving offset-free tracking of constant reference values. Additionally, in all instances, the number of control inputs exceeds the number of outputs that need adjustment to specific reference values.

To ensure offset-free reference tracking, integrator states are added to the process model. This can be realized using the velocity form model [38] or by employing a disturbance model to correct for any plant-model mismatch or constant disturbances [39]. Using the velocity form model is equivalent to the use of a particular disturbance model, as shown in [40]. In this work, disturbance models are applied to achieve offset-free control, enabling the weighting of the absolute values of control inputs. This approach is especially advantageous here, as the surplus of control inputs over outputs allows the MPC to incorporate objectives such as minimizing heating oil consumption into the control formulation. The methodology is briefly explained below.

The linear, discrete-time model

$$\begin{aligned} \mathbf{x}_{k+1} &= \mathbf{A}\mathbf{x}_k + \mathbf{B}\mathbf{u}_k + \mathbf{E}\mathbf{z}_k, \\ \mathbf{y}_k &= \mathbf{C}\mathbf{x}_k, \\ \mathbf{y}_k^* &= \mathbf{H}\mathbf{y}_k, \end{aligned} \quad (15)$$

is used as a plant model, with the state vector \mathbf{x} , the control input vector \mathbf{u} , the vector of measured disturbances \mathbf{z} , the output vector \mathbf{y} and the vector of controlled outputs \mathbf{y}^* . The matrices \mathbf{A} , \mathbf{B} , \mathbf{C} and \mathbf{E} are the system matrix, the input matrix, the output matrix, and the disturbance input matrix, respectively. The matrix \mathbf{H} selects the controlled outputs from the output vector. The index k denotes the time step.

The high-level DFB MPC utilizes the following states, inputs, and outputs:

$$\begin{aligned} \mathbf{x} &= [\dot{m}_{\text{PG}}, \dot{m}_{\text{FG}}, T_{\text{GR}}, T_{\text{GR,wall}}, T_{\text{CR}}, T_{\text{CR,wall}}, y_{\text{O}_2}]^T, \\ \mathbf{u} &= [\dot{m}_{\text{bm}}, \dot{m}_{\text{oil}}, \dot{m}_{\text{steam,GR}}, \dot{V}_{\text{air}}, \Delta p]^T, \\ \mathbf{z} &= [\dot{m}_{\text{steam,ILS}}, \dot{m}_{\text{steam,ULS}}, \dot{m}_{\text{steam,LLS}}, T_{\text{steam}}, T_{\text{air}}]^T, \\ \mathbf{y} &= [\dot{m}_{\text{PG}}, \dot{m}_{\text{FG}}, T_{\text{GR}}, T_{\text{CR}}, y_{\text{O}_2}]^T, \\ \mathbf{y}^* &= [\dot{m}_{\text{PG}}, T_{\text{GR}}]^T, \end{aligned}$$

whereas for the circulation MPC, the following variables are used:

$$\begin{aligned} x &= y = y^* = \Delta p, \\ \mathbf{u} &= [\dot{V}_{\text{air1}}, \dot{V}_{\text{air2}}, \dot{V}_{\text{air3}}]^T, \\ z &= \dot{m}_{\text{bm}}. \end{aligned}$$

A disturbance state vector \mathbf{d} is introduced, and model (15) is augmented as follows:

$$\begin{aligned} \begin{bmatrix} \mathbf{x}_{k+1} \\ \mathbf{d}_{k+1} \end{bmatrix} &= \begin{bmatrix} \mathbf{A} & \mathbf{B}_d \\ \mathbf{0} & \mathbf{I} \end{bmatrix} \begin{bmatrix} \mathbf{x}_k \\ \mathbf{d}_k \end{bmatrix} + \begin{bmatrix} \mathbf{B} \\ \mathbf{0} \end{bmatrix} \mathbf{u}_k + \begin{bmatrix} \mathbf{E} \\ \mathbf{0} \end{bmatrix} \mathbf{z}_k + \mathbf{w}_k, \\ \mathbf{y}_k &= \mathbf{C}\mathbf{x}_k + \mathbf{C}_d\mathbf{d}_k + \mathbf{v}_k. \end{aligned} \quad (16)$$

It is assumed that process noise \mathbf{w} is acting on the augmented state vector and output noise \mathbf{v} is acting on the output, both are assumed to be zero-mean and normally distributed. Offset-free reference tracking can be achieved if the number of disturbance states matches the number of measured outputs, for the case that the closed-loop system is stable and there are no active constraints at steady state. However, if the number of disturbance states is chosen to be smaller than the number of measured outputs, this may no longer hold true [39]. Thus, in this work, the number of disturbance states is chosen to be equal to the number of measured outputs. The matrix \mathbf{C}_d is chosen to be the zero matrix and \mathbf{B}_d is designed in a way that the disturbance states have a physical meaning, such as unmodeled heat flows to the reactors.

To control the DFB gasification plant, the following three steps are performed at each time step:

1. A Kalman filter estimates both the system state \mathbf{x} , and the disturbance state \mathbf{d} .
2. A target input vector and target state vector are calculated so that the controlled outputs meet their reference values at steady state.
3. The MPC optimization problem is solved to track the target operating point determined in Step 2.

The steady-state Kalman gain for the filter is precomputed by solving the discrete-time algebraic Riccati equation, as outlined in [39]. Further details on Steps 2 and 3 are provided below.

Computation of the target operating point

A target operating point is defined by a target state $\bar{\mathbf{x}}$ and a target control input $\bar{\mathbf{u}}$, calculated so that the controlled output vector \mathbf{y}^* aligns with the reference \mathbf{r} at steady state. Since there are more control inputs available than required output variables to track, the solution for this problem is not unique. To address this, a desired control input vector \mathbf{u}^* can be specified. An optimization problem is then formulated to ensure that the steady-state input $\bar{\mathbf{u}}$ is as close as possible to \mathbf{u}^* in a least-squares sense. This approach also allows additional considerations, such as economic objectives, to be incorporated into the target computation. The target operating point is determined by minimizing the cost function

$$J_t = \|\bar{\mathbf{u}}_k - \mathbf{u}^*\|_{\mathbf{R}_\infty}^2, \quad (17)$$

where \mathbf{R}_∞ is a weighting matrix, with respect to the following constraints:

- Model equations, describing the stationary relationships of \mathbf{x} , \mathbf{u} , \mathbf{z} and \mathbf{d} , and demanding the controlled outputs to meet their reference values \mathbf{r} :

$$\begin{bmatrix} \mathbf{A} - \mathbf{I} & \mathbf{B} \\ \mathbf{HC} & \mathbf{0} \end{bmatrix} \begin{bmatrix} \bar{\mathbf{x}}_k \\ \bar{\mathbf{u}}_k \end{bmatrix} = \begin{bmatrix} -\mathbf{E}\mathbf{z}_k - \mathbf{B}_d\hat{\mathbf{d}}_k \\ \mathbf{r}_k - \mathbf{HC}_d\hat{\mathbf{d}}_k \end{bmatrix} \quad (18)$$

- Process constraints, such as minimum and maximum values for control inputs, a minimum concentration of oxygen in the flue gas, a predefined steam-to-fuel ratio, or constraints to ensure the desired fluidization regime of the reactors

MPC optimization problem

The MPC optimization problem is formulated to track the target point computed in step 2 by solving an optimization problem with the cost function

$$J_{\text{MPC}} = \sum_{i=1}^{N_p} (\|\mathbf{x}_{k+i} - \bar{\mathbf{x}}_k\|_{\mathbf{Q}_i}^2 + w_\eta \eta_{k+i}^2) + \sum_{i=0}^{N_c-1} (\|\mathbf{u}_{k+i} - \bar{\mathbf{u}}_k\|_{\mathbf{R}_i}^2 + \|\Delta \mathbf{u}_{k+i}\|_{\mathbf{R}_\Delta}^2), \quad (19)$$

where \mathbf{Q} , \mathbf{R} , and \mathbf{R}_Δ are weighting matrices, N_p represents the prediction horizon, N_c is the control horizon, η is a slack variable, and w_η is its associated weight. The term $w_\eta \eta_{k+i}^2$ is included to enforce a soft constraint on the output, which is used only for the high-level DFB MPC in maintaining a minimum oxygen concentration in the flue gas. The last term can be used to prevent rapid changes in the control variables. The optimization problem includes the following constraints:

- system dynamics,
- initialization of the states by their estimates, and
- process constraints, such as minimum and maximum values for the control inputs, a soft constraint formulation to ensure a minimum concentration of oxygen in the flue gas, or constraints to ensure the desired fluidization regime of the reactors.

The time constants of the DFB gasification plant differ significantly. Mass flows and gas compositions change rapidly, while reactor temperatures evolve more slowly due to the high reactor heat capacity. To address these differences, the high-level DFB MPC uses two sampling times to predict the process behavior within the prediction horizon. The initial prediction steps use a short sampling time of 5 s to capture the fast-changing dynamics. After that, predictions are made with a longer sampling time of 250 s. This approach allows the process behavior to be predicted for approximately two hours in total while reducing the number of decision variables and keeping the computation times short.

4.3 Gaussian process regression-based control of solids circulation rate

While linear models accurately describe the relationship between control inputs and the circulation rate in the 100 kW pilot plant, they were found to be unsuitable for a second system investigated within this work - a 1 MW demonstration plant. This discrepancy arises because, unlike the 100 kW plant, the 1 MW system does not allow for adjusting the air volume flows of individual stages. Instead, only the total volume flow across all stages and the valve positions of the individual stages can be controlled. In particular, a nonlinear relationship has been shown between the valve positions and the circulation rate. Therefore, a nonlinear approach is introduced for circulation control, offering a method that can be employed more independently of the system configuration. The approach is based on GP regression, a method that explicitly provides a measure of uncertainty in its predictions. The presented controller considers this uncertainty measure as well as the availability of redundant control actuators to drive the system into a region of low model uncertainty.

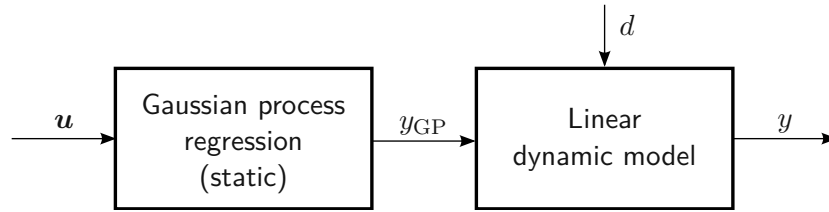


Figure 6: Structure of the Hammerstein model for the solids circulation rate. Figure adapted from [Publication D](#).

Model structure

A model is developed to describe the pressure difference Δp in the upper CR, which serves as an indicator of the solids circulation rate. Due to the nonlinear nature of the static input-output relationship, combined with the suitability of a linear time-invariant (LTI) model for representing system dynamics, a Hammerstein model is employed. The structure of the Hammerstein model is illustrated in Figure 6.

The Hammerstein model combines a nonlinear static component and a linear dynamic component. The nonlinear static part uses GP regression for the steady-state input-output relationship, using steady-state process data as training data. The linear dynamic component models the system's dynamic behavior and incorporates a disturbance model to address discrepancies between the plant and model, as well as unmeasured disturbances. This disturbance model introduces an integrator into the plant model, enabling offset-free tracking of constant reference signals.

The overall model is defined by the differential equations

$$\begin{aligned} \dot{x}(t) &= \frac{1}{\tau_c} (-x(t) + y_{\text{GP}}(\mathbf{u}(t)) + d(t)), \\ \dot{d}(t) &= 0, \\ y(t) &= x(t), \end{aligned} \tag{20}$$

where $x(t)$ and $d(t)$ represent the system state and disturbance state, respectively. The input to the model is $\mathbf{u}(t)$, the output is $y(t)$, and τ_c denotes the time constant. The term $y_{\text{GP}}(\mathbf{u}(t))$ is the GP regression prediction, which is a static function of the input $\mathbf{u}(t)$.

Gaussian process regression

This section provides a brief overview of GP regression, with detailed explanations available in sources such as [41, 42].

Consider a training dataset comprising input vectors $\bar{\mathbf{U}} = [\bar{\mathbf{u}}_1, \dots, \bar{\mathbf{u}}_N]$ and corresponding output measurements $\bar{\mathbf{Y}} = [\bar{y}_1, \dots, \bar{y}_N]$. The objective is to predict the output \bar{y}_* for a new input vector $\bar{\mathbf{u}}_*$.

The outputs $\bar{\mathbf{Y}} = [\bar{y}_1(\bar{\mathbf{u}}_1), \dots, \bar{y}_N(\bar{\mathbf{u}}_N)]$ are modeled as random variables following a joint normal distribution:

$$\bar{\mathbf{y}} \sim \mathcal{N}(\boldsymbol{\mu}, \mathbf{K}), \tag{21}$$

where $\boldsymbol{\mu}$ is the mean vector, and \mathbf{K} is the covariance matrix. In practice, the mean vector is often assumed to be zero after appropriate data normalization. The covariance matrix measures the relationship between inputs and is determined by a covariance function $k(\cdot, \cdot)$:

$$\mathbf{K} = k(\bar{\mathbf{U}}, \bar{\mathbf{U}}). \quad (22)$$

A commonly used choice is the squared exponential covariance function, which depends on hyperparameters $\boldsymbol{\theta}$ controlling the function's amplitude, length scale, and noise level. These parameters are critical in defining how closely related outputs are for inputs that are near each other in the input space.

To predict \bar{y}_* , a joint Gaussian distribution is assumed for the training outputs and the new output:

$$\begin{bmatrix} \bar{\mathbf{y}} \\ \bar{y}_* \end{bmatrix} \sim \mathcal{N} \left(\mathbf{0}, \begin{bmatrix} \mathbf{K} & \mathbf{k}_* \\ \mathbf{k}_*^T & k_{**} \end{bmatrix} \right). \quad (23)$$

Here, \mathbf{k}_* is the covariance between the training outputs and the new output, and k_{**} is the variance of the new output. These are given by:

$$\mathbf{k}_* = k(\bar{\mathbf{U}}, \bar{\mathbf{u}}_*), \quad k_{**} = k(\bar{\mathbf{u}}_*, \bar{\mathbf{u}}_*). \quad (24)$$

Given the observed training outputs $\bar{\mathbf{y}}$, the predicted mean μ_* and variance σ_*^2 of \bar{y}_* are derived from the conditional Gaussian distribution:

$$\begin{aligned} \mu_* &= \mathbf{k}_*^T \mathbf{K}^{-1} \bar{\mathbf{y}}, \\ \sigma_*^2 &= k_{**} - \mathbf{k}_*^T \mathbf{K}^{-1} \mathbf{k}_*. \end{aligned} \quad (25)$$

Training the GP model involves optimizing the hyperparameters of the covariance function to best explain the observed data. This is typically done by maximizing the logarithm of the marginal likelihood,

$$\log p(\bar{\mathbf{y}} | \mathbf{U}, \boldsymbol{\theta}) = -\frac{1}{2} \bar{\mathbf{y}}^T \mathbf{K}^{-1} \bar{\mathbf{y}} - \frac{1}{2} \log |\mathbf{K}| - \frac{N}{2} \log 2\pi, \quad (26)$$

where $p(\bar{\mathbf{y}} | \mathbf{U}, \boldsymbol{\theta})$ is the probability that the training data was generated by the model given the input data and the hyperparameters. This approach balances data fit and model complexity.

The computational cost of a GP prediction increases with the number of training points, as the entire dataset is used for each prediction. For a large dataset, approximation methods can be employed to reduce this cost, as detailed in [41]. However, the approach in this work uses the full dataset for predictions.

Control approach

An extended Kalman filter is employed to estimate both the system state and the disturbance state. For this purpose, a discrete-time version of the model (20) is utilized within both the Kalman filter and the controller.

The process under consideration involves multiple control inputs to control a single output. Additionally, the GP prediction provides confidence information, which is used in the control design. Specifically, the objective is to determine a steady-state input vector $\bar{\mathbf{u}}_k$ such that the

output aligns with the reference r_k at steady state while minimizing the prediction uncertainty. This is done by solving the following optimization problem:

$$\min_{\bar{\mathbf{u}}_k} J_{\text{GP}} = \sigma_{\text{GP}}^2(\bar{\mathbf{u}}_k) + \lambda \|\bar{\mathbf{u}}_k - \mathbf{u}_{k-1}\|, \quad (27a)$$

subject to

$$\mu_{\text{GP}}(\bar{\mathbf{u}}_k) = r_k - \hat{d}_k, \quad (27b)$$

$$\bar{\mathbf{u}}_k \in \mathbb{U}. \quad (27c)$$

This optimization is performed at each time step k , under the assumption that certain regions of the input space exhibit higher uncertainty in GP predictions than others. The cost function (27a) consists of two terms. The first term, $\sigma_{\text{GP}}^2(\bar{\mathbf{u}}_k)$, represents the GP prediction uncertainty, which is generally a non-convex function. To discourage large input-space changes that offer only marginal uncertainty reductions, a second term, $\lambda \|\bar{\mathbf{u}}_k - \mathbf{u}_{k-1}\|$, is included, where $\lambda \geq 0$ is a weighting factor.

Constraint (27b) ensures that the GP prediction equals the reference r_k , adjusted by the estimated disturbance state \hat{d}_k . This correction facilitates offset-free tracking of constant references, despite mismatches in the plant model or unmeasured disturbances and integrates feedback into the closed-loop system. Additionally, constraint (27c) restricts the input space, enabling specific control inputs, such as feedstock feed rate, to be fixed or bounded within specified limits.

Given the non-convex nature of the cost function, the optimization problem (27) is solved multiple times using different initial conditions generated via Latin hypercube sampling [43]. Among the feasible solutions, the one with the lowest cost is selected.

The optimization problem may sometimes become infeasible, for instance, when the reference value is set beyond the range achievable according to the GP regression model. In such cases, a fallback optimization problem is solved to find the best possible solution. This alternative approach minimizes the squared difference between the GP prediction and the reference, adjusted by the estimated disturbance state.

4.4 Experimental investigation

In this work, experiments were conducted on the 100 kW pilot plant, which also served as a testing platform for controllers. Additionally, experimental studies were carried out on the following systems:

- In [Publication C](#) data from a cold flow model of the DFB system were utilized to investigate solids circulation, model the circulation, and design a minimum-variance MPC for the cold flow model. The controller was tested in simulations.
- In [Publication D](#) the methodology for GP-based circulation control was examined also for a 1 MW demonstration plant using measurement data. While the control strategy was tested in simulations, it was not implemented on this plant.

This section focuses on describing the experimental procedures carried out at the 100 kW pilot plant. For further details on the cold model, please refer to [44, 45], and for information on the 1 MW plant, refer to [46, 47].

Table 1: Measurement equipment at the TU Wien pilot plant. Table adapted from [Publication A](#).

Process variable	Device
Temperature	Type K thermocouple
Pressure	Kalinsky pressure sensor
Steam and airflows	Variable area flowmeter
Product gas and flue gas flows	Barthel orifice meter
Main gas compositions	Rosemount NGA 2000
Fuel feed	Rot. speed of dosing screws*

* The dosing screws are calibrated before every test run.

The experiments at the 100 kW plant have been conducted using softwood pellets as feedstock. The bed material was composed of a mixture of 80 % olivine and 20 % limestone.

Table 1 provides an overview of the equipment utilized for measurement purposes. Detailed information regarding the measurement devices and actuators used at the pilot plant can be found in [48].

All the algorithms are implemented in MATLAB. Measurement data from the plant's process control system is collected and transmitted to a cloud platform using the Modbus/TCP and MQTT protocols. The computer running the controller in MATLAB accesses this data over the internet via an HTTP-based web API. The computed control inputs are sent back to the plant in the reverse direction.

The MPC optimization problems are formulated using YALMIP [49] and solved with the quadprog solver from MATLAB's Optimization Toolbox [50]. For the GP regression algorithms, the MATLAB Statistics and Machine Learning Toolbox [51] is utilized. The nonlinear optimization problem in the GP-based control algorithm is solved using `fmincon`, also from MATLAB's Optimization Toolbox [50].

Experimental results from the DFB MPC implementation at the 100 kW pilot plant

The DFB control strategy, which integrates a high-level DFB MPC and a circulation MPC, was successfully implemented and tested at the 100 kW pilot plant at TU Wien. The results from this eight-hour test run are presented in Figure 7.

During the experiment, the following reference value adjustments were applied:

- (a) The reference for the PG mass flow was reduced by 20 %.
- (b) The oil feed in the desired input vector \mathbf{u}^* was adjusted from 4.386 kg/h to 0 kg/h, requiring the MPC to reduce the oil feed accordingly.
- (c) The reference value for the gasification temperature was increased to 810 °C.
- (d) The reference value for the gasification temperature was then decreased to 750 °C.

The experimental results demonstrate the effectiveness of the DFB MPC in controlling the gasification process. The product gas mass flow showed fast and accurate tracking of the

reference values. Similarly, changes in the gasification temperature reference were successfully tracked. The circulation MPC effectively controlled the solids circulation rate and, due to its fast dynamics, quickly responded to the high demands of the DFB MPC.

An increase in the gasification temperature reference was initially implemented just prior to $t = 3$ h. However, due to necessary maintenance of the gas analysis system, the reference was temporarily reset to 780°C . During this maintenance period, incorrect product gas mass flow measurements required manual operation of the plant. This manual phase is indicated by a grey background in the corresponding graph.

A detailed discussion of the experimental results can be found in [Publication B](#).

Simulation results of the GP-based circulation controller for the 1 MW demonstration plant

The developed GP-based circulation controller was evaluated through simulations for both the 100 kW pilot plant and the 1 MW demonstration plant. Additionally, the controller for the 100 kW pilot plant was experimentally tested on-site. A comprehensive discussion of the results is provided in [Publication D](#).

Here, exemplary results from a closed-loop simulation of the 1 MW demonstration plant are presented in [Figure 8](#). The two plots on the left show the controlled output - the solids circulation rate - represented by the pressure drop in the upper CR (top plot). The lower plot shows the control inputs corresponding to the valve positions of air 2 and air 3. A change in the circulation rate set point occurs at $t = 30$ min. The plot on the right illustrates the uncertainty in the GP prediction (contour lines), the distribution of the training data, and the control sequence within the input space. It can be seen that the GP-based controller operates the process close to the training data points, ensuring low prediction uncertainty.

5 Scientific contribution

This section summarizes how the research conducted in this thesis addresses the research questions and ultimately contributes to achieving the overarching goal.

Development of a dynamic model for DFB gasification

To answer [RQ-1](#), *How can a dynamic model of the DFB gasification process be developed to support model-based control design, and which approaches are suitable for accurately capturing key dynamics?*, this thesis makes the following contributions:

- The developed model captures how control inputs and disturbances affect key variables, internal states and their couplings, providing a foundation for model-based control.
- A first-principles modeling approach, which incorporates mass and energy balances along with thermodynamic equilibrium models, has been demonstrated to be sufficient for capturing the relationships and couplings of major process variables. Model parameters were identified using measurement data from both previous experiments and targeted identification experiments.

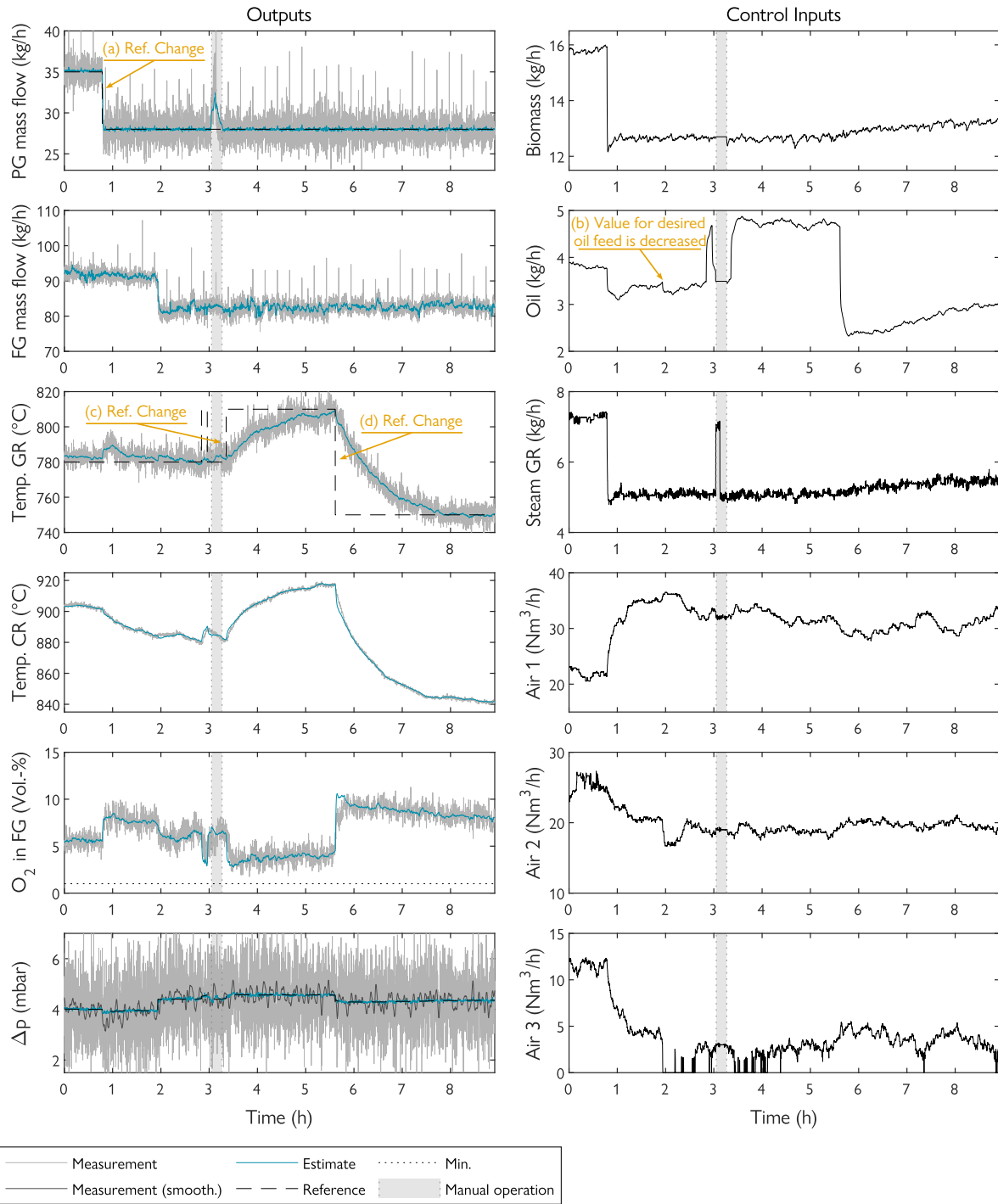


Figure 7: Experimental results obtained in implementing the proposed controller for the 100 kW pilot plant. Adapted from [Publication B](#).

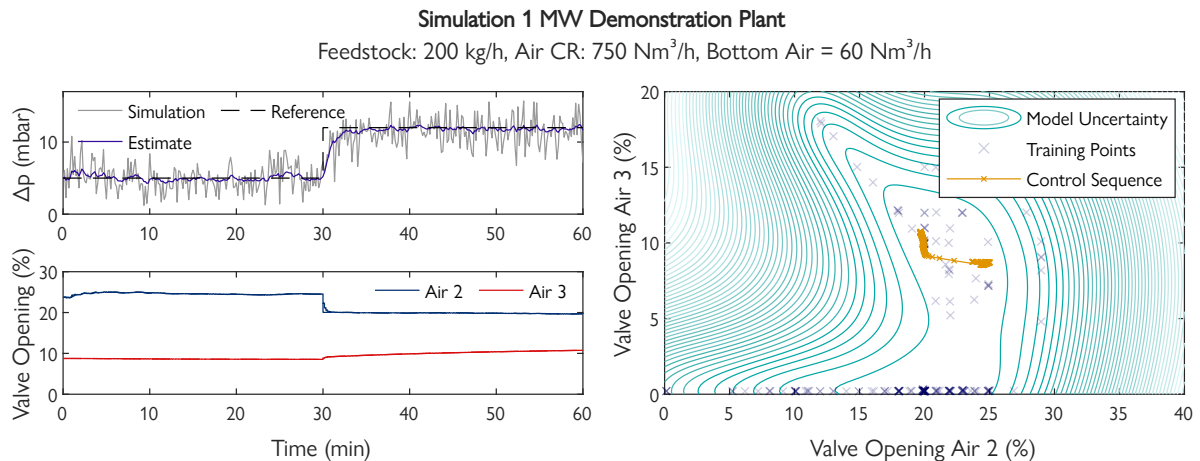


Figure 8: Closed-loop simulation of the proposed GP-based controller for the 1 MW demonstration plant. Adapted from [Publication D](#).

- For solids circulation rate, where first-principles modeling is challenging to implement with reasonable effort, black-box models were successfully applied. For the 100 kW pilot plant and a cold flow model, where the individual airflows of the air stages can be adjusted, a linear black-box model was adequate to describe system dynamics. In contrast, for a 1 MW demonstration plant, where only the overall airflow and valve opening positions of the air stages can be manipulated, strong nonlinearities between inputs and outputs were observed. To address these nonlinearities, nonlinear black-box models, such as artificial neural networks and GP regression, were successfully applied.

Application of model predictive control

To address [RQ-2](#), *How can model predictive control be employed to control key variables such as gasification temperature and product gas flow rate, ensuring offset-free tracking of constant references in the presence of system disturbances, model uncertainties, and process constraints?*, the work contributed as follows:

- A hierarchical MPC structure was developed, with a high-level DFB MPC controlling gasification temperature and product gas quantity, and a circulation MPC controlling the solids circulation rate via air staging. This modular structure will enhance transferability to other plants.
- Offset-free tracking was achieved by incorporating disturbance states into the plant model, compensating for model mismatches and disturbances. This approach is also advantageous in this application because the system has more control inputs than outputs to be controlled. The absolute values of the control inputs can be weighted so that secondary objectives, such as minimizing fuel oil consumption, can be incorporated without compromising the primary control objectives.
- Non-constant prediction steps in the MPC addressed varying time constants, ensuring accurate control for both fast (e.g., mass flows) and slow (e.g., temperatures) dynamics.

- The MPC framework was successfully implemented and validated on the 100 kW pilot plant, demonstrating its ability to control the DFB system under real operating conditions.

Addressing model uncertainties and actuator redundancy

To answer [RQ-3](#), *How can model uncertainties and actuator redundancy be effectively addressed in the control strategy for the solids circulation rate in DFB gasification plants?*, the contributions include:

- Two control approaches were developed for solids circulation: A linear minimum-variance MPC, tested through simulations on a cold flow model, and a nonlinear GP regression-based control approach, validated through simulations on both the 100 kW and 1 MW plants, and experimentally tested on the 100 kW plant.
- Both approaches utilized actuator redundancy by explicitly integrating model uncertainty information into the control algorithms. This allowed the process to be guided toward regions with low model uncertainty.
- Disturbance models were incorporated into both control strategies, enabling offset-free tracking of constant reference signals by compensating for plant-model mismatches and unmeasured disturbances.

Contribution to the thesis objective

The overall contributions of this work align closely with the [thesis objective](#): developing a multivariable control strategy for a DFB gasification pilot plant with real-world applicability and transferability. Key points include:

- An initial contribution to closing the research gap in control strategies was achieved by presenting MPC-based control for important process variables.
- Experimental results from the 100 kW pilot plant confirm the successful application of the proposed control methods.
- The emphasis on first-principles modeling, with black-box models used only where necessary, should support transferability to other plants. The model structure can often be reused with minor adjustments to account for differences in process design, while known parameters (e.g., fuel properties) can be adopted, and unknown parameters can be identified through targeted experiments.

6 Outlook

This work provides a contribution to the development of advanced control strategies for DFB gasification plants. However, there are several areas where future research can further improve and extend the presented concepts:

- **Control strategies for industrial plants.** While the control strategies were tested on pilot-scale systems, applying them to industrial-scale plants introduces additional challenges.

For example, heating oil in the CR is typically replaced by recirculating product gas, requiring adjustments to the control strategy. It may also become important to control the product gas flow rate after water separation. Furthermore, industrial plants must meet stricter safety regulations, so future work should include safety mechanisms in the control system design.

- **Alternative feedstocks.** Future research could focus on applying the control strategies to alternative feedstocks such as biomass residues or waste materials. These materials often have different properties compared to softwood pellets as mainly used in this work. To handle this, the models would need to be adapted, and additional experiments might be required to identify unknown parameters. This would make the DFB gasification system more flexible and capable of using a wider range of feedstocks.
- **Comparison of different control strategies.** Although this thesis demonstrates the benefits of MPC, comparing it with simpler control strategies, such as multiple SISO PID controllers, could provide valuable insights. This comparison could highlight the advantages of MPC, such as its ability to handle interactions between variables and enforce constraints, versus the simplicity and widespread use of PID controllers. Such comparisons could guide the design of control systems for DFB gasification.
- **Potential model improvements.** The models used in this work were developed based on reasonable simplifications, but further refinements could improve their accuracy and predictive capabilities. For example, the assumption that the char flow from the CR is a constant fraction of the biomass feed could be replaced by adding dependencies on the gasification temperature and circulation rate. Similarly, improving the model for predicting product gas composition would make it possible to control gas quality more precisely.
- **Enhancing circulation control.** In this work, the circulation control strategies did not consider potential flooding in the counter-current column, which could disrupt the system's operation. Future research could include methods to detect flooding using additional measurements, making the control system more robust and reliable.

By addressing these points, future work can build on the contributions of this thesis, improving the control of DFB gasification plants and supporting their implementation in larger industrial systems.

Bibliography

- [1] IPCC. *Climate Change 2023: Synthesis Report*. Geneva, Switzerland, 2023. DOI: [10.59327/IPCC/AR6-9789291691647](https://doi.org/10.59327/IPCC/AR6-9789291691647).
- [2] M. Kaltschmitt, H. Hofbauer, and V. Lenz, eds. *Energie aus Biomasse*. Wiesbaden: Springer Fachmedien Wiesbaden, 2024. DOI: [10.1007/978-3-658-41216-6](https://doi.org/10.1007/978-3-658-41216-6).
- [3] N. Hanchate, S. Ramani, C. S. Mathpati, and V. H. Dalvi. “Biomass gasification using dual fluidized bed gasification systems: A review”. In: *Journal of Cleaner Production* 280 (Jan. 2021), p. 123148. DOI: [10.1016/J.JCLEPRO.2020.123148](https://doi.org/10.1016/J.JCLEPRO.2020.123148).
- [4] F. Benedikt. *Fuel flexible advanced dual fluidized bed steam gasification*. Dissertation, TU Wien, 2020. DOI: [10.34726/hss.2020.39988](https://doi.org/10.34726/hss.2020.39988).
- [5] A. Chiodini, L. Bua, L. Carnelli, R. Zwart, B. Vreugdenhil, and M. Vocciante. “Enhancements in Biomass-to-Liquid processes: Gasification aiming at high hydrogen/carbon monoxide ratios for direct Fischer-Tropsch synthesis applications”. In: *Biomass and Bioenergy* 106 (Nov. 2017), pp. 104–114. DOI: [10.1016/J.BIOMBIOE.2017.08.022](https://doi.org/10.1016/J.BIOMBIOE.2017.08.022).
- [6] A. Bartik, F. Benedikt, J. Fuchs, H. Hofbauer, and S. Müller. “Experimental investigation of hydrogen-intensified synthetic natural gas production via biomass gasification: a technical comparison of different production pathways”. In: *Biomass Conversion and Biorefinery* (2023). DOI: [10.1007/s13399-023-04341-3](https://doi.org/10.1007/s13399-023-04341-3).
- [7] J. Loipersböck, M. Luisser, S. Müller, H. Hofbauer, and R. Rauch. “Experimental Demonstration and Validation of Hydrogen Production Based on Gasification of Lignocellulosic Feedstock”. In: *ChemEngineering* 2.4 (2018). DOI: [10.3390/chemengineering2040061](https://doi.org/10.3390/chemengineering2040061).
- [8] H. Hofbauer, A. M. Mauerhofer, F. Benedikt, M. Hammerschmid, A. Bartik, M. Veress, R. Haas, M. Siebenhofer, and G. Resch. *Reallabor zur Herstellung von Holzdiesel und Holzgas aus Biomasse und biogenen Reststoffen für die Land-und Forstwirtschaft*. 2020.
- [9] J. Karl and T. Pröll. “Steam gasification of biomass in dual fluidized bed gasifiers: A review”. In: *Renewable and Sustainable Energy Reviews* 98 (Dec. 2018), pp. 64–78. DOI: [10.1016/J.RSER.2018.09.010](https://doi.org/10.1016/J.RSER.2018.09.010).
- [10] T. Glad and L. Ljung. *Control theory*. CRC press, 2000. DOI: [10.1201/9781315274737](https://doi.org/10.1201/9781315274737).
- [11] M. Schwenzer, M. Ay, T. Bergs, and D. Abel. “Review on model predictive control: an engineering perspective”. In: *The International Journal of Advanced Manufacturing Technology* 117.5 (2021), pp. 1327–1349. DOI: [10.1007/s00170-021-07682-3](https://doi.org/10.1007/s00170-021-07682-3).
- [12] H. Hofbauer, M. Kaltschmitt, F. Keil, U. Neuling, and H. Wagner. “Vergasung in der Gasatmosphäre”. In: *Energie aus Biomasse*. Berlin, Heidelberg: Springer Berlin Heidelberg, 2016, pp. 1059–1182. DOI: [10.1007/978-3-662-47438-9_{\ }13](https://doi.org/10.1007/978-3-662-47438-9_{\ }13).
- [13] F. Benedikt, J. C. Schmid, J. Fuchs, A. M. Mauerhofer, S. Müller, and H. Hofbauer. “Fuel flexible gasification with an advanced 100 kW dual fluidized bed steam gasification pilot plant”. In: *Energy* 164 (Dec. 2018), pp. 329–343. DOI: [10.1016/j.energy.2018.08.146](https://doi.org/10.1016/j.energy.2018.08.146).
- [14] J. Schmid, C. Pfeifer, H. Kitzler, T. Pröll, and H. Hofbauer. “A new dual fluidized bed gasifier design for improved in situ conversion of hydrocarbons”. In: *Proc. Int. Conf. Polygeneration Strateg.* Aug. 2011.

- [15] J. C. Schmid, F. Benedikt, J. Fuchs, A. M. Mauerhofer, S. Müller, and H. Hofbauer. “Syngas for biorefineries from thermochemical gasification of lignocellulosic fuels and residues—5 years’ experience with an advanced dual fluidized bed gasifier design”. In: *Biomass Conversion and Biorefinery* 11.6 (2021), pp. 2405–2442. DOI: [10.1007/s13399-019-00486-2](https://doi.org/10.1007/s13399-019-00486-2).
- [16] K. Göransson, U. Söderlind, and W. Zhang. “Experimental test on a novel dual fluidised bed biomass gasifier for synthetic fuel production”. In: *Fuel* 90.4 (Apr. 2011), pp. 1340–1349. DOI: [10.1016/J.FUEL.2010.12.035](https://doi.org/10.1016/J.FUEL.2010.12.035).
- [17] X. Liu, M. Zhang, S. Zhang, Y. Ding, Z. Huang, T. Zhou, H. Yang, and G. Yue. “Measuring Technologies for CFB Solid Circulation Rate: A Review and Future Perspectives”. In: *Energies* 15.2 (Jan. 2022), p. 417. DOI: [10.3390/en15020417](https://doi.org/10.3390/en15020417).
- [18] A. Kreuzeder, C. Pfeifer, and H. Hofbauer. “Fluid-Dynamic Investigations in a Scaled Cold Model for a Dual Fluidized Bed Biomass Steam Gasification Process: Solid Flux Measurements and Optimization of the Cyclone”. In: *International Journal of Chemical Reactor Engineering* 5.1 (Aug. 2007). DOI: [10.2202/1542-6580.1394](https://doi.org/10.2202/1542-6580.1394).
- [19] T. Karlsson, X. Liu, D. Pallarès, and F. Johnsson. “Solids circulation in circulating fluidized beds with low riser aspect ratio and varying total solids inventory”. In: *Powder Technology* 316 (July 2017), pp. 670–676. DOI: [10.1016/J.POWTEC.2016.09.028](https://doi.org/10.1016/J.POWTEC.2016.09.028).
- [20] S. Matsuda. “Measurement of solid circulation rate in a circulating fluidized bed”. In: *Powder Technology* 187.2 (Oct. 2008), pp. 200–204. DOI: [10.1016/J.POWTEC.2008.02.004](https://doi.org/10.1016/J.POWTEC.2008.02.004).
- [21] X. Liu, Y. Zhang, H. Yang, X. Liu, Y. Zhang, and G. Yue. “A method for measuring the solid circulation rates of CFB boilers based on the particle flow-around principle”. In: *Chemical Engineering Journal* 481 (Feb. 2024), p. 148424. DOI: [10.1016/J.CEJ.2023.148424](https://doi.org/10.1016/J.CEJ.2023.148424).
- [22] Y. Alghamdi, Z. Peng, K. Shah, B. Moghtaderi, and E. Doroodchi. “Predicting the solid circulation rate in chemical looping combustion systems using pressure drop measurements”. In: *Powder Technology* 286 (Dec. 2015), pp. 572–581. DOI: [10.1016/J.POWTEC.2015.09.004](https://doi.org/10.1016/J.POWTEC.2015.09.004).
- [23] J. Fuchs, J. Schmid, F. Benedikt, A. Mauerhofer, S. Müller, and H. Hofbauer. “A general method for the determination of the entrainment in fluidized beds”. In: *The International Journal of Multiphysics* 12.4 (Dec. 2018), pp. 359–372. DOI: [10.21152/1750-9548.12.4.359](https://doi.org/10.21152/1750-9548.12.4.359).
- [24] M. Stollhof, S. Penthor, K. Mayer, and H. Hofbauer. “Estimation of the solid circulation rate in circulating fluidized bed systems”. In: *Powder Technology* 336 (Aug. 2018), pp. 1–11. DOI: [10.1016/J.POWTEC.2018.05.033](https://doi.org/10.1016/J.POWTEC.2018.05.033).
- [25] C. C. Sreejith, P. Arun, and C. Muraleedharan. “Thermochemical analysis of biomass gasification by Gibbs free energy minimization model - Part: I (Optimization of Pressure and Temperature)”. In: *International Journal of Green Energy* 10.3 (Mar. 2013), pp. 231–256. DOI: [10.1080/15435075.2011.653846](https://doi.org/10.1080/15435075.2011.653846).

- [26] C. C. Sreejith, C. Muraleedharan, and P. Arun. “Thermo-chemical analysis of biomass gasification by gibbs free energy minimization model-part: II (Optimization of biomass feed and steam to biomass ratio)”. In: *International Journal of Green Energy* 10.6 (July 2013), pp. 610–639. DOI: [10.1080/15435075.2012.709203](https://doi.org/10.1080/15435075.2012.709203).
- [27] G. Schuster, G. Löffler, K. Weigl, and H. Hofbauer. “Biomass steam gasification – an extensive parametric modeling study”. In: *Bioresource Technology* 77.1 (Mar. 2001), pp. 71–79. DOI: [10.1016/S0960-8524\(00\)00115-2](https://doi.org/10.1016/S0960-8524(00)00115-2).
- [28] A. Aghaalikhani, J. C. Schmid, D. Borello, J. Fuchs, F. Benedikt, H. Hofbauer, F. Rispoli, U. B. Henriksen, Z. Sárosy, and L. Cedola. “Detailed modelling of biomass steam gasification in a dual fluidized bed gasifier with temperature variation”. In: *Renewable Energy* 143 (Dec. 2019), pp. 703–718. DOI: [10.1016/J.RENENE.2019.05.022](https://doi.org/10.1016/J.RENENE.2019.05.022).
- [29] S. I. Ngo, T. D. Nguyen, Y. I. Lim, B. H. Song, U. D. Lee, Y. T. Choi, and J. H. Song. “Performance evaluation for dual circulating fluidized-bed steam gasifier of biomass using quasi-equilibrium three-stage gasification model”. In: *Applied Energy* 88.12 (2011), pp. 5208–5220. DOI: [10.1016/j.apenergy.2011.07.046](https://doi.org/10.1016/j.apenergy.2011.07.046).
- [30] S. Koppatz, C. Pfeifer, and H. Hofbauer. “Comparison of the performance behaviour of silica sand and olivine in a dual fluidised bed reactor system for steam gasification of biomass at pilot plant scale”. In: *Chemical Engineering Journal* 175.1 (Nov. 2011), pp. 468–483. DOI: [10.1016/j.cej.2011.09.071](https://doi.org/10.1016/j.cej.2011.09.071).
- [31] A. M. Mauerhofer, F. Benedikt, J. C. Schmid, J. Fuchs, S. Müller, and H. Hofbauer. “Influence of different bed material mixtures on dual fluidized bed steam gasification”. In: *Energy* 157 (Aug. 2018), pp. 957–968. DOI: [10.1016/j.energy.2018.05.158](https://doi.org/10.1016/j.energy.2018.05.158).
- [32] T. Pröll and H. Hofbauer. “H₂ rich syngas by selective CO₂ removal from biomass gasification in a dual fluidized bed system - Process modelling approach”. In: *Fuel Processing Technology* 89.11 (Nov. 2008), pp. 1207–1217. DOI: [10.1016/j.fuproc.2008.05.020](https://doi.org/10.1016/j.fuproc.2008.05.020).
- [33] P. Kaushal, T. Pröll, and H. Hofbauer. “Application of a detailed mathematical model to the gasifier unit of the dual fluidized bed gasification plant”. In: *Biomass and Bioenergy* 35.7 (July 2011), pp. 2491–2498. DOI: [10.1016/J.BIOMBIOE.2011.01.025](https://doi.org/10.1016/J.BIOMBIOE.2011.01.025).
- [34] P. Kaushal, T. Pröll, and H. Hofbauer. “Model development and validation: Co-combustion of residual char, gases and volatile fuels in the fast fluidized combustion chamber of a dual fluidized bed biomass gasifier”. In: *Fuel* 86.17-18 (Dec. 2007), pp. 2687–2695. DOI: [10.1016/j.fuel.2007.03.032](https://doi.org/10.1016/j.fuel.2007.03.032).
- [35] S. Kraft, F. Kirnbauer, and H. Hofbauer. “CPFD simulations of an industrial-sized dual fluidized bed steam gasification system of biomass with 8 MW fuel input”. In: *Applied Energy* 190 (Mar. 2017), pp. 408–420. DOI: [10.1016/J.APENERGY.2016.12.113](https://doi.org/10.1016/J.APENERGY.2016.12.113).
- [36] T. Pröll and H. Hofbauer. “Process and device for providing a constant product gas rate from a fluidized bed gas generation plant”. In: *WO201006353A3* (2010).
- [37] T. Nigitz, M. Gölles, C. Aichernig, S. Schneider, H. Hofbauer, and M. Horn. “Increased efficiency of dual fluidized bed plants via a novel control strategy”. In: *Biomass and Bioenergy* 141 (Oct. 2020), p. 105688. DOI: [10.1016/J.BIOMBIOE.2020.105688](https://doi.org/10.1016/J.BIOMBIOE.2020.105688).

- [38] L. Wang. “A Tutorial on Model Predictive Control: Using a Linear Velocity-Form Model”. In: *Developments in Chemical Engineering and Mineral Processing* 12.5-6 (Jan. 2004), pp. 573–614. DOI: <https://doi.org/10.1002/apj.5500120511>.
- [39] G. Pannocchia and J. B. Rawlings. “Disturbance models for offset-free model-predictive control”. In: *AIChE Journal* 49.2 (Feb. 2003), pp. 426–437. DOI: <https://doi.org/10.1002/aic.690490213>. URL: <https://doi.org/10.1002/aic.690490213>.
- [40] G. Pannocchia, M. Gabiccini, and A. Artoni. “Offset-free MPC explained: Novelties, subtleties, and applications”. In: *IFAC-PapersOnLine* 48.23 (2015), pp. 342–351. DOI: [10.1016/j.ifacol.2015.11.304](https://doi.org/10.1016/j.ifacol.2015.11.304).
- [41] C. E. Rasmussen and C. K. I. Williams. *Gaussian Processes for Machine Learning*. MIT Press, 2006. DOI: [10.7551/mitpress/3206.001.0001](https://doi.org/10.7551/mitpress/3206.001.0001).
- [42] M. N. Gibbs. *Bayesian Gaussian Processes for Regression and Classification*. Dissertation, University of Cambridge, 1997.
- [43] M. D. McKay, R. J. Beckman, and W. J. Conover. “A Comparison of Three Methods for Selecting Values of Input Variables in the Analysis of Output from a Computer Code”. In: *Technometrics* 21.2 (1979), pp. 239–245. DOI: [10.2307/1268522](https://doi.org/10.2307/1268522).
- [44] A. Lunzer, S. Kraft, S. Müller, and H. Hofbauer. “CPFD simulation of a dual fluidized bed cold flow model”. In: *Biomass Conversion and Biorefinery* 11.1 (2021), pp. 189–203. DOI: [10.1007/s13399-020-01229-4](https://doi.org/10.1007/s13399-020-01229-4). URL: <https://doi.org/10.1007/s13399-020-01229-4>.
- [45] J. Fuchs. *Ermittlung des Betriebskennfeldes einer innovativen Zweibett-wirbelschicht anhand von Kaltmodelluntersuchungen*. Master thesis, Montanuniversität Leoben, 2013.
- [46] D. Kadlez, F. Benedikt, M. Huber, K. Fürsatz, J. C. Schmid, H. Hofbauer, and S. Müller. “Technology development of advanced dual fluidized bed steam gasification from pilot to demonstration scale – First results from a newly commissioned 1 MW demonstration plant”. In: *Fuel* 381 (Feb. 2025), p. 133376. DOI: [10.1016/j.fuel.2024.133376](https://doi.org/10.1016/j.fuel.2024.133376).
- [47] D. Hochstätger. *Performance evaluation of DFB gas generation based on a comparison of two research plants with 100 kW and 1 MW*. Wien: Master thesis, TU Wien, 2023. DOI: [10.34726/hss.2023.96261](https://doi.org/10.34726/hss.2023.96261).
- [48] M. Schmalzl. *Implementierung der MSR-Technik einer 100 kW Dual Fluid Versuchsanlage zur Vergasung von Festbrennstoffen*. ger. Master thesis, TU Wien, 2014.
- [49] J. Lofberg. “YALMIP : a toolbox for modeling and optimization in MATLAB”. In: *2004 IEEE International Conference on Robotics and Automation (IEEE Cat. No.04CH37508)*. 2004, pp. 284–289. DOI: [10.1109/CACSD.2004.1393890](https://doi.org/10.1109/CACSD.2004.1393890).
- [50] The Mathworks Inc. *MATLAB Optimization Toolbox*. 2023. URL: <https://www.mathworks.com/products/optimization.html>.
- [51] The MathWorks Inc. *MATLAB Statistics and Machine Learning Toolbox*. 2023. URL: <https://www.mathworks.com/products/statistics.html>.

Publications

Publication A

Dynamic modeling of dual fluidized bed steam gasification for control design

Lukas Stanger, Alexander Schirrer, Florian Benedikt, Alexander Bartik, Stefan Jankovic, Stefan Müller, and Martin Kozek

Energy 265 (2023) p. 126378

DOI: [10.1016/J.ENERGY.2022.126378](https://doi.org/10.1016/J.ENERGY.2022.126378)

Publication B

Model predictive control of a dual fluidized bed gasification plant

Lukas Stanger, Alexander Bartik, Martin Hammerschmid, Stefan Jankovic, Florian Benedikt, Stefan Müller, Alexander Schirrer, Stefan Jakubek, and Martin Kozek

Applied Energy 361 (2024) p. 122917

DOI: [10.1016/J.APENERGY.2024.122917](https://doi.org/10.1016/J.APENERGY.2024.122917)

Publication C

Minimum-Variance Model Predictive Control for Dual Fluidized Bed Circulation Control

Lukas Stanger, Alexander Schirrer, Alexander Bartik, and Martin Kozek

IFAC-PapersOnLine 56 (2023) pp. 2701–2706

DOI: [10.1016/j.ifacol.2023.10.1364](https://doi.org/10.1016/j.ifacol.2023.10.1364)

Publication D

Gaussian Process Regression-Based Control of Solids Circulation Rate in Dual Fluidized Bed Gasification

Lukas Stanger, Alexander Bartik, Matthias Binder, Alexander Schirrer, Stefan Jakubek, and Martin Kozek

IEEE Access 12 (2024) pp. 138535–138546

DOI: [10.1109/ACCESS.2024.3466394](https://doi.org/10.1109/ACCESS.2024.3466394)

Publication A

Dynamic modeling of dual fluidized bed steam gasification for control design

Lukas Stanger, Alexander Schirrer, Florian Benedikt, Alexander Bartik, Stefan Jankovic, Stefan Müller, and Martin Kozek

Energy 265 (2023) p. 126378

DOI: [10.1016/J.ENERGY.2022.126378](https://doi.org/10.1016/J.ENERGY.2022.126378)

Own Contribution: Conceptualization, Methodology, Validation, Software, Visualization, Writing - original draft



Contents lists available at ScienceDirect

Energy

journal homepage: www.elsevier.com/locate/energy

Dynamic modeling of dual fluidized bed steam gasification for control design

Lukas Stanger^{a,*}, Alexander Schirrer^a, Florian Benedikt^b, Alexander Bartik^b, Stefan Jankovic^c, Stefan Müller^{b,c}, Martin Kozek^a

^a TU Wien, Institute of Mechanics and Mechatronics, Getreidemarkt 9, 1060 Vienna, Austria

^b TU Wien, Institute of Chemical, Environmental and Bioscience Engineering, Getreidemarkt 9, 1060 Vienna, Austria

^c Verto Engineering GmbH, Franz-Josefs Kai 53/13, 1010 Vienna, Austria

ARTICLE INFO

Keywords:

Dual fluidized bed
Biomass gasification
Dynamic prediction model
Gray-box modeling
Artificial neural network

ABSTRACT

Dual fluidized bed steam gasification allows the production of high-value product gas from woody biomass or biogenic residuals. Advanced control concepts such as model predictive control are promising approaches to improve the process performance and efficiency. These control techniques require dynamic models of the process that can predict the plant's behavior as a function of the manipulated variables. This paper presents a gray-box modeling approach based on mass and energy balances to obtain a mathematical description of the temperatures inside the two reactors and the total mass flows leaving the reactors. The model incorporates data-driven components where first-principle modeling is hardly possible with reasonable effort. An artificial neural network is utilized to model the bed material circulation between the two reactors. Experiments were carried out at a 100 kW pilot plant to generate measurement data both for system identification and model validation. Simulations verify that the model achieves reliable predictions for the dual fluidized bed gasification process.

1. Introduction

The globally increasing demand for energy and the need to reduce greenhouse gases require the use of environmentally friendly energy carriers [1]. Dual fluidized bed (DFB) steam gasification is a promising technology that allows the thermo-chemical conversion of woody biomass or biogenic residuals to a high-value product gas, and can therefore help to decrease the dependency on fossil fuels. The product gas can be used e.g. in combined heat and power plants [2] or for synthetic natural gas (SNG) production [3,4].

In DFB plants, several inputs, such as fuel feed, steam, and air flows need to be chosen to accurately control the process. State-of-the-art DFB plants use several single-input single-output (SISO) controllers to control the relevant process variables [5]. In [6], a procedure is presented to control a DFB plant based on SISO controllers controlling individual process variables. However, these SISO controllers do not take into account the couplings between those process variables. In [5], a model-based control strategy is presented to control the product gas quantity, which led to a reduction in fuel consumption by 5% compared to the state-of-the-art controller.

Multiple-input multiple-output (MIMO) controllers which control multiple process variables, such as product gas mass flow and reactor temperatures, which take coupling between variables into account,

cannot be found in the literature, yet these offer the chance for further improvements in process efficiency. Model predictive control (MPC) has been applied successfully in the process industry for multivariable processes [7] and can explicitly consider constraints on process variables. However, this requires a model of the DFB process that is capable of predicting the variables and their dynamic coupling that should be controlled in dependence on the input variables that can be manipulated, such as fuel, steam and air flows into the plant.

In literature, various modeling approaches can be found for steam gasification. A thermodynamic equilibrium model for steam gasification of biomass to derive the product gas composition for different gasification temperatures is presented in [8]. In [9], the influence of the steam-to-fuel ratio on the product gas composition is modeled by a thermodynamic equilibrium model, where the gasification temperature is set to a fixed value. In both works [8,9], the calculation of the thermodynamic equilibrium is based on the minimization of Gibbs free energy. A model for the product gas composition of DFB steam gasification as a function of the gasification temperature and the fuel water content is given in [10], where the product gas composition is computed based on the thermodynamic equilibrium. In [11] the product gas composition is modeled by considering the pyrolysis and the results are compared to the measurements of a DFB pilot plant.

* Corresponding author.

E-mail address: lukas.stanger@tuwien.ac.at (L. Stanger).

<https://doi.org/10.1016/j.energy.2022.126378>

Received 7 September 2022; Received in revised form 25 November 2022; Accepted 8 December 2022

Available online 9 December 2022

0360-5442/© 2022 The Authors. Published by Elsevier Ltd. This is an open access article under the CC BY license (<http://creativecommons.org/licenses/by/4.0/>).

Nomenclature**Abbreviations**

ANN	artificial neural network
bm	biomass
CR	combustion reactor
db	dry basis
DFB	dual fluidized bed
FG	flue gas
GR	gasification reactor
ILS	internal loop seal
LLS	lower loop seal
MPC	model predictive control
PG	product gas
RMSE	root-mean-square error
ULS	upper loop seal
wt	weight

Symbols

α_{CR}	heat transfer coefficient reactor wall combustion reactor (kW/°C)
$\beta_0, \alpha_1, \alpha_2$	heat loss parameters (kW and kW/°C)
θ	parameter vector
d	measured disturbances
u	manipulated variables
y	output vector
Δh_R^{750}	enthalpy of reaction at 750 °C (kJ/mol)
Δp	pressure difference in the upper part of the combustion reactor (mbar)
ΔT	Temperature difference between combustion reactor and gasification reactor (°C)

$\Delta^R G(T)$	Gibbs free energy of reactions (J/mol)
\dot{H}	enthalpy flow rate (kW)
\dot{m}	mass flow rate (kg/h)
\dot{n}	molar flow rate (mol/h)
\dot{Q}	heat flow rate (kW)
\dot{V}	volumetric flow rate (Nm ³ /h)
\hat{y}	model output vector
τ_{FG}	time constant flue gas mass flow (s)
τ_{PG}	time constant product gas mass flow (s)
$c_{bm,CR}$	weight fraction of dry and ash-free biomass transported to the combustion reactor
$C_{CR,wall}$	heat capacity of the combustion reactor's wall (kJ/°C)
C_{CR}	heat capacity of the combustion reactor (kJ/°C)
C_{GR}	heat capacity of the gasification reactor (kJ/°C)
c_{PG}	correction factor product gas mass flow
K_{eq}	equilibrium constant
k_{PG}	product gas mass flow correction factor
p_0, p_1	heat transport (bed material) parameters (kW/°C and kW/(mbar·°C))
R	gas constant (J/(K·mol))
R^2	Coefficient of determination
t	Time (h or min)
T_{amb}	ambient temperature (°C)
$T_{CR,wall}$	wall temperature of the combustion reactor (°C)
T_{CR}	temperature in the upper part of the combustion reactor (°C)
T_{GR}	temperature in the bubbling bed of the gasification reactor (°C)
w_{ash}	ash content in biomass (weight fraction)
w_{H_2O}	water content in biomass (weight fraction)

A quasi-equilibrium model is used in [12] to investigate the product gas composition and the process performance for different gasification temperatures and steam-to-fuel ratios. The product gas composition is experimentally investigated in [13,14] for different bed material mixtures as well as in [15] for different fuels. In [16], the process efficiency and the product gas composition is simulated for different fuel water contents. All these models treat the gasification temperature as an input variable.

Models for both the gas compositions and the reactor temperatures that incorporate mass and energy balances can be found in [17,18] for the gasification reactor (GR) and combustion reactor (CR), respectively. However, mass flow and temperature of the incoming bed material are treated as model inputs, hence the couplings between the two reactors are not depicted in the model. In [19], a method is presented to estimate the mass flow of bed material circulating between the GR and the CR based on the measured pressure gradient in the upper part of the CR and the volume flow in the CR. A model for the bed material circulation as a function of the process inputs, such as air streams to the reactors, can be found in [20]. Computational fluid dynamics is used to model the bed material circulation, what results in a complex model and high computational effort.

An extensive overview of different DFB gasification modeling approaches is given in [21].

No DFB plant model can yet be found in literature that describes the influence of plant inputs, that actually can be manipulated, on the process variables, which should be controlled (e.g. gasification temperature, combustion temperature, bed material circulation, product gas

quantities) and considers all relevant couplings between those process variables.

The aim of this work is to develop a dynamic model of the coupled DFB process that can then be used to develop efficient multi-variable model-based control concepts and

- is based on mass and energy balances using physical parameters for fuel and gas streams into and out of the reactor,
- incorporates data-driven components to describe the heat loss and the heat transported by the bed material between the reactors, and
- uses an artificial neural network to describe the circulation of bed material between the GR and the CR.

The process model needs to be able to predict the temperatures in the GR and the CR, and the total mass flow of product gas and flue gas. Thus, this model can be used to implement model-based control schemes such as MPC. This allows the accurate tracking of desirable operating points in order to achieve a high-quality product gas and increase plant availability e.g. by reducing problems caused by an abnormal product gas composition.

The remainder of this paper is structured as follows: A brief introduction to the DFB gasification process is given in Section 2. In Section 3 the modeling methods are presented. The dynamic parameters in the model are estimated using time-series measurement data. The estimation procedure is described in Section 4. Finally, results are presented in Section 5.

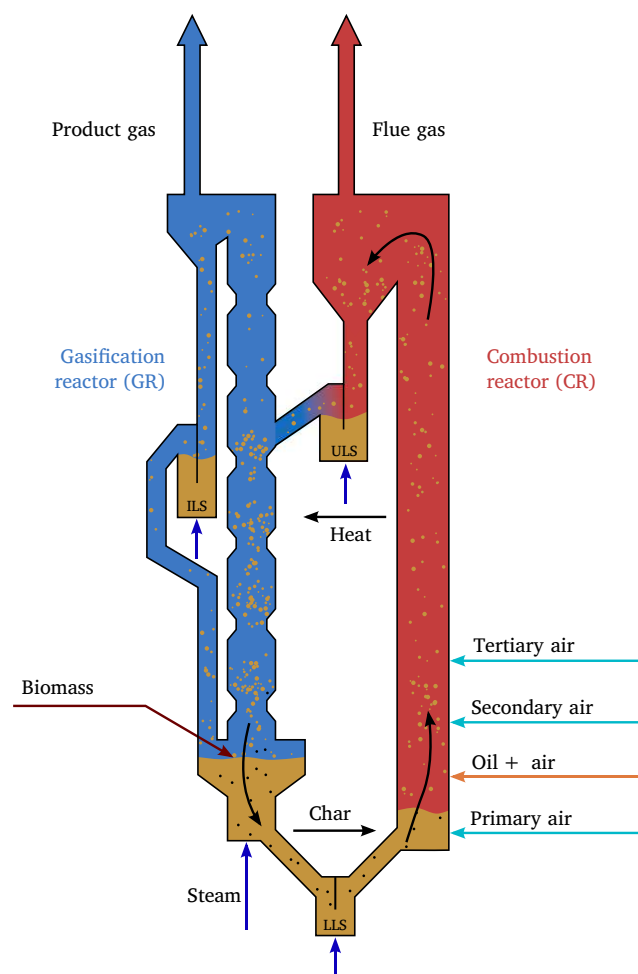


Fig. 1. Advanced 100 kW dual fluidized bed (DFB) steam gasification pilot plant, with the gasification reactor (GR) at the left side and the combustion reactor (CR) at the right side.

2. Dual fluidized bed gasification

In DFB gasification, product gas generation is divided into gasification, which takes place in the gasification reactor (GR), and combustion, which takes place in the combustion reactor (CR). Due to the separation of these processes, the air needed for combustion cannot enter the GR and an almost nitrogen-free product gas can be generated.

2.1. Advanced 100 kW DFB steam gasification pilot plant at TU Wien

Fig. 1 shows the principle of the DFB plant with the GR at the left and the CR at the right. The lower GR is operated as a bubbling fluidized bed reactor, whereas the upper GR is equipped with constrictions and is operated as turbulent fluidized bed. The CR is operated as a fast-fluidized bed reactor. Steam is used as a gasification agent in the GR and air is used in the CR. Also, the internal loop seal (ILS), the upper loop seal (ULS) and the lower loop seal (LLS) are fluidized with steam. The ILS is necessary for the internal circulation of the GR. The ULS and the LLS are connecting the GR and the CR. The biomass is fed onto the bubbling bed of the GR. For a fixed feedstock, the temperature in the gasification reactor is the most important influence on the product gas



Fig. 2. Upper part of the advanced 100 kW pilot plant at TU Wien [24].



Fig. 3. Lower part of the advanced 100 kW pilot plant at TU Wien [24].

composition. The product gas rises in the reactor and passes through a counter-current column which is outfitted with constrictions to enhance the contact between the product gas and the bed material. Thereby, the product gas quality is enhanced in terms of main gas composition and reduced tar contents [22]. However, this design constrains the biomass input flow as well as the circulation rate because flooding of the column can be induced if these flows are too high.

The overall endothermic gasification in the GR requires heat. This heat is provided by the hot bed material coming from the CR via the ULS. A fraction of the char is not gasified in the GR, but transported to the CR with the bed material via the LLS. In the CR, the char is combusted and therefore heats up the bed material. Oil serves as an auxiliary fuel to equalize the high specific heat loss of the pilot plant. Air staging in the CR (primary, secondary and tertiary air) is used to control the bed material circulation between the two reactors. An indicator for the bed material circulation is the measured pressure gradient in the upper part of the CR, as described in [19].

Detailed descriptions of the TU Wien pilot plant are given in [23–25] (see **Figs. 2** and **3**).

Table 1
Measurement equipment at the TU Wien pilot plant.

Process variable	Device
Temperature	Type K thermocouple
Pressure	Kalinsky pressure sensor
Steam and air flows	variable area flowmeter
Product gas and flue gas flows	Barthel orifice meter
Main gas compositions	Rosemount NGA 2000
Fuel feed	Rot. speed of dosing screws ^a

^aThe dosing screws are calibrated before every test run.

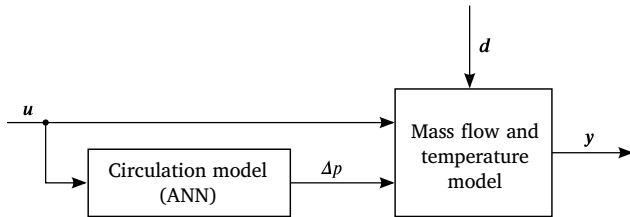


Fig. 4. Structure of the DFB process model, consisting of a gray box model for the mass flows and reactor temperatures and an artificial neural network (ANN) to model the bed material circulation.

2.1.1. Measurement equipment

The TU Wien pilot plant is equipped with a variety of measurement devices to monitor the process. Table 1 shows the sensors used to generate measurement data that is used in this work. A detailed description of the experimental setup including the measurement equipment is given in [15,26].

3. Modeling

The aim of this work is to identify a DFB plant model that can be used for model-based control. The modeling addresses steam-gasification of **softwood pellets** using an **olivine-limestone** mixture as bed material.

The output variables that are modeled are

- the product gas mass flow \dot{m}_{PG} ,
- the flue gas mass flow \dot{m}_{FG} ,
- the gasification temperature T_{GR} and
- the combustion temperature T_{CR} .

Fig. 4 show the structure of the overall DFB plant model. It consists of a physical model (mass and energy balances) and a circulation model (artificial neural network, ANN). The physical model uses the output of the circulation model Δp as an input variable. The inputs to the overall DFB plant model are manipulated variables u as well as measured disturbances d . Both are inputs to the model, however, only the manipulated variables can be used to control the process, whereas disturbances cannot be manipulated or are held on a constant level during operations. The following assumptions are made:

- Both the product gas and the flue gas consist of ideal gases.
- The temperature of the product gas and the bed material leaving the GR corresponds to the temperature in the bubbling bed of the GR.
- The temperature of the flue gas and the bed material leaving the CR correspond to the temperature in the upper part of the CR.
- Both the bed material and the ash remain in the DFB system.
- Char particles that leave the GR entrained into the product gas flow is not taken into account.

3.1. Mass balance

A mass balance is derived both for the GR and the CR. First, the mass balances are formulated for a steady state. Afterwards, the equations are extended to differential equations, in order to describe the plant's dynamic behavior.

3.1.1. Gasification reactor

At steady state, the mass of product gas \dot{m}_{PG} leaving the GR must be equal to the amount of biomass \dot{m}_{bm} and steam $\dot{m}_{steam,GR}$ fed into the reactor reduced by the ungasified char \dot{m}_{char} flowing to the CR and the ash remaining in the DFB system:

$$\dot{m}_{PG} = k_{PG}(\dot{m}_{bm}(1 - w_{ash}) + \dot{m}_{steam,GR} - \dot{m}_{char}), \quad (1)$$

where w_{ash} is the mass fraction of ash in the dry biomass. It is assumed that the ash remains in the reactor system. The mass of steam $\dot{m}_{steam,GR}$ streaming to the GR consists of the steam used for fluidizing the GR, the ILS and a partial flow from the ULS and LLS. We assume that 50% of the steam that is used for fluidizing the ULS and the LLS streams to the GR, the other 50% streams to the CR.

At steady state, the mass of bed material entering the GR is equal to the mass of bed material leaving the GR. Therefore, the bed material is not considered in the mass balance. The parameter k_{PG} allows the correction of the product gas mass flow, which is necessary due to measurement uncertainty. This measurement uncertainty depends on the gasification temperature T_{GR} and is estimated using measurement data.

The amount of char that is transported to the CR via the bed material is modeled as

$$\dot{m}_{char} = c_{bm,CR}\dot{m}_{bm}(1 - w_{H_2O} - w_{ash}), \quad (2)$$

where $c_{bm,CR}$ refers to the weight fraction of dry and ash-free biomass that is transported to the CR.

According to (1), an increase in one input (e.g. the biomass feed) would instantly increase the product gas mass flow rate, which is physically impossible for a real process. Therefore, a time constant τ_{PG} is introduced, yielding a first-order differential equation for \dot{m}_{PG} :

$$\frac{d\dot{m}_{PG}}{dt} = \frac{1}{\tau_{PG}} \left(-\dot{m}_{PG} + k_{PG} \left(\dot{m}_{bm}(1 - w_{ash}) + \dot{m}_{steam,GR} - \dot{m}_{char} \right) \right). \quad (3)$$

3.1.2. Combustion reactor

The mass of flue gas leaving the CR in a steady state is described by

$$\dot{m}_{FG} = \dot{m}_{char} + \dot{m}_{steam,CR} + \dot{m}_{air} + \dot{m}_{oil}, \quad (4)$$

with the mass flows of air \dot{m}_{air} and oil \dot{m}_{oil} fed into the reactor. Full combustion of the oil and the char is assumed. $\dot{m}_{steam,CR}$ consists of the partial flow of steam from the ULS and the LLS to the CR.

Again, a time constant τ_{FG} is introduced to describe the dynamic behavior and obtain a differential equation for the flue gas mass flow:

$$\frac{d\dot{m}_{FG}}{dt} = \frac{1}{\tau_{FG}} (-\dot{m}_{FG} + \dot{m}_{char} + \dot{m}_{steam,CR} + \dot{m}_{air} + \dot{m}_{oil}) \quad (5)$$

3.2. Energy balance

To model the temperature T_{GR} in the GR and the temperature T_{CR} in the CR, an energy balance is formulated for both the GR and the CR. For the GR, this leads to

$$C_{GR} \frac{dT_{GR}}{dt} = \dot{H}_{bm} + \dot{H}_{steam,GR} - \dot{H}_{char} - \dot{H}_{PG} - \dot{Q}_{loss,GR} + \dot{Q}_{bed}, \quad (6)$$

with the GR's heat capacity C_{GR} and the temperature's time derivative at the left side of the equation and the enthalpy flow rates \dot{H}_i as well as the heat flow rates \dot{Q}_i at the right side. The enthalpy flow rates of

steam $\dot{H}_{steam,GR}$ and product gas \dot{H}_{PG} are calculated using the NASA polynomials and the coefficients from [27]. To calculate \dot{H}_{PG} a model for its composition is needed. This model is presented in Section 3.2.1. The calculation of the enthalpy of biomass \dot{H}_{bm} and char \dot{H}_{char} is based on their lower heating values. Models for the heat loss $\dot{Q}_{loss,GR}$ and the heat that is transported via the bed material circulation \dot{Q}_{bed} from the GR to the CR are presented in Sections 3.2.2 and 3.2.3, respectively.

For the combustion reactor, a first-order differential equation was not able to describe the reactor's dynamic behavior sufficiently well. Therefore, besides the temperature in the reactor T_{CR} , a second state is introduced, representing the reactor wall temperature $T_{CR,wall}$. This leads to two coupled first-order differential equations, one describing the temperature inside the reactor

$$C_{CR} \frac{dT_{CR}}{dt} = \dot{H}_{char} + \dot{H}_{oil} + \dot{H}_{air} + \dot{H}_{steam,CR} - \dot{H}_{FG} - \dot{Q}_{bed} - \dot{Q}_{wall}, \quad (7)$$

and a second equation describing the reactor wall temperature

$$C_{CR,wall} \frac{dT_{CR,wall}}{dt} = \dot{Q}_{wall} - \dot{Q}_{loss,CR}, \quad (8)$$

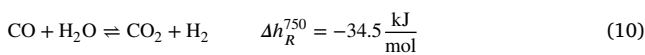
with the heat capacities C_{CR} and $C_{CR,wall}$. The enthalpy flow rates of the air \dot{H}_{air} , the steam $\dot{H}_{steam,CR}$, and the flue gas \dot{H}_{FG} are again calculated using the NASA polynomials. For calculation of the flue gas composition, full combustion of the char and the oil is assumed. The enthalpies of char \dot{H}_{char} and oil \dot{H}_{oil} are calculated based on their lower heating values. The two differential equations for the gas in the reactor and the reactor wall are coupled by the heat flow between the wall and the gas

$$\dot{Q}_{wall} = \alpha_{CR}(T_{CR} - T_{CR,wall}), \quad (9)$$

with a parameter α_{CR} that is estimated using measurement data.

3.2.1. Product gas enthalpy

To calculate the enthalpy flow of the product gas \dot{H}_{PG} , a model for its composition is needed. In this work, we use a model based on the thermodynamic equilibrium. The species remaining in the GR are calculated by the biomass feed with its known composition and the steam feed, reduced by the amount of ungasified char according to (2). For the equilibrium calculation, only the water–gas shift reaction



is considered. The equilibrium is calculated by solving the non-linear system of equations

$$\dot{n}_{\text{CO}} + \dot{n}_{\text{CO}_2} - \dot{n}_{\text{in,C}} = 0, \quad (11a)$$

$$2\dot{n}_{\text{H}_2} + 2\dot{n}_{\text{H}_2\text{O}} - \dot{n}_{\text{in,H}} = 0, \quad (11b)$$

$$\dot{n}_{\text{CO}} + 2\dot{n}_{\text{CO}_2} + \dot{n}_{\text{H}_2\text{O}} - \dot{n}_{\text{in,O}} = 0 \text{ and} \quad (11c)$$

$$K_{eq}(T_{GR})\dot{n}_{\text{CO}}\dot{n}_{\text{H}_2\text{O}} - \dot{n}_{\text{CO}_2}\dot{n}_{\text{H}_2} = 0, \quad (11d)$$

consisting of three balances for carbon, hydrogen and oxygen, and the equilibrium condition [28]. The pressure in the GR is always close to atmospheric pressure, therefore the pressure is assumed to be the standard pressure. The molar flow rates $\dot{n}_{\text{in,C}}$, $\dot{n}_{\text{in,H}}$ and $\dot{n}_{\text{in,O}}$ describe the molar flow rates of carbon, hydrogen and oxygen considered in the water–gas shift reaction. The molar flow rates \dot{n}_{H_2} , \dot{n}_{CO} , \dot{n}_{CO_2} , and $\dot{n}_{\text{H}_2\text{O}}$ describe the molar flows in the equilibrium leaving the GR. The equilibrium constant

$$K_{eq}(T_{GR}) = \exp \frac{\Delta^R G(T_{GR})}{RT_{GR}} \quad (12)$$

is calculated using the Gibbs free energy change for the reaction $\Delta^R G(T_{GR})$, which is derived using the enthalpies and entropies of the species from the NASA polynomials. Methane (CH_4) and ethylene (C_2H_4) are not taken into account in the equilibrium calculation, since

these components are usually underestimated by equilibrium models as reported in [10,29]. Here, a model for CH_4 and C_2H_4 based on measured quantities is used. Other components like C_2H_6 or N_2 can also be measured in the product gas. However, their concentrations are typically low and they are therefore not considered in this model.

3.2.2. Heat loss

To model the heat loss of the GR $\dot{Q}_{loss,GR}$ and the CR $\dot{Q}_{loss,CR}$, the energy balance is formulated for the whole DFB system and evaluated for steady-state points. For steady-state points, the energy balance needs to be closed, which leads to

$$0 = \dot{H}_{bm} + \dot{H}_{oil} + \dot{H}_{steam,GR} + \dot{H}_{steam,CR} + \dot{H}_{air} - \dot{H}_{PG} - \dot{H}_{FG} - \dot{Q}_{loss,DFB}. \quad (13)$$

This energy balance allows the computation of the DFB system's heat loss $\dot{Q}_{loss,DFB}$. It is assumed that this heat loss depends on the difference between the reactor temperatures T_{GR} and T_{CR} , and the ambient temperature T_{amb} . The heat loss is calculated for multiple steady-state points and a linear model for the heat loss

$$\dot{Q}_{loss,DFB} = \beta_0 + \alpha_1(T_{GR} - T_{amb}) + \alpha_2(T_{CR} - T_{amb}), \quad (14)$$

with the parameters β_0 , α_1 and α_2 is fitted. The overall heat loss is then divided into a part for the GR

$$\dot{Q}_{loss,GR} = \frac{\beta_0}{2} + \alpha_1(T_{GR} - T_{amb}), \quad (15)$$

and a part for the CR

$$\dot{Q}_{loss,CR} = \frac{\beta_0}{2} + \alpha_2(T_{CR} - T_{amb}), \quad (16)$$

where the constant term is equally split to the GR and the CR.

3.2.3. Bed material heat transport

Bed material is constantly circulating between the GR and the CR. Since the temperature is typically higher in the CR, the bed material streaming from the CR to the GR is hotter than the bed material streaming back to the CR. Therefore, there is a net heat flow from the CR to the GR via the bed material, indicated as \dot{Q}_{bed} . To find a model for this heat transport, steady-state points are investigated. The energy balances are formulated for the GR and the CR separately. For the GR, this leads to

$$0 = \dot{H}_{bm} + \dot{H}_{steam,GR} - \dot{H}_{char} - \dot{H}_{PG} - \dot{Q}_{loss,GR} + \dot{Q}_{bed,GR}, \quad (17)$$

whereas for the CR we get

$$0 = \dot{H}_{char} + \dot{H}_{oil} + \dot{H}_{air} + \dot{H}_{steam,CR} - \dot{H}_{FG} - \dot{Q}_{loss,CR} - \dot{Q}_{bed,CR}. \quad (18)$$

This allows the calculation of the heat transported between the reactors from the GR's perspective $\dot{Q}_{bed,GR}$ and from the CR's perspective $\dot{Q}_{bed,CR}$. In order to close the overall energy balance, these two heat flows must be the same. However, due to model uncertainties and measurement inaccuracies, these values differ. Next, a model for the heat transport is defined with the structure

$$\dot{Q}_{bed} = (p_0 + p_1 \Delta p)(T_{CR} - T_{GR}), \quad (19)$$

and the parameters p_0 and p_1 . Using this approach, the model for the heat transported by the bed material \dot{Q}_{bed} depends on the temperature difference between the two reactors and the pressure gradient in the upper part of the CR Δp . We assume this structure, since it has been reported in [19] that the pressure gradient Δp is a strong indicator for the mass of bed material circulating between the two reactors. This heat transport model, and thus the model for the reactor temperatures, is now a function of the pressure gradient Δp in the upper part of the CR. This pressure gradient can be measured, however, it cannot

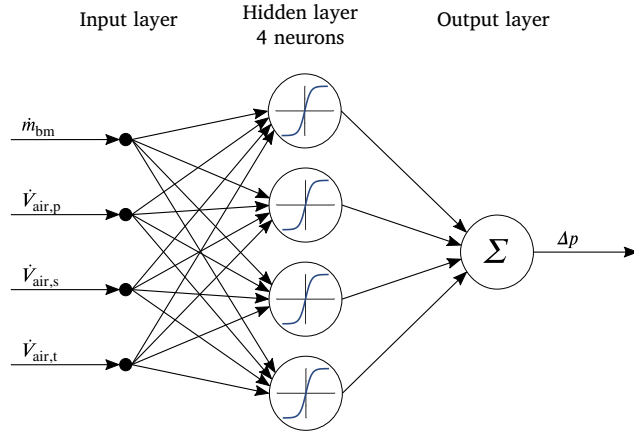


Fig. 5. Structure of the circulation model (static artificial neural network).

be manipulated directly. Since the aim of this work is to identify a DFB plant model that allows the calculation of the temperatures using only manipulable input variables, a Δp -model is needed. This model is presented in Section 3.3.

3.3. Circulation model

A circulation model is presented to describe the pressure gradient Δp in the upper part of the CR as a function of the manipulated variables and can therefore be used for control purposes.

3.3.1. Model structure

Since no simple first-principle model is available and linear data-based approaches have failed to achieve the necessary fidelity of Δp , an ANN is used. The ANN uses the biomass feed and the volumetric flow rates of the three air flows into the CR as inputs and is designed as a static feedforward neural network (Fig. 5). The hidden layer consists of 4 neurons with hyperbolic tangent sigmoid activation functions.

3.3.2. Model training

Time-series data of Δp and the four inputs are used to train the network. The weights and biases are estimated using a Levenberg–Marquardt algorithm that minimizes a cost function including the squared output error and a regularization term to avoid overfitting. The MATLAB® Deep Learning Toolbox is used for the identification of the ANN [30].

4. Parameter identification

The DFB model with the output vector

$$y = [\dot{m}_{PG}, \dot{m}_{FG}, T_{GR}, T_{CR}]^T \quad (20)$$

and 5 ordinary differential equations incorporates unknown parameters that need to be identified by time series data. Note that the parameters in the heat loss model and in the bed material heat transport are identified by investigating steady-state operating points and are thus not considered in this section. Moreover, the parameters in the circulation model (ANN) are estimated separately, as described in Section 3.3.2. The parameters identified using time-series data are collected into the parameter vector

$$\theta = [\tau_{PG}, \tau_{FG}, C_{GR}, C_{CR}, C_{CR,wall}, \alpha_{CR}]^T. \quad (21)$$

The parameter vector θ is estimated by minimizing the output error of the model. This is done by minimization of the cost function

$$V(\hat{\theta}) = \frac{1}{N} \sum_{k=1}^N (y(k) - \hat{y}(k))^T (y(k) - \hat{y}(k)), \quad (22)$$

Table 2

Properties of the fuel used in the test run and the char.

		Softwood	Char
Water content	wt.-%	7.2	0
Ash content	wt.-% _{db}	0.2	0
Carbon (C)	wt.-% _{db}	50.7	89.0
Hydrogen (H)	wt.-% _{db}	5.9	3.0
Oxygen (O)	wt.-% _{db}	43.0	8.0
Nitrogen (N)	wt.-% _{db}	0.2	0
Sulfur (S)	wt.-% _{db}	0.005	0
Chlorine (Cl)	wt.-% _{db}	0.005	0

taking into account the squared output error for N data points. $y(k)$ refers to the measured output vector at sample k , whereas $\hat{y}(k)$ describes the simulated model output that is calculated by numerically solving the ODEs forward in time.

5. Results

The measurement data presented in this section has been generated at the advanced 100 kW pilot plant at TU Wien as described in Section 2.1.

5.1. Identification experiment

The experimental identification of the parameters was carried out with the DFB pilot plant. During these test runs, the process was excited by varying the manipulated variables

$$u = [\dot{m}_{bm}, \dot{m}_{oil}, \dot{m}_{steam,GR}, \dot{V}_{air,p}, \dot{V}_{air,s}, \dot{V}_{air,t}]^T. \quad (23)$$

In the experiment, softwood pellets were fed to the GR. The properties of the softwood pellets as well of the char transported from the GR to the CR are listed in Table 2 [25]. An olivine-limestone mixture has been used as bed material, consisting of 80 % olivine and 20 % limestone with 70 kg of initial bed material inventory.

5.2. Temperature model

In order to model the heat loss and the heat transported via the bed material, steady-state operating points from the identification experiment are evaluated. Moreover, steady-state points from previous test runs are used to enlarge the operating space covered by the model.

5.2.1. Heat loss

Fig. 6 shows the heat loss of the DFB system calculated for different data points. As expected, the heat loss increases with higher reactor temperatures. With a coefficient of determination $R^2 = 0.83$, the simple model structure in (14) is shown to be a good modeling approach.

5.2.2. Bed material heat transport

To find a model for the heat transported with the bed material \dot{Q}_{bed} from the CR to the GR, steady-state operating points are investigated again. For this purpose, energy balances are evaluated for the two reactors individually. This allows computing the amount of heat transported between those two reactors from two perspectives: The heat transported via the bed material necessary to close the GR's energy balance is calculated using the energy balance for the GR. This heat is defined as $\dot{Q}_{bed,GR}$. Likewise, $\dot{Q}_{bed,CR}$ is calculated for the CR. This leads to two different values for each steady-state point that are shown in Fig. 7 (in blue for the GR and in red for the CR). These two data points of the same steady-state point are connected by a gray line. If these two points lie on top of each other, the energy balance for the overall DFB system is perfectly closed by the heat loss model, which means the data point in Fig. 6 lies on the surface that shows the heat loss model. In Fig. 7, $\dot{Q}_{bed,GR}$ and $\dot{Q}_{bed,CR}$ are referred to the temperature difference $\Delta T = T_{CR} - T_{GR}$. With the model defined in (19), a coefficient of determination $R^2 = 0.95$ can be achieved.

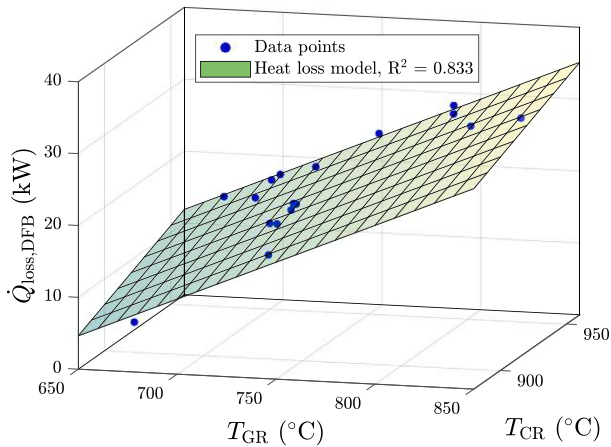


Fig. 6. The heat loss of the DFB system was calculated for several steady-state points (blue points). A linear model (shown by the surface) fits the data points to describe the heat loss as a function of the reactor temperatures T_{GR} and T_{CR} .

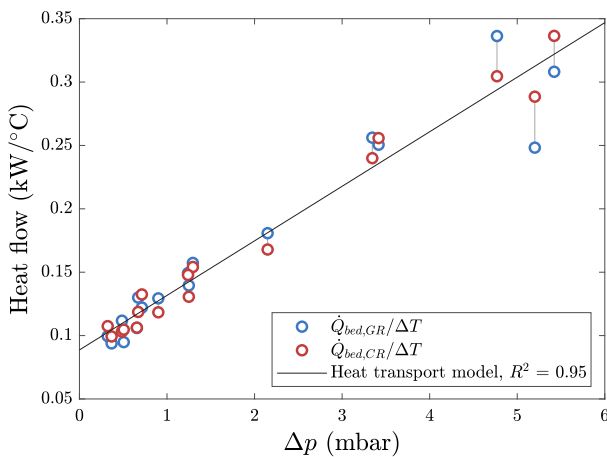


Fig. 7. The amount of heat transported by the bed material from the combustion reactor (CR) to the gasification reactor (GR) as a function of the pressure gradient Δp in the upper part of the CR.

5.3. Circulation model

For the training of the circulation model (ANN), data from three different test runs is used. Fig. 8 shows the model output of the pressure gradient Δp in the upper part of the CR and a comparison to the measured data. The measured data can be tracked by the model accurately, even for the cross-validation data (highlighted by a blue background).

5.4. Overall DFB plant model

The overall DFB plant model consists of the physical model (mass and energy balances) and the circulation model (ANN), as shown in Fig. 4. The output of the circulation model acts as an input to the physical model. In Figs. 9 and 10, simulations of the overall DFB plant model are shown for two different test runs. The model is initialized at $t = 0$ using measured temperatures. Afterwards, the measured inputs are fed to the model and the ODEs are solved forward in time. The model outputs are then compared to the measurement values.

For the first test run (Fig. 9) the coefficient of determination is rather small for the flue gas mass flow and the temperature in the

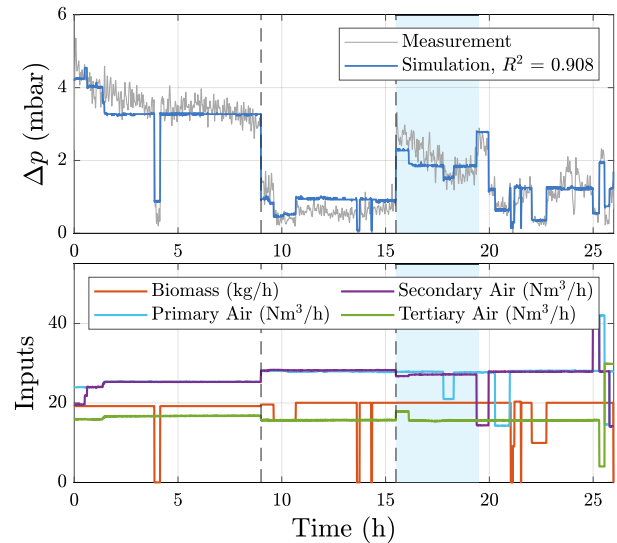


Fig. 8. Comparison of the model output and the measured data for the pressure gradient Δp in the upper part of the CR. The blue background indicates the cross-validation data (data that has not been used for model training).

Table 3

Numerical simulation results: Model output compared to measurement data.

	Test run day 1		Test run day 2	
	R^2	RMSE	R^2	RMSE
\dot{m}_{PG}	0.548	1.89 kg/h	0.66	2.09 kg/h
\dot{m}_{FG}	-0.231	1.62 kg/h	0.818	2.73 kg/h
T_{GR}	0.313	13.31 °C	0.632	8.02 °C
T_{CR}	0.656	12.28 °C	0.64	9.51 °C

Table 4

Steady state inputs (chosen) and states (derived).

Inputs	States		
\dot{m}_{bm}	20 kg/h	\dot{m}_{PG}	26.4 kg/h
\dot{m}_{oil}	4 kg/h	\dot{m}_{FG}	101.0 kg/h
$\dot{m}_{steam,GR}$	8 kg/h	T_{GR}	756.1 °C
$\dot{V}_{air,p}$	27 Nm ³ /h	T_{CR}	924.5 °C
$\dot{V}_{air,s}$	27 Nm ³ /h	$T_{CR,wall}$	907.7 °C
$\dot{V}_{air,t}$	14 Nm ³ /h		

gasification reactor. However, this can be explained by the lack of excitation of these outputs. For the second test run (Fig. 10), these outputs are excited stronger by the input variations and it can be seen that the model is capable of predicting those outputs.

Table 3 summarizes the numerical results of both simulations. The root-mean-square error (RMSE) lies for product gas and flue gas mass flow around 2 kg/h and for the reactor temperatures between 8 and 13 °C. However, it must be noted that besides the plant-model mismatch also the noise in the measurement data contributes to the RMSE.

5.5. Simulation of input variations

The identified model is now used to simulate the process' response to input variations. The inputs are varied individually, starting from a steady state. The steady-state is derived from the model for a chosen input vector, which is chosen in a way that corresponds to typical operating conditions. Table 4 shows the steady state inputs and states. In this simulation, only the manipulated variables (inputs that are later used to control the process) are varied, whereas disturbance variables are held constant.

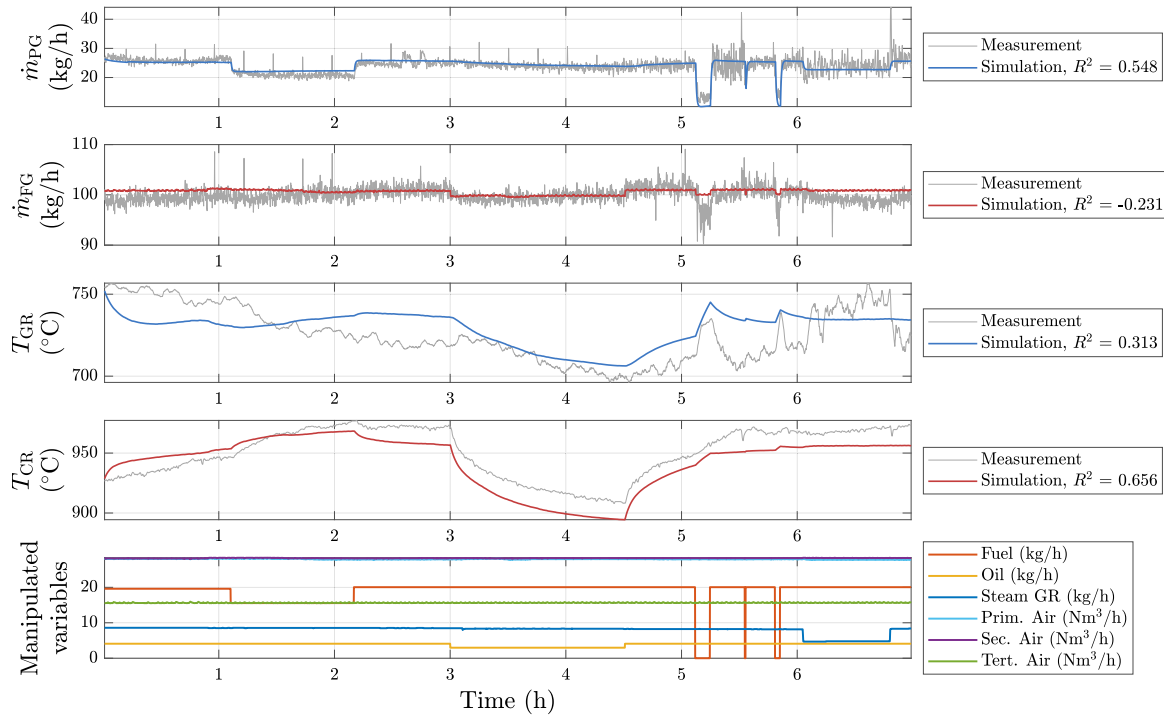


Fig. 9. DFB plant model validation, test run day 1. The gray lines show the measured mass flows and reactor temperatures whereas the colored lines show the simulated model outputs.

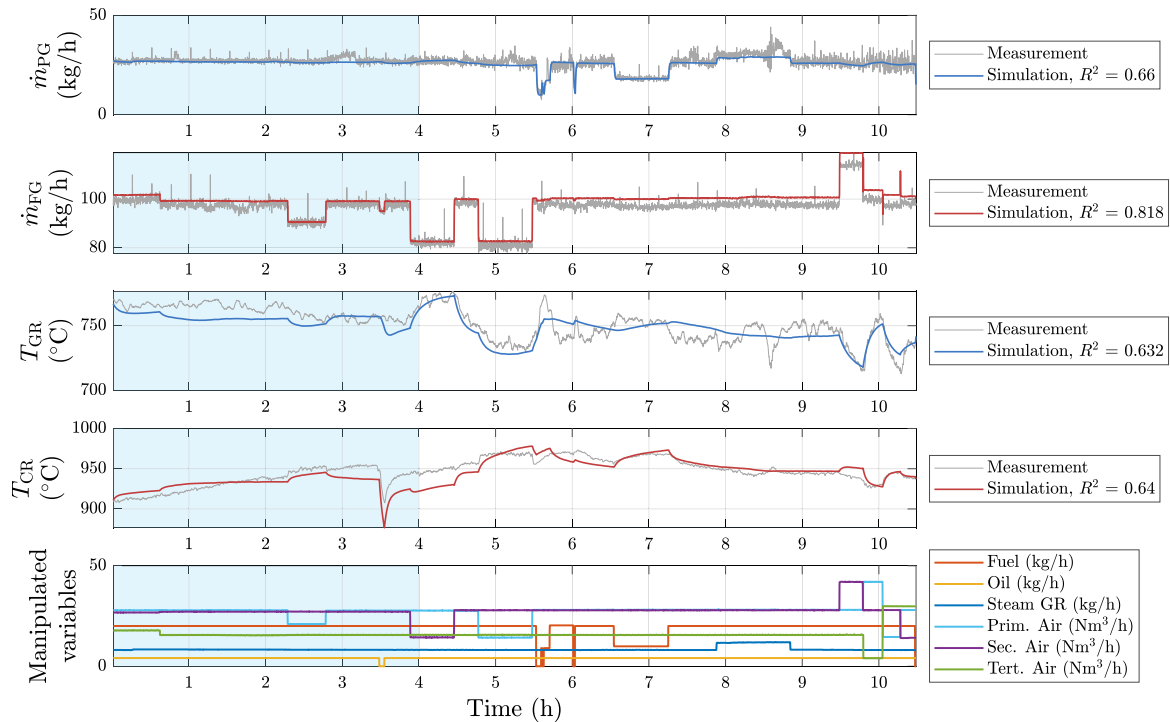


Fig. 10. DFB plant model validation, test run day 2. The blue background indicates the cross-validation data.

Since especially the reactor temperatures T_{GR} and T_{CR} are of interest due to their coupled behavior, their responses to steps in the individual inputs are shown in Fig. 11. At $t = 0$, the input steps are applied. The heights of the steps are given in Fig. 11 as well. A decrease in biomass feed leads to an increase in the reactor temperatures due

to the endothermic gasification reactions. The temperature rise in the CR is even higher than in the GR. This is because a decrease in biomass input also leads to a reduction in bed material circulation. Therefore, less heat is transported via the bed material from the CR to the GR. A decrease in the oil feed leads to a drop in the reactor

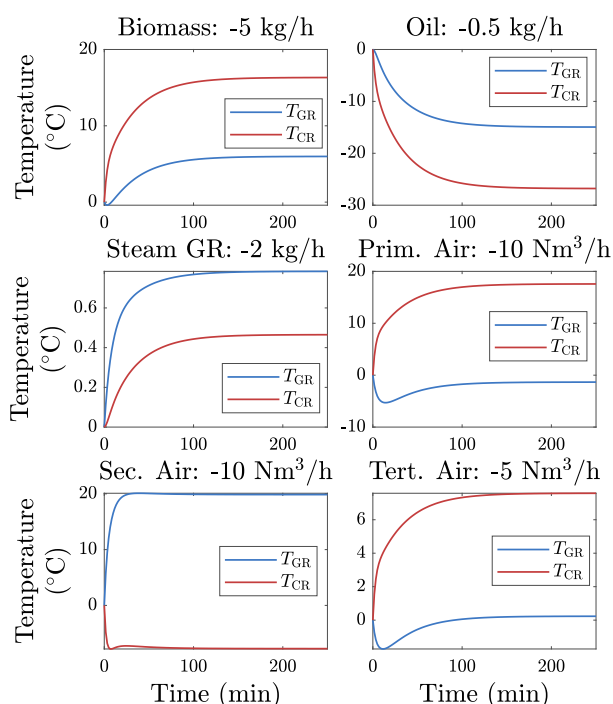


Fig. 11. Simulated responses of the reactor temperatures to input variations. The simulation is started from the steady-state operating point defined in Table 4.

temperatures, whereas a reduction in steam leads to an increase in reactor temperatures. An interesting behavior can be observed in the air streams: On the one hand, the air is cooling the reactor. On the other hand, the air streams play a significant role in the bed material circulation between the two reactors. For the primary and tertiary air, a reduction leads to a lower circulation rate, leading to less heat transport from the CR to the GR. Therefore, the temperatures in the GR are decreasing. For the secondary air, a decrease in the air stream leads to an increase in the circulation rate (this can be seen in Fig. 8 at hour 20). Thus, more hot bed material is transported to the GR, and its temperature rises. The reason for the reverse influence of the secondary air on the bed material circulation is not clarified so far. Further investigations are necessary to explain this behavior.

6. Conclusion and outlook

The following contributions have been made in this work:

- We presented a method to develop a fully coupled model for a DFB gasifier that can be used for model-based control.
- The model structure is given by mass and energy balances.
- Physical parameters are used in the model wherever possible, such as describing the fuel composition.
- Parameters describing the heat loss and the heat transported by the bed material have been estimated by steady-state measurement points from various test runs.
- Parameters describing the dynamic plant behavior such as time constants and the reactor heat capacities have been estimated using time series data from test runs, where the process has been excited by steps in the input signals.
- An artificial neural network has been used to model the bed material circulation as a function of process inputs, since first-principle modeling is hardly possible with reasonable effort.

- Simulations show that the model is capable of predicting the product gas mass flow, the flue gas mass flow as well as the reactor temperatures and allows predictions needed for example for model predictive control.

Since the model is based on physical equations, the modeling procedure can be applied to other fuels or plants, what allows a straightforward development of dynamic process models of industrial-sized DFB plants. For that purpose, re-estimation of the unknown parameters has to be done by utilizing data generated by identification experiments.

The aim of future research can be to extend the model to further outputs, e.g. the product gas composition, in order to control these variables as well. This can be beneficial for following synthesis processes such as methanation in a SNG production chain. In the future, the holistic and dynamic approach in cooperation with other digital tools is expected to directly influence parameters such as cold gas efficiency, carbon utilization efficiency or production costs during operation.

CRedit authorship contribution statement

Lukas Stanger: Conceptualization, Methodology, Validation, Software, Visualization, Writing – original draft. **Alexander Schirrer:** Conceptualization, Methodology, Writing – review & editing. **Florian Benedikt:** Investigation, Resources, Writing – review & editing. **Alexander Bartik:** Investigation, Resources, Writing – review & editing. **Stefan Jankovic:** Investigation, Writing – review & editing. **Stefan Müller:** Funding acquisition, Resources, Writing – review & editing. **Martin Kozek:** Conceptualization, Funding acquisition, Supervision, Writing – review & editing.

Declaration of competing interest

The authors declare that they have no known competing financial interests or personal relationships that could have appeared to influence the work reported in this paper.

Data availability

The data that has been used is confidential.

Acknowledgments

This work was supported by the project ADORe-SNG, which is funded by the Austrian Climate and Energy Fund (FFG, No. 881135).

The authors acknowledge TU Wien Bibliothek for financial support through its Open Access Funding Programme.

References

- [1] Codina Gironès V, Moret S, Peduzzi E, Nasato M, Maréchal F. Optimal use of biomass in large-scale energy systems: Insights for energy policy. *Energy* 2017;137:789–97. <http://dx.doi.org/10.1016/J.ENERGY.2017.05.027>.
- [2] Hofbauer H, Rauch R, Bosch K, Koch R, Aichernig C. Biomass CHP plant Güssing—a success story. In: *Proceedings of the expert meeting on pyrolysis and gasification of biomass and waste*, Strasbourg, France. Vol. 30. 2002.
- [3] Thunman H, Seemann M, Berdugo Vilches T, Maric J, Pallares D, Ström H, et al. Advanced biofuel production via gasification – lessons learned from 200 man-years of research activity with Chalmers' research gasifier and the GoBiGas demonstration plant. *Energy Sci Eng* 2018;6(1):6–34. <http://dx.doi.org/10.1002/ese3.188>.
- [4] Bartik A, Benedikt F, Lunzer A, Walcher C, Müller S, Hofbauer H. Thermodynamic investigation of SNG production based on dual fluidized bed gasification of biogenic residues. *Biomass Convers Biorefinery* 2021;11(1):95–110. <http://dx.doi.org/10.1007/s13399-020-00910-y>.
- [5] Nigitz T, Gölles M, Aichernig C, Schneider S, Hofbauer H, Horn M. Increased efficiency of dual fluidized bed plants via a novel control strategy. *Biomass Bioenergy* 2020;141:105688. <http://dx.doi.org/10.1016/J.BIOMBIOE.2020.105688>.

- [6] Pröll T, Hofbauer H. Process and device for providing a constant product gas rate from a fluidized bed gas generation plant. 2010, WO2010006353A3. URL <https://patents.google.com/patent/WO2010006353A3/en>.
- [7] Morari M, Jay H. Model predictive control: past, present and future. *Comput Chem Eng* 1999;23(4-5):667-82. [http://dx.doi.org/10.1016/S0098-1354\(98\)00301-9](http://dx.doi.org/10.1016/S0098-1354(98)00301-9).
- [8] Sreejith CC, Arun P, Muraleedharan C. Thermochemical analysis of biomass gasification by Gibbs free energy minimization model - Part: I (optimization of pressure and temperature). *Int J Green Energy* 2013;10(3):231-56. <http://dx.doi.org/10.1080/15435075.2011.653846>.
- [9] Sreejith CC, Muraleedharan C, Arun P. Thermo-chemical analysis of biomass gasification by gibbs free energy minimization model-Part: II (optimization of biomass feed and steam to biomass ratio). *Int J Green Energy* 2013;10(6):610-39. <http://dx.doi.org/10.1080/15435075.2012.709203>.
- [10] Schuster G, Löffler G, Weigl K, Hofbauer H. Biomass steam gasification – an extensive parametric modeling study. *Bioresour Technol* 2001;77(1):71-9. [http://dx.doi.org/10.1016/S0960-8524\(00\)00115-2](http://dx.doi.org/10.1016/S0960-8524(00)00115-2).
- [11] Aghaalikhani A, Schmid JC, Borello D, Fuchs J, Benedikt F, Hofbauer H, et al. Detailed modelling of biomass steam gasification in a dual fluidized bed gasifier with temperature variation. *Renew Energy* 2019;143:703-18. <http://dx.doi.org/10.1016/J.RENENE.2019.05.022>.
- [12] Ngo SI, Nguyen TD, Lim YI, Song BH, Lee UD, Choi YT, et al. Performance evaluation for dual circulating fluidized-bed steam gasifier of biomass using quasi-equilibrium three-stage gasification model. *Appl Energy* 2011;88(12):5208-20. <http://dx.doi.org/10.1016/j.apenergy.2011.07.046>.
- [13] Koppatz S, Pfeifer C, Hofbauer H. Comparison of the performance behaviour of silica sand and olivine in a dual fluidised bed reactor system for steam gasification of biomass at pilot plant scale. *Chem Eng J* 2011;175(1):468-83. <http://dx.doi.org/10.1016/j.cej.2011.09.071>.
- [14] Mauerhofer AM, Benedikt F, Schmid JC, Fuchs J, Müller S, Hofbauer H. Influence of different bed material mixtures on dual fluidized bed steam gasification. *Energy* 2018;157:957-68. <http://dx.doi.org/10.1016/j.energy.2018.05.158>.
- [15] Benedikt F, Schmid JC, Fuchs J, Mauerhofer AM, Müller S, Hofbauer H. Fuel flexible gasification with an advanced 100 kW dual fluidized bed steam gasification pilot plant. *Energy* 2018;164:329-43. <http://dx.doi.org/10.1016/j.energy.2018.08.146>.
- [16] Pröll T, Hofbauer H. H₂ rich syngas by selective CO₂ removal from biomass gasification in a dual fluidized bed system - process modelling approach. *Fuel Process Technol* 2008;89(11):1207-17. <http://dx.doi.org/10.1016/j.fuproc.2008.05.020>.
- [17] Kaushal P, Pröll T, Hofbauer H. Application of a detailed mathematical model to the gasifier unit of the dual fluidized bed gasification plant. *Biomass Bioenergy* 2011;35(7):2491-8. <http://dx.doi.org/10.1016/J.BIOMBIOE.2011.01.025>.
- [18] Kaushal P, Pröll T, Hofbauer H. Model development and validation: Co-combustion of residual char, gases and volatile fuels in the fast fluidized combustion chamber of a dual fluidized bed biomass gasifier. *Fuel* 2007;86(17-18):2687-95. <http://dx.doi.org/10.1016/j.fuel.2007.03.032>.
- [19] Fuchs J, Schmid J, Benedikt F, Mauerhofer A, Müller S, Hofbauer H. A general method for the determination of the entrainment in fluidized beds. *Int J Multiphys* 2018;12(4):359-72. <http://dx.doi.org/10.21152/1750-9548.12.4.359>.
- [20] Kraft S, Kirnbauer F, Hofbauer H. CPFD simulations of an industrial-sized dual fluidized bed steam gasification system of biomass with 8 MW fuel input. *Appl Energy* 2017;190:408-20. <http://dx.doi.org/10.1016/J.APENERGY.2016.12.113>.
- [21] Hanchate N, Ramani S, Mathpati CS, Dalvi VH. Biomass gasification using dual fluidized bed gasification systems: A review. *J Clean Prod* 2021;280:123148. <http://dx.doi.org/10.1016/J.JCLEPRO.2020.123148>.
- [22] Mauerhofer AM, Schmid JC, Benedikt F, Fuchs J, Müller S, Hofbauer H. Dual fluidized bed steam gasification: Change of product gas quality along the reactor height. *Energy* 2019;173:1256-72. <http://dx.doi.org/10.1016/J.ENERGY.2019.02.025>.
- [23] Schmid JC. Development of a novel dual fluidized bed gasification system for increased fuel flexibility (Ph.D. thesis), 2014.
- [24] Schmid JC, Benedikt F, Fuchs J, Mauerhofer AM, Müller S, Hofbauer H. Syngas for biorefineries from thermochemical gasification of lignocellulosic fuels and residues—5 years' experience with an advanced dual fluidized bed gasifier design. *Biomass Convers Biorefinery* 2021;11(6):2405-42. <http://dx.doi.org/10.1007/s13399-019-00486-2>.
- [25] Benedikt F, Fuchs J, Schmid JC, Müller S, Hofbauer H. Advanced dual fluidized bed steam gasification of wood and lignite with calcite as bed material. *Korean J Chem Eng* 2017;34(9):2548-58. <http://dx.doi.org/10.1007/s11814-017-0141-y>.
- [26] Schmalzl M. Implementierung der MSR-Technik einer 100 kW dual fluid Versuchsanlage zur Vergasung Von Festbrennstoffen. 2014.
- [27] Burcat A, Gardiner WC. Ideal gas thermochemical data for combustion and air pollution use. In: Gardiner WC, editor. *Gas-phase combustion chemistry*. New York, NY: Springer; 2000, p. 489-538. <http://dx.doi.org/10.1007/978-1-4612-1310-9>, URL <http://garfield.chem.elte.hu/Burcat/burcat.html>.
- [28] Baehr HD. *Thermodynamik Grundlagen und technische Anwendungen* : Zwölfte, neu bearbeitete und erweiterte Auflage Unter Mitarbeit Von Stephan Kabelac. Springer-lehrbuch, Berlin, Heidelberg: Springer-Verlag Berlin Heidelberg; 2005, <http://dx.doi.org/10.1007/b138786>.
- [29] Fuchs J, Schmid JC, Müller S, Mauerhofer AM, Benedikt F, Hofbauer H. The impact of gasification temperature on the process characteristics of sorption enhanced reforming of biomass. *Biomass Convers Biorefinery* 2020;10(4):925-36. <http://dx.doi.org/10.1007/s13399-019-00439-9>.
- [30] The Mathworks Inc. MATLAB and deep learning toolbox release 2021b. 2021, URL <https://www.mathworks.com/products/deep-learning.html>.

Publication B

Model predictive control of a dual fluidized bed gasification plant

Lukas Stanger, Alexander Bartik, Martin Hammerschmid, Stefan Jankovic, Florian Benedikt, Stefan Müller, Alexander Schirrer, Stefan Jakubek, and Martin Kozek

Applied Energy 361 (2024) p. 122917

DOI: [10.1016/J.APENERGY.2024.122917](https://doi.org/10.1016/J.APENERGY.2024.122917)

Own Contribution: Conceptualization, Methodology, Validation, Software, Visualization, Writing - original draft



Contents lists available at ScienceDirect

Applied Energy

journal homepage: www.elsevier.com/locate/apenergy

Model predictive control of a dual fluidized bed gasification plant

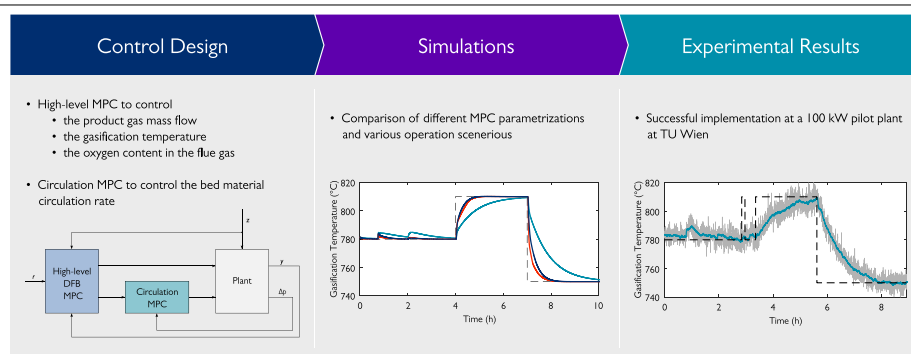
Lukas Stanger^{a,*}, Alexander Bartik^b, Martin Hammerschmid^b, Stefan Jankovic^c, Florian Benedikt^b, Stefan Müller^{b,c}, Alexander Schirrer^a, Stefan Jakubek^a, Martin Kozek^a

^a TU Wien, Institute of Mechanics and Mechatronics, Getreidemarkt 9, 1060 Vienna, Austria

^b TU Wien, Institute of Chemical, Environmental and Bioscience Engineering, Getreidemarkt 9, 1060 Vienna, Austria

^c Verto Engineering GmbH, Franz-Josefs Kai 53/13, 1010 Vienna, Austria

GRAPHICAL ABSTRACT



ARTICLE INFO

Keywords:

Model predictive control
Automatic control
DFB
Gasification
Biomass
Fluidized bed

ABSTRACT

Dual fluidized bed (DFB) gasification is a promising method for producing valuable gaseous energy carriers from biogenic feedstocks as a substitute for fossil fuels. State-of-the-art DFB gasification plants mainly rely on manual operation or single-input single-output control loops, and scientific contributions only exist for controlling individual process variables. This leaves a research gap in terms of comprehensive control strategies for DFB gasification. To address this gap, we propose a multivariate control strategy that focuses on crucial process variables, such as product gas quantity, gasification temperature, and bed material circulation rate. Our approach utilizes model predictive control (MPC), which enables effective process control while explicitly considering process constraints. A simulation study is given demonstrating how different MPC parametrizations influence the behavior of the closed-loop system. Experimental results from a 100 kW pilot plant at TU Wien demonstrate the successful control achieved by the proposed control algorithm.

1. Introduction

The need to reduce greenhouse gas emissions calls for substitutes for fossil fuels [1]. Thermo-chemical conversion of biogenic feedstock is promising to generate environmentally friendly energy carriers. Dual fluidized bed (DFB) steam gasification offers a method to produce a product gas containing mainly hydrogen, carbon monoxide, and

methane from different biogenic feedstocks [2]. The product gas is almost free of nitrogen and can undergo further processing, such as converting it into synthetic natural gas [3,4], Fischer-Tropsch products [5, 6], or pure hydrogen [7,8].

DFB gasification has been successfully implemented on an industrial scale at various locations, including Güssing (AT) [9], Senden

* Corresponding author.

E-mail address: lukas.stanger@tuwien.ac.at (L. Stanger).

<https://doi.org/10.1016/j.apenergy.2024.122917>

Received 15 September 2023; Received in revised form 1 February 2024; Accepted 23 February 2024

Available online 26 February 2024

0306-2619/© 2024 The Authors. Published by Elsevier Ltd. This is an open access article under the CC BY license (<http://creativecommons.org/licenses/by/4.0/>).

Nomenclature**Abbreviations**

bm	Biomass
CR	Combustion reactor
DFB	Dual fluidized bed
FG	Flue gas
GR	Gasification reactor
ILS	Internal loop seal
LLS	Lower loop seal
MPC	Model predictive control(ler)
PG	Product gas
ULS	Upper loop seal

Mathematical notation and accents

\bar{x}	Steady-state target value for x
\mathbf{x}^T	Transpose of \mathbf{x}
\hat{x}	Estimate of x
$\ \mathbf{x}\ $	Euclidean norm of \mathbf{x}
$\text{diag}(\mathbf{x})$	Matrix with the elements of vector \mathbf{x} on the main diagonal
$x_{k j}$	j th element of the vector \mathbf{x}_k
x^+	One-step-ahead prediction of x

Subscripts

i	Time step within prediction horizon
k	Time step
c	Circulation MPC
m	Measurement

Variables and parameters

α	Heat transfer coefficient (kW/°C)
β_0, β_1	Heat transport (bed material) parameters (kW/°C and kW/(mbar °C))
A	System matrix
B	Control input matrix
B_d	Disturbance state input matrix
C	Output matrix
C_d	Disturbance state output matrix
d	Disturbance state vector
E	Disturbance input matrix
H	Controlled output matrix
$h_{O_2}^T$	Oxygen content selection vector
I	Identity matrix
L	Kalman gain matrix
Q	State deviation weighting matrix
R	Input deviation weighting matrix
r	Reference vector
R_Δ	Input rate weighting matrix
R_∞	Weighting matrix for steady-state control inputs
u	Control input vector
u^*	Desired input vector
v	Output noise
w	Process noise
x	State vector
y	Output vector

y^*	Controlled output vector
z	Disturbance input vector
Δp	Pressure difference in the upper part of the combustion reactor (mbar)
Δt_f	Sampling time for fast sampled model (s)
Δt_s	Sampling time for slowly sampled model (s)
\dot{H}	Enthalpy flow rate (kW)
\dot{m}	Mass flow rate (kg/h)
\dot{Q}	Heat flow rate (kW)
\dot{V}	Volumetric flow rate (Nm ³ /h)
η	Slack variable
τ	Time constant (s)
φ_{SF}	Steam-to-fuel ratio
b_{0-4}	Circulation model parameters
C	Heat capacity (kJ/°C)
c_{LS}	Loop seal split factor
N_c	Length of control horizon
N_p	Total length of prediction horizon
$N_{p,f}$	Length of fast sampled prediction horizon
$N_{p,s}$	Length of slowly sampled prediction horizon
T	Temperature (°C)
t	Time (s)
u	Gas velocity (m/s)
u_{mf}	Superficial gas velocity for minimum fluidization (m/s)
u_{se}	Superficial gas velocity for fast fluidization (m/s)
w_η	Slack variable weight
w_{ash}	Ash content in biomass (weight fraction)
w_{H_2O}	Water content in biomass (weight fraction)
y_{O_2}	Oxygen concentration in the dry flue gas (Vol.-%)

(DE) [10], and Gothenburg (SE) [11]. Numerous studies deal with process modeling [2] or the evaluation of process efficiency [12]. Nevertheless, there is a gap in the literature regarding automatic control strategies for DFB gasifiers. Typically, DFB gasification plants are operated manually or employ multiple single-input single-output controllers to regulate important process variables such as product gas quantity, gasification temperature, and oxygen content in the flue gas, as suggested in [13].

In [14], a PID control strategy is presented, which effectively controls the product gas quantity and leads to reduced fuel consumption. Additionally, in [15], a model-based control concept for controlling the circulation of bed material between the gasification reactor (GR) and the combustion reactor (CR) is introduced.

Currently, no multivariate control strategies can be found in literature for DFB gasification plants, capable of simultaneously controlling all relevant process variables. However, implementing such control concepts presents the possibility to enhance process efficiency and reducing operational costs, while combined single-input single-output control loops can lead to unexpected results and even instability in multivariable coupled systems [16].

Model predictive control (MPC) has proven to be highly effective in various process control applications [17]. It has been shown to be efficient in handling multivariate control problems and is able to explicitly account for constraints in the process variables.

In this study, we introduce an MPC strategy for effectively controlling the product gas quantity and the gasification temperature.

Additionally, the controller takes into consideration a predetermined lower limit for the oxygen content in the flue gas, as set by the plant operator. The control problem explicitly incorporates constraints on various variables, including minimum and maximum values for plant feeds, as well as the essential fluidization requirements of the reactors. Our proposed dual-stage control strategy comprises a high-level DFB MPC, responsible for controlling the product gas quantity and the gasification temperature, along with an underlying MPC controlling the bed material circulation.

The remainder of this paper is organized as follows: In Section 2, we provide a concise overview on the process, highlighting its key characteristics relevant for automatic control. In Section 3, we present the model that the MPC utilizes for its predictions. Subsequently, we introduce the control algorithm employed in this study in Section 4. In Section 5, we present a simulation study comparing different controller parametrization as well as experimental results obtained from implementing the controller at a 100 kW pilot plant located at TU Wien.

2. Process description

In this section, we want to give a brief description of DFB gasification. More detailed process descriptions are given in [2,18].

In DFB gasification, the process of generating a product gas from biomass is divided into gasification, which takes place in the GR, and combustion in the CR. Bed material constantly circulates between these two reactors and transports ungasified char from the GR to the CR and heat from the CR to the GR. This heat is essential for the overall endothermic steam gasification reactions. Air is fed to the CR only, meaning that the product gas leaving the GR is almost free of nitrogen which would dilute the product gas and reduce its quality.

2.1. 100 kW advanced DFB steam gasification pilot plant at TU Wien

Fig. 1 illustrates the design of the advanced DFB gasification pilot plant at TU Wien. The lower GR utilizes steam for fluidization and is operated as a bubbling fluidized bed reactor. A counter-column is positioned above the bubbling bed that contains constrictions in its cross-sectional area. These constrictions enhance the gas-solid contact and residence time of the bed material, thereby aiding in the reduction of tar content [19]. The CR is fluidized by air and is operated as a fast fluidized bed reactor. The two reactors are connected by a lower loop seal (LLS) at the bottom and an upper loop seal (ULS) at the top. The internal loop seal (ILS) is necessary for the internal bed material circulation of the GR. All loop seals are fluidized with steam.

The biomass is fed to the fluidized bed of the GR, where drying, devolatilization, and gasification take place. A part of the biomass remains ungasified and is transported via the LLS to the CR. There, the char is combusted, thereby heating up the bed material. Heating oil is used as an auxiliary fuel in the CR, which is required to compensate for the relatively high heat loss of the pilot plant. The air necessary for combustion is fed into the reactor in three stages. These air flows are referred to as primary air (air 1), secondary air (air 2), and tertiary air (air 3), whereby the primary air is the lowest airflow and the secondary and tertiary air are above it. A larger volume flow of air at a lower entry point leads to increased circulation of the bed material and vice versa. Thus, this air staging can be used to control the mass flow of bed material circulating between the two reactors. The mass flow of circulating bed material cannot be measured directly. However, the pressure difference Δp in the upper part of the CR is a reliable indicator of bed material circulation [20]. Therefore, it is subsequently used for bed material circulation control.

Fig. 2 depicts the TU Wien pilot plant. More comprehensive descriptions of this plant are given in [21,22].

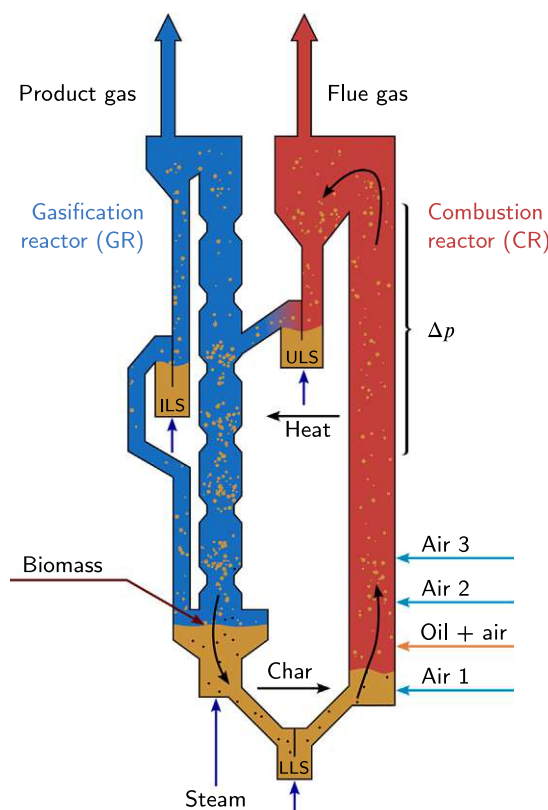
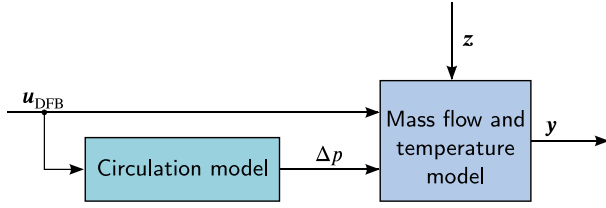


Fig. 1. DFB gasification pilot plant at TU Wien (100 kW), with the gasification reactor (GR) at the left and the combustion reactor (CR) at the right. Source: Adapted from [23].



Fig. 2. Upper part of the advanced 100 kW pilot plant at TU Wien.



$$\mathbf{u}_{\text{DFB}} = [\dot{m}_{\text{bm}}, \dot{m}_{\text{oil}}, \dot{m}_{\text{steam,GR}}, \dot{V}_{\text{air1}}, \dot{V}_{\text{air2}}, \dot{V}_{\text{air3}}]^T$$

$$\mathbf{y} = [\dot{m}_{\text{PG}}, \dot{m}_{\text{FG}}, T_{\text{GR}}, T_{\text{CR}}, y_{\text{O}_2,\text{FG}}]^T$$

$$\mathbf{z} = [\dot{m}_{\text{steam,ILS}}, \dot{m}_{\text{steam,ULS}}, \dot{m}_{\text{steam,LLS}}, T_{\text{steam}}, T_{\text{air}}]^T$$

Fig. 3. Structure of the DFB process model, consisting of a gray box model for the mass flows and reactor temperatures and a linear model for the bed material circulation.

3. Modeling

The MPC requires a dynamic model that can predict future states and outputs based on system inputs. This model enables the MPC to optimize the future manipulated variables, allowing the process to behave optimally according to predefined objectives.

The majority of dynamic models of DFB gasification rely on computational fluid dynamics, such as the ones presented in [24,25]. These models require a high computational effort and are thus not suitable for MPC. In this work, we are using a model based on the work presented in [23]. This model is based on non-steady-state mass and energy balances.

Maintaining a consistent level of product gas quantity is crucial for subsequent synthesis processes. Thus, it is desirable to control it at a specific value. The gasification temperature has a significant impact on the composition of the product gas [18]. Therefore, it is essential to control these process variables accordingly. The flue gas mass flow and the temperature in the CR are coupled to the product gas mass flow and the gasification temperature, respectively. Thus, these variables are considered in the model as well. In order to achieve complete combustion in the CR, it is desirable to maintain a specific oxygen content in the flue gas. The oxygen content is therefore considered in the model so that it can later be taken into account by the MPC. Thus,

- the product gas mass flow \dot{m}_{PG} ,
- the flue gas mass flow \dot{m}_{FG} ,
- the temperature in the bubbling bed of the GR T_{GR} , hereinafter referred to as gasification temperature,
- the temperature at the top of the CR T_{CR} , and
- the oxygen content in the dry flue gas y_{O_2}

are modeled, which is summarized in this section. Since the bed material circulation is crucial for the process, a submodel is used to model the pressure difference Δp in the upper part of the CR. This variable is then used as an input to the energy balance as the bed material circulation determines how much heat is transported from the CR to the GR. Fig. 3 shows the model structure of the dynamic DFB plant model.

3.1. Mass balance

A first-order differential equation is used to model the mass flow of product gas \dot{m}_{PG} leaving the gasification reactor:

$$\frac{d\dot{m}_{\text{PG}}}{dt} = \frac{1}{\tau_{\text{PG}}} (-\dot{m}_{\text{PG}} + \dot{m}_{\text{bm}}(1 - w_{\text{ash}}) + \dot{m}_{\text{steam,GR,total}} - \dot{m}_{\text{char}}), \quad (1)$$

with the time constant τ_{PG} , the mass of biomass fed to the GR \dot{m}_{bm} , the ash content in the biomass $w_{\text{ash}} \in [0, 1]$, the total amount of steam entering the GR $\dot{m}_{\text{steam,GR,total}}$, and the char that is transported to the CR

via the LLS \dot{m}_{char} . Thus, it is assumed that at steady state, the product gas mass flow is equal to the mass of ash-free biomass, plus the total amount of steam fed to the GR, reduced by the mass of char leaving the GR. Eq. (1) can be interpreted as this static relationship followed by a first-order linear dynamic model. For the char, it is assumed that a constant fraction of the biomass remains ungasified and is transported to the CR. The total amount of steam entering the GR $\dot{m}_{\text{steam,GR,total}}$ is computed as

$$\dot{m}_{\text{steam,GR,total}} = \dot{m}_{\text{steam,GR}} + \dot{m}_{\text{steam,ILS}} + c_{\text{LS}}(\dot{m}_{\text{steam,ULS}} + \dot{m}_{\text{steam,LLS}}), \quad (2)$$

where $\dot{m}_{\text{steam,GR}}$ is the mass flow of steam fed to the bubbling bed of the GR, and $\dot{m}_{\text{steam,ILS}}$, $\dot{m}_{\text{steam,ULS}}$, and $\dot{m}_{\text{steam,LLS}}$ are the mass flows of steam used to fluidize the ILS, the ULS, and the LLS, respectively. The split factor c_{LS} defines what fraction of steam used to fluidize the ULS and the LLS enters the GR and is assumed to be constant.

Likewise, the mass flow of flue gas \dot{m}_{FG} is modeled by a first-order differential equation, with

$$\frac{d\dot{m}_{\text{FG}}}{dt} = \frac{1}{\tau_{\text{FG}}} (-\dot{m}_{\text{FG}} + \dot{m}_{\text{char}} + \dot{m}_{\text{steam,CR}} + \dot{m}_{\text{air}} + \dot{m}_{\text{oil}}), \quad (3)$$

where τ_{FG} is a time constant, $\dot{m}_{\text{steam,CR}}$ is the steam streaming to the CR from the LLS and the ULS, and \dot{m}_{air} and \dot{m}_{oil} are the air and oil feed, respectively.

3.2. Energy balance

The reactor temperatures are modeled using energy balances for both reactors. The model incorporates two temperature state variables for each reactor. One state variable represents the temperature inside the reactor while the second state variable represents the reactor wall temperature.

For the GR, the energy balance

$$C_{\text{GR}} \frac{dT_{\text{GR}}}{dt} = \dot{H}_{\text{bm}} + \dot{H}_{\text{steam,GR,total}} - \dot{H}_{\text{char}} - \dot{H}_{\text{PG}} + \dot{Q}_{\text{bed}} - \dot{Q}_{\text{wall,GR}}, \quad (4)$$

models the gasification temperature T_{GR} , where C_{GR} is a heat capacity and \dot{H}_{bm} , $\dot{H}_{\text{steam,GR,total}}$, \dot{H}_{char} and \dot{H}_{PG} are the flows of conventional enthalpy of the biomass, steam, char, and product gas, respectively. The specific values of conventional enthalpy of biomass and char are calculated based on their lower heating values. The lower heating values are computed using Boie's formula, which considers their compositions obtained from compositional analysis. The conventional enthalpy of the product gas is computed using a pseudo-equilibrium model for its composition. \dot{Q}_{bed} is the heat transported by the bed material from the CR to the GR. $\dot{Q}_{\text{wall,GR}}$ is the heat flow from the gas inside the reactor to the reactor wall and thus represents the coupling between the reactor inside temperature state variable and the reactor wall temperature state variable. The heat balance for the reactor wall

$$C_{\text{GR,wall}} \frac{dT_{\text{GR,wall}}}{dt} = \dot{Q}_{\text{wall,GR}} - \dot{Q}_{\text{loss,GR}}, \quad (5)$$

models the temperature of the reactor wall $T_{\text{GR,wall}}$, with the heat capacity $C_{\text{GR,wall}}$ and the heat loss $\dot{Q}_{\text{loss,GR}}$. The heat flow from the GR to the reactor wall is modeled by the equation

$$\dot{Q}_{\text{wall,GR}} = \alpha_{\text{GR}}(T_{\text{GR}} - T_{\text{GR,wall}}), \quad (6)$$

with the heat transfer coefficient α_{GR} . The heat loss $\dot{Q}_{\text{loss,GR}}$ is modeled to be a linear function of T_{GR} , as suggested in [23]. Likewise, for the CR there is one energy balance

$$C_{\text{CR}} \frac{dT_{\text{CR}}}{dt} = \dot{H}_{\text{char}} + \dot{H}_{\text{oil}} + \dot{H}_{\text{air}} + \dot{H}_{\text{steam,CR}} - \dot{H}_{\text{FG}} - \dot{Q}_{\text{bed}} - \dot{Q}_{\text{wall,CR}}, \quad (7)$$

for the temperature at the top of the CR T_{CR} , with the heat capacity C_{CR} , the flows of conventional enthalpy \dot{H}_{oil} , \dot{H}_{air} , $\dot{H}_{\text{steam,CR}}$ and \dot{H}_{FG} of oil, air from the three stages, steam, and flue gas, respectively. For calculating the conventional enthalpy of the flue gas, the composition

calculated as described in Section 3.3 is used. Again, there is a second energy balance

$$C_{CR,wall} \frac{dT_{CR,wall}}{dt} = \dot{Q}_{wall,CR} - \dot{Q}_{loss,CR}, \quad (8)$$

describing the reactor wall temperature $T_{CR,wall}$, with the heat capacity $C_{CR,wall}$ and the coupling term

$$\dot{Q}_{wall,CR} = \alpha_{CR}(T_{CR} - T_{CR,wall}), \quad (9)$$

where α_{CR} is a heat transfer coefficient. The heat flow of bed material \dot{Q}_{bed} couples the temperature state variables T_{GR} and T_{CR} . The work presented in [23] demonstrated a high linear correlation between the heat transported by the bed material per degree temperature difference $\dot{Q}_{bed}/(T_{CR} - T_{GR})$ and the pressure difference in the CR Δp . Thus, the model

$$\dot{Q}_{bed} = (\beta_0 + \beta_1 \Delta p)(T_{CR} - T_{GR}), \quad (10)$$

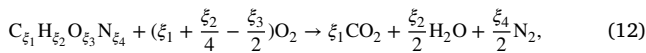
is used in this work as well. The parameters β_0 and β_1 are estimated from measurement data. Note that this model may not hold true for low Δp values. However, it exhibits high accuracy under conditions typical for plant operation.

3.3. Combustion model

In the CR, complete combustion and thus a surplus of oxygen is desired. Therefore, the oxygen content of the dry flue gas y_{O_2} is modeled, which allows the MPC to predict the oxygen content and ensure that complete combustion is maintained. It is assumed, that there is always enough air \dot{V}_{air} available, and that complete combustion of the char \dot{m}_{char} and the oil \dot{m}_{oil} is possible. Assuming ideal gases, the oxygen content of the dry flue gas can be computed by

$$y_{O_2} = \frac{\dot{n}_{O_2,FG}}{\dot{n}_{CO_2,FG} + \dot{n}_{N_2,FG} + \dot{n}_{O_2,FG}}, \quad (11)$$

where $\dot{n}_{O_2,FG}$, $\dot{n}_{CO_2,FG}$, and $\dot{n}_{N_2,FG}$ are the molar flows of O_2 , CO_2 , and N_2 in the flue gas, respectively. Other minor components are neglected in this work. Using the stoichiometric combustion equation



the steady-state oxygen content in the flue gas can be calculated as

$$y_{O_2} = \frac{\dot{n}_{O_2,in} - 2\dot{n}_{C,in} - 0.5\dot{n}_{H,in}}{\dot{n}_{N_2,in} + \dot{n}_{O_2,in} - 0.5\dot{n}_{H,in}}, \quad (13)$$

where $\dot{n}_{O_2,in}$, $\dot{n}_{C,in}$, $\dot{n}_{H,in}$, and $\dot{n}_{N_2,in}$ are the flows of oxygen, carbon, hydrogen, and nitrogen to the CR, that are depending on the flow rates of char, oil, and air as well as on their compositions. Samples of the char were collected to analyze its composition. In [26], the composition of the char was investigated in a simulation study for varying gasification temperatures during DFB gasification. Their results show that there are only small variations in the composition of char within the temperature range typically used in the pilot plant operation. These small variations are neglected in this work and a constant char composition is assumed. The composition of the heating oil and the air is known as well. It can be seen from (13), that the steam feed does not influence the oxygen content. Thus, (13) is a nonlinear function of the mass flows of char, oil, and air:

$$y_{O_2} = \phi(\dot{m}_{char}, \dot{m}_{oil}, \dot{V}_{air}). \quad (14)$$

Since it is observed that a change in the fuel feed or the air feed does not instantly change the oxygen content in the flue gas, the first-order differential equation

$$\frac{dy_{O_2}}{dt} = \frac{1}{\tau_{O_2}} (-y_{O_2} + \phi(\dot{m}_{char}, \dot{m}_{oil}, \dot{V}_{air})), \quad (15)$$

with the time constant τ_{O_2} is used to model y_{O_2} . This type of model is known in the literature as a Hammerstein model, a static nonlinear function followed by a linear dynamic model. As per the complete combustion assumption, $y_{O_2} \geq 0$ has to hold.

3.4. Bed material circulation model

The pressure difference Δp in the upper part of the CR is an indicator for the amount of bed material circulating between the CR and the GR and can be measured directly. It is used in (10) to compute the heat transported by the bed material. However, this pressure difference cannot be manipulated directly by a controller. Thus, a model is used describing how the variables that can be manipulated affect Δp . A linear approach

$$\Delta p = b_0 + b_1 \dot{V}_{air1} + b_2 \dot{V}_{air2} + b_3 \dot{V}_{air3} + b_4 \dot{m}_{bm} \quad (16)$$

is used to model Δp at steady state as a function of the biomass feed \dot{m}_{bm} , the primary air flow \dot{V}_{air1} , the secondary air flow \dot{V}_{air2} , and the tertiary air flow \dot{V}_{air3} . The coefficients b_0 , b_1 , b_2 , b_3 and b_4 are estimated from measurement data. In the identification experiment, the total airflow was always higher than 50 Nm³/h. The model may be invalid for smaller total air volumes.

An increase in the biomass feed or in the air flows cannot instantly lead to a change in the bed material circulation, due to the inertia of the bed material. Moreover, no oscillations can be observed in the bed material circulation when increasing an input step-wise. Therefore, the simplest modeling approach, a first-order differential equation

$$\frac{d(\Delta p)}{dt} = \frac{1}{\tau_c} (-\Delta p + b_0 + b_1 \dot{V}_{air1} + b_2 \dot{V}_{air2} + b_3 \dot{V}_{air3} + b_4 \dot{m}_{bm}), \quad (17)$$

with the time constant τ_c is used to model the lumped dynamic behavior of the bed material circulation.

The equations of the DFB process model are also provided as supplementary material, together with the structure of the linearized model.

4. Controller design

DFB gasification plants are typically operated at a steady-state operating point and constant references need to be tracked. Around an operating point, the system behavior can be approximated sufficiently by a linear model. Therefore, linear MPC formulations are used.

Offset-free reference tracking can be achieved by using the so-called velocity form model [27], or by using a disturbance model to account for a plant-model mismatch and constant disturbances [28]. In this work, we use disturbance models to achieve offset-free control. This allows the absolute values of the control inputs to be weighted, which is beneficial in this application as there are more control inputs available than outputs to track.

The subsequent sections discuss the control structure, followed by the design of the high-level DFB MPC and the circulation MPC.

4.1. Control structure

The controller for the DFB gasification plant is designed in a way that a constant reference for the product gas mass flow and for the gasification temperature can be tracked without stationary error. For the oxygen content in the flue gas, a lower bound can be set that is considered by the controller. The control scheme for the DFB gasification plant is illustrated in Fig. 4. The high-level DFB MPC uses the biomass feed, the oil feed, the steam feed, the total airflow to the CR, and the bed material circulation rate as control inputs. The adjustment of the steam used to fluidize the loop seals relies on manual valves for the pilot plant and can thus not be manipulated by the controller. Therefore, the mass flows of steam fed to the seals, together with the temperatures of both the incoming air and steam supplied to the plant, are considered as measured disturbances. A secondary MPC serves as a circulation controller, ensuring the desired circulation of bed material by appropriately distributing the total airflow among the three air stages. This hierarchical control structure allows for easier adaptation to different plants, as the specific air staging required for circulation control may vary across different plants.

Both MPCs use linearized discrete-time models for state estimation and prediction. These models are augmented by disturbance states as proposed in [28,29]. In operation, the steps

close as possible to \mathbf{u}^* in a least-squares sense. Using this, additional factors such as economic objectives can be incorporated into the target calculation. We define the optimization problem as follows:

$$\min_{\bar{\mathbf{x}}_k, \bar{\mathbf{u}}_k} \|\bar{\mathbf{u}}_k - \mathbf{u}^*\|_{\mathbf{R}_\infty}^2, \quad (23a)$$

subject to

$$\begin{bmatrix} \mathbf{A} - \mathbf{I} & \mathbf{B} \\ \mathbf{H}\mathbf{C} & \mathbf{0} \end{bmatrix} \begin{bmatrix} \bar{\mathbf{x}}_k \\ \bar{\mathbf{u}}_k \end{bmatrix} = \begin{bmatrix} -\mathbf{E}\mathbf{z}_k - \mathbf{B}_d \hat{\mathbf{d}}_k \\ \mathbf{r}_k - \mathbf{H}\mathbf{C}_d \hat{\mathbf{d}}_k \end{bmatrix}, \quad (23b)$$

$$\mathbf{h}_{\text{O}_2}^T (\mathbf{C}\bar{\mathbf{x}}_k + \mathbf{C}_d \hat{\mathbf{d}}_k) \geq y_{\text{O}_2, \min}, \quad (23c)$$

$$\varphi_{\text{SF}} = \frac{\bar{u}_{k|3} + \bar{u}_{k|1} w_{\text{H}_2\text{O}} + z_{k|1} + c_{\text{LS}}(z_{k|2} + z_{k|3})}{\bar{u}_{k|1}(1 - w_{\text{H}_2\text{O}} - w_{\text{ash}})}, \quad (23d)$$

$$\bar{\mathbf{u}}_k \in \mathbb{U}, \quad (23e)$$

where $u_{k|j}$ denotes the j th element of the vector \mathbf{u}_k . The matrix \mathbf{R}_∞ facilitates the weighting of the individual control inputs' deviation.

The system dynamics is incorporated by the constraint in (23b). The constraint (23c) ensures that the oxygen content in the flue gas is above a predefined limit that can be set by the plant operator. The vector $\mathbf{h}_{\text{O}_2}^T = [0, 0, 0, 0, 1]^T$ selects the oxygen concentration in the flue gas from the output vector. With (23d), the steam-to-fuel ratio φ_{SF} can be set to a specific value by the plant operator, where $w_{\text{H}_2\text{O}}$ represents the water content in the fuel and c_{LS} the split factor of both the LLS and the ULS. To further restrict the input space, the constraint (23e) is introduced, which is necessary for two reasons. Firstly, control inputs typically have minimum and maximum values, also due to necessary reactor fluidizations. Secondly, the total airflow to the CR and the bed material circulation rate are interdependent. Consequently, the possible bed material circulation rate heavily relies on the total airflow to the CR. The input constraints are described in detail in Section 4.2.5 and numerical values are given.

The target calculation is performed at every time step k utilizing the current measured disturbance \mathbf{z} and the estimate of the disturbance state $\hat{\mathbf{d}}$.

Due to the input restrictions, the optimization problem can become infeasible, meaning that no control input can be found so that the reference is reached at steady state. In this case, an alternative optimization problem is solved as suggested in [30]: The distance of the controlled outputs to their reference values is minimized in a least-squares sense instead of (23a). The constraints considered in the alternative optimization problem stay the same as in the original optimization problem (23). This serves as a safety mechanism and was never necessary during the experiment presented in Section 5.

4.2.4. DFB MPC problem

The DFB MPC problem is designed to track the target point computed in Section 4.2.3 by solving the optimization problem

$$\min_{\mathbf{U}} \sum_{i=1}^{N_p} (\|\mathbf{x}_{k+i} - \bar{\mathbf{x}}_k\|_{\mathbf{Q}_i}^2 + w_\eta \eta_{k+i}^2) + \sum_{i=0}^{N_c-1} (\|\mathbf{u}_{k+i} - \bar{\mathbf{u}}_k\|_{\mathbf{R}_i}^2 + \|\Delta \mathbf{u}_{k+i}\|_{\mathbf{R}_\Delta}^2), \quad (24a)$$

subject to

$$\mathbf{x}_{k+i+1} = \mathbf{A}_i \mathbf{x}_{k+i} + \mathbf{B}_i \mathbf{u}_{k+i} + \mathbf{E}_i \mathbf{z}_k + \mathbf{B}_{d,i} \hat{\mathbf{d}}_k, \quad \forall i \in \{0, 1, \dots, N_p - 1\} \quad (24b)$$

$$\mathbf{u}_{k+i} = \mathbf{u}_{k+N_c-1}, \quad \forall i \geq N_c, \quad (24c)$$

$$\Delta \mathbf{u}_{k+i} = \mathbf{u}_{k+i} - \mathbf{u}_{k+i-1}, \quad \forall i \in \{0, 1, \dots, N_c - 1\}, \quad (24d)$$

$$\mathbf{x}_k = \hat{\mathbf{x}}_k, \quad (24e)$$

$$\mathbf{d}_k = \hat{\mathbf{d}}_k, \quad (24f)$$

$$\mathbf{h}_{\text{O}_2}^T (\mathbf{C}\bar{\mathbf{x}}_k + \mathbf{C}_d \hat{\mathbf{d}}_k) \geq y_{\text{O}_2, \min} - \eta_{k+i}, \quad \eta_{k+i} \geq 0, \quad (24g)$$

$$\varphi_{\text{SF}} = \frac{u_{k+i|3} + u_{k+i|1} w_{\text{H}_2\text{O}} + z_{k|1} + c_{\text{LS}}(z_{k|2} + z_{k|3})}{u_{k+i|1}(1 - w_{\text{H}_2\text{O}} - w_{\text{ash}})}, \quad (24h)$$

$$\mathbf{u}_{k+i} \in \mathbb{U}. \quad (24i)$$

Cost function. The cost function (24a) penalizes a deviation from the target state $\bar{\mathbf{x}}_k$ and from the target control input $\bar{\mathbf{u}}_k$, weighted by the matrix \mathbf{Q}_i and the matrix \mathbf{R}_i , respectively. The prediction horizon N_p and the control horizon N_c are design parameters. Furthermore, changes in the control input are penalized and weighted by \mathbf{R}_Δ . To ensure a positive oxygen content in the flue gas, a soft constraint is used, where η is a slack variable and w_η is the corresponding penalty cost coefficient.

Constraints. With (24b) the system dynamics is taken into account. The control horizon can be chosen shorter than the prediction horizon to limit the computational effort. Thus, the control inputs are held constant with (24c) for $i \geq N_c$. Eqs. (24e) and (24f) consider the initialization of the state predictions with their estimated values. The soft constraint for the oxygen content in the flue gas requires the constraints (24g). The steam-to-fuel ratio is limited to a predefined value as determined by (24h). Finally, the input space is bounded according to the physical limitations of the process by (24i) as specified in Section 4.2.5.

Non-constant prediction-step MPC. The time constants of the DFB gasification plant differ strongly. Mass flows and gas compositions change quickly, whereas reactor temperatures change slowly due to the high heat capacities. Therefore, two different models are employed to compute the MPC predictions as proposed in [31]. The first model is created by discretizing the system using a fast sampling time Δt_f and is used to compute the first $N_{p,f}$ prediction steps. The second model is obtained by discretization using a slow sampling time Δt_s to compute further $N_{p,s}$ predictions. The total number of prediction steps is

$$N_p = N_{p,f} + N_{p,s}. \quad (25)$$

The state deviation in (24a) is weighted by the matrix \mathbf{Q}_i , where

$$\mathbf{Q}_i = \begin{cases} \Delta t_f \mathbf{Q} & \forall i \in \{1, \dots, N_{p,f}\} \\ \Delta t_s \mathbf{Q} & \forall i \in \{N_{p,f} + 1, \dots, N_p\}. \end{cases} \quad (26)$$

Thus, the integration of the weighted state deviation over time is approximated. The control input deviation is weighted by

$$\mathbf{R}_i = \begin{cases} \Delta t_f \mathbf{R} & \forall i \in \{1, \dots, N_{p,f}\} \\ \Delta t_s \mathbf{R} & \forall i \in \{N_{p,f} + 1, \dots, N_c\}. \end{cases} \quad (27)$$

It is assumed that $N_{p,f} < N_c < N_p$.

Riccati terminal costs and suitable terminal constraints around $(\bar{\mathbf{x}}_k, \bar{\mathbf{u}}_k)$ can be included to ensure closed-loop nominal stability. Extension to robust stability guarantees in the presence of model uncertainties are available in literature [32], but not used in this work.

4.2.5. Input constraints for the high-level DFB MPC

Table 1 presents the implemented minimum and maximum values for the control inputs.

Furthermore, the gas velocities inside the reactors need to satisfy constraints regarding fluidization. For the GR, the boundaries

$$2u_{\text{mf}} \leq u_{\text{GR}} \leq u_{\text{se}} \quad (28)$$

are applied. u_{GR} denotes the gas velocity to the GR, depending on the steam feed, the reactor temperature, and the reactor cross-sectional area. The minimum superficial gas velocity u_{mf} required for the formation of a bubbling fluidized bed as well as the superficial gas velocity for fast fluidization u_{se} depend on gas and bed material properties. For the CR, it is demanded that

$$u_{\text{CR}} > 0.7u_{\text{se}}, \quad (29)$$

Table 1
Minimum and maximum values for control inputs (high-level DFB MPC).

Control input	Min	Max
\dot{m}_{bm}	0 kg/h	25 kg/h
\dot{m}_{oil}	0 kg/h	6.88 kg/h
$\dot{m}_{\text{steam,GR}}$	(28)	20 kg/h ^a
\dot{V}_{air}	(29)	100 Nm ³ /h
Δp	2 mbar	10 mbar

^a Additionally subject to fluidization constraint (28).

with the gas velocity u_{CR} in the CR. This has been shown to be an adequate lower limit for the fluidization of the CR. These non-linear fluidization constraints are linearized at an operating point. Further information on fluidization and the calculation of superficial gas velocities can be found in [33].

Additionally, the total airflow to the CR \dot{V}_{air} and the pressure difference in the CR Δp cannot be chosen independently by the high-level DFB MPC. The pressure difference that can be achieved by varying the air staging depends on the total airflow. These limitations are computed using the circulation model (16).

4.3. Circulation MPC

The circulation MPC controls the circulation of bed material between the CR and the GR as demanded by the high-level DFB MPC while ensuring a total volume flow of air to the CR.

4.3.1. Circulation model

For offset-free control of the bed material circulation, the model (17) is augmented by a disturbance state d_c , leading to the augmented model

$$\dot{x}_c = \frac{1}{\tau_c} (-x_c + b_0 + [b_1 \ b_2 \ b_3] u_c + b_4 z_c + d_c),$$

$$\dot{d}_c = 0, \quad (30)$$

$$y_c = x_c,$$

with

$$y_c = \Delta p, u_c = [\dot{V}_{\text{air}1}, \dot{V}_{\text{air}2}, \dot{V}_{\text{air}3}]^T, z_c = \dot{m}_{\text{bm}}. \quad (31)$$

4.3.2. Circulation observer design

A Kalman filter is designed for the discrete-time model

$$\begin{bmatrix} x_{c|k+1} \\ d_{c|k+1} \end{bmatrix} = \begin{bmatrix} a_c & b_{c|d} \\ 0 & 1 \end{bmatrix} \begin{bmatrix} x_{c|k} \\ d_{c|k} \end{bmatrix} + \begin{bmatrix} b_c \\ 0 \end{bmatrix} u_{c|k} + \begin{bmatrix} e_c \\ 0 \end{bmatrix} z_{c|k} + w_{c|k}, \quad (32)$$

$$y_{c|k} = x_{c|k} + v_{c|k},$$

where a_c , $b_{c|d}$, b_c , and e_c are a function of the continuous-time parameters in (30) as well as the sampling time. The estimates for both the system state and the disturbance state are computed by a prediction step

$$\begin{bmatrix} \hat{x}_{c|k+1}^+ \\ \hat{d}_{c|k+1}^+ \end{bmatrix} = \begin{bmatrix} a_c & b_{c|d} \\ 0 & 1 \end{bmatrix} \begin{bmatrix} \hat{x}_{c|k} \\ \hat{d}_{c|k} \end{bmatrix} + \begin{bmatrix} b_c \\ 0 \end{bmatrix} u_{c|k} + \begin{bmatrix} e_c \\ 0 \end{bmatrix} z_{c|k} \quad (33)$$

and a correction step

$$\begin{bmatrix} \hat{x}_{c|k} \\ \hat{d}_{c|k} \end{bmatrix} = \begin{bmatrix} \hat{x}_{c|k}^+ \\ \hat{d}_{c|k}^+ \end{bmatrix} + \begin{bmatrix} l_{c|x} \\ l_{c|d} \end{bmatrix} (-y_{c|m|k} + \hat{x}_{c|k}^+), \quad (34)$$

with the output measurement $y_{c|m|k}$. The steady-state Kalman gain $l_c = [l_{c|x}, l_{c|d}]^T$ is computed by solving the discrete-time algebraic Riccati equation [28].

Table 2
Minimum and maximum values for control inputs (Circulation MPC).

Control input	Min	Max
$\dot{V}_{\text{air}1}$	0 Nm ³ /h	40 Nm ³ /h
$\dot{V}_{\text{air}2}$	0 Nm ³ /h	40 Nm ³ /h
$\dot{V}_{\text{air}3}$	0 Nm ³ /h	20 Nm ³ /h

4.3.3. Circulation target calculation

Since three control inputs are available to control the circulation of the bed material while simultaneously ensuring a certain total airflow, there is no unique solution for the air staging. An optimization problem is therefore formulated again. This keeps the control input as close as possible to a desired control input u_c^* . The calculation of the target point to be tracked by the MPC is done by solving the optimization problem

$$\min_{\bar{u}_{c|k}} \|\bar{u}_{c|k} - u_c^*\|^2, \quad (35a)$$

subject to

$$r_{c|k} = b_0 + [b_1 \ b_2 \ b_3] \bar{u}_{c|k} + b_4 z_{c|k} + \hat{d}_{c|k}, \quad (35b)$$

$$\bar{u}_{c|1|k} + \bar{u}_{c|2|k} + \bar{u}_{c|3|k} = \dot{V}_{\text{air,CR}|k}, \quad (35c)$$

$$\bar{u}_{c|k} \in \mathbb{U}_c. \quad (35d)$$

The circulation reference value $r_{c|k}$ and the total amount of air $\dot{V}_{\text{air,CR}|k}$ are the first values of the control input sequence computed by the high-level DFB MPC. The input space is bounded by (35d) as described in Section 4.3.5.

4.3.4. Circulation MPC problem

The MPC tracks the target point by solving the optimization problem

$$\min_{U_c} \sum_{i=1}^{N_p} (x_{c|k+i} - r_{c|k})^2 q_c$$

$$+ \sum_{i=0}^{N_c-1} (\|u_{c|k+i} - \bar{u}_{c|k}\|_{R_c}^2 + \|\Delta u_{c|k+i}\|_{R_{c|\Delta}}^2), \quad (36a)$$

subject to

$$x_{c|k+i+1} = a_c x_{c|k+i} + b_c u_{c|k+i} + e_c z_{c|k} + b_{c|d} d_{c|k},$$

$$\forall i \in \{0, 1, \dots, N_p - 1\} \quad (36b)$$

$$u_{c|k+i} = u_{c|k+N_c-1}, \quad \forall i \geq N_c, \quad (36c)$$

$$\Delta u_{c|k+i} = u_{c|k+i} - u_{c|k+i-1}, \quad \forall i \in \{0, 1, \dots, N_c - 1\}, \quad (36d)$$

$$x_{c|k} = \hat{x}_{c|k}, \quad (36e)$$

$$d_{c|k} = \hat{d}_{c|k}, \quad (36f)$$

$$u_{c|1|k+i} + u_{c|2|k+i} + u_{c|3|k+i} \geq \dot{V}_{\text{air,CR}|k}, \quad (36g)$$

$$u_{c|k+i} \in \mathbb{U}_c, \quad (36h)$$

where q_c is the weighting for the state deviation, R_c the weighting for the input deviation, and $R_{c|\Delta}$ the weighting for changes in the control input. To ensure complete combustion, the sum of the three air streams must always be higher than the total amount of air demanded from the high-level DFB MPC. This is taken into account by (36g). Again, the input space is bounded by (36h) according to the input constraints presented in 4.3.5.

4.3.5. Input constraints for the circulation MPC

The minimum and maximum values for the control inputs of the circulation MPC are given in Table 2.

5. Results and discussion

The results are presented for the 100 kW pilot plant at TU Wien described in Section 2.1. Before the MPC was implemented, the system was operated manually.

Table 3
Prediction and control horizons of the different high-level DFB MPCs.

	$N_{p,f}$	$N_{p,s}$	Δt_f	Δt_s	N_c
MPC I	20	–	5 s	–	20
MPC II	10	30	5 s	250 s	20
MPC III ^a	10	30	5 s	250 s	20

^a High weighting of the control input responsible for the bed material circulation rate.

5.1. Controller simulation

In order to show the influence of different MPC parametrizations, a simulation study is conducted. Three DFB MPC configurations with different high-level DFB MPC configurations are compared. The three versions differ in their prediction horizons and in their weighting matrices. MPC I utilizes a single time scale for its predictions, resulting in a prediction time of 100 s. MPC II and MPC III utilize the non-constant prediction-step MPC method, which leads to a longer total prediction time of approximately 2 h. Table 3 shows the prediction and control horizons of each MPC. Notably, MPC II and MPC III differ in terms of their weighting matrices. For MPC III, the values in the weighting matrix R_∞ as well as in R , penalizing strong deviations from the desired bed material circulation, are chosen very high. This results in constant bed material circulation. The state observer as well as the circulation MPC are the same across all controller configurations. The circulation MPC utilizes a prediction and control horizon of 20 samples. The specific weighting matrices for both the high-level DFB MPCs and the circulation MPC as well as the state observer design matrices are provided in Appendix A. Measurement data from previous test runs were used to determine the covariance matrices for the observer in order to obtain a sufficient result for state estimation. The MPC weighting matrices were tuned in closed-loop simulations.

Two simulations are performed, both starting with reference values for the PG mass flow and the gasification temperature of 30 kg/h and 780 °C, respectively. The minimum value for the O₂ concentration in the flue gas is set to 1 Vol.-%, which is appropriate for the pilot plant as the flue gas passes through a post-combustion chamber. For industrial DFB gasification plants, this value may have to be increased. The desired control inputs are set to

$$\mathbf{u}^* = [20, 4.386, 7.526, 64, 3.5]^T \quad (37)$$

for the high-level DFB MPC and to

$$\mathbf{u}_c^* = [27, 27, 12]^T \quad (38)$$

for the circulation MPC. This corresponds to values, where the plant is typically operated and has been operated for identification experiments. The desired steam-to-fuel ratio is set to 0.7.

5.1.1. Tracking of changes in the references

During the first simulation, the following changes in the reference values are applied:

- (a): The reference for the PG mass flow is reduced by 20 %.
- (b): The oil feed in the desired input vector \mathbf{u}^* is set from 4.386 kg/h to 0 kg/h. Thus, the oil feed should be reduced by the MPC.
- (c): The reference value for the gasification temperature is increased to 810 °C.
- (d): The reference value for the gasification temperature is decreased to 750 °C.

The simulation results are shown in Fig. 5. The results show the influence of the different MPC parameterizations on the closed-loop dynamics. MPC I focuses on computing steady-state control inputs to achieve desired reference values, resulting in slow dynamics for setpoint changes. MPC II uses an extended prediction horizon and higher

weighting on deviations of the tracked outputs from their references. This leads to faster closed-loop responses. In the design of MPC III, the bed material circulation is restricted to a specific value. This can be beneficial to ensure a consistent amount of bed material in the counter column of the GR, necessary for gasification reactions. For the simulated plant operation shown in Fig. 5, the following closed-loop behavior can be observed:

- (a): By reducing the product gas mass flow reference, the MPCs reduce biomass and steam inputs. In addition, less heat is required for the endothermic gasification reactions. Therefore, the oil feed is also reduced. The MPC III ensures a constant circulation of the bed material. Since reducing the biomass feed would reduce the bed material circulation, the controller increases air 1 while decreasing air 2 and air 3 to ensure constant circulation. MPC I and MPC II also reduce the bed material circulation due to the lower heat demand.
- (b): MPC I and MPC II are able to reduce the oil feed from a steady-state value of 3.85 kg/h before the change made at $t = 2$ h to a steady-state value of 3.65 kg/h before $t = 4$ h, which is a reduction of approximately 5%. This can be achieved by increasing the bed material circulation. MPC III can hardly reduce the oil consumption, since the bed material circulation has to be held constant.
- (c): MPC I and MPC II achieve the increase in gasification temperature by increasing both the oil feed and the bed material circulation. In addition, the total amount of air must be increased to keep the oxygen content in the flue gas above its lower limit. To increase the bed material circulation, air 1 is increased while air 2 and air 3 are reduced. MPC III achieves the increase in gasification temperature solely by increasing the oil feed, which results in higher oil consumption compared to MPC I and MPC II. The total amount of air to the CR must also be increased, resulting in an increase in all three air streams to keep the circulation rate constant with a higher amount of air. Thus, MPC III increases air 2 and air 3 while MPC I and MPC II decrease them.
- (d): To reduce the gasification temperature, proceed in reverse to the setpoint change (c).

The computation time for each time step, which involves solving the optimization problems for both the high-level DFB MPC and the circulation MPC, is approximately 0.04 s for the configuration with MPC I and approximately 0.07 s for the configuration including MPC II and MPC III.

5.1.2. Simulation with parameter errors in the simulation model

In reality, the plant parameters will differ from the model parameters. In order to investigate the effect of parameter uncertainties, a second simulation is performed. In this simulation, the following parameters are varied in the nonlinear simulation model:

- (e): It is assumed that a constant mass fraction of the dry and ash-free biomass remains ungasified and is transported to the CR as char. This parameter value is increased from 0.05 to 0.065 (+25 %).
- (f): The split factor c_{LS} , determining which part of the steam is used to fluidize the ULS and the LLS streams to the GR is increased from 0.5 to 0.7.
- (g): The water content of the biomass is increased from 7.2 % to 20 %.

The results of this simulation are shown in Fig. 6. Here, not all outputs and control inputs are shown, but the most essential ones for investigating these parameter variations. In the following, the closed-loop behavior is discussed for the individual parameter variations:

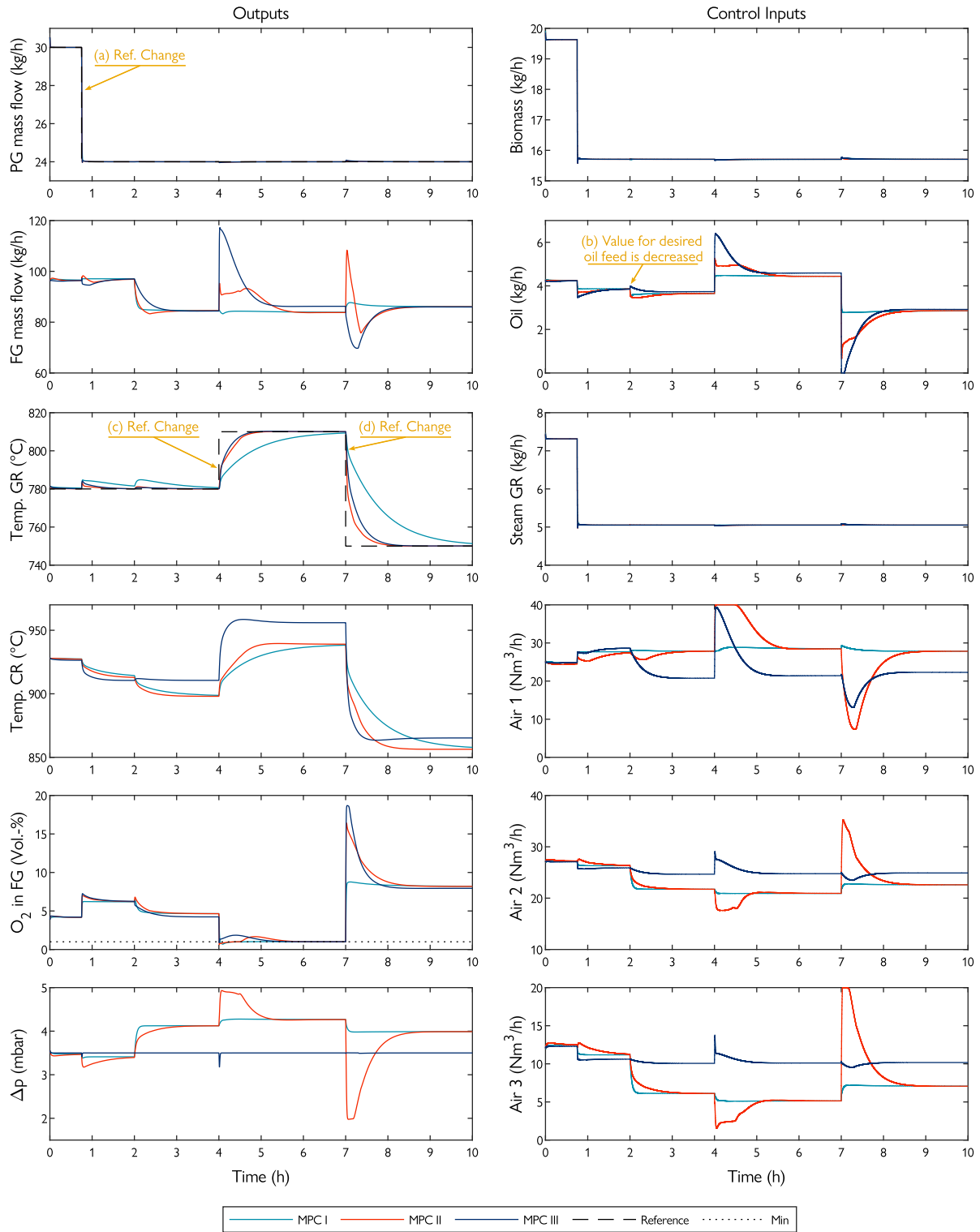


Fig. 5. Simulation results comparing three different controllers for the DFB gasification plant. Reference tracking is applied for the PG mass flow and the gasification temperature (Temp. GR) while ensuring a minimum oxygen concentration in the FG. MPC I has been implemented at the TU Wien pilot plant.

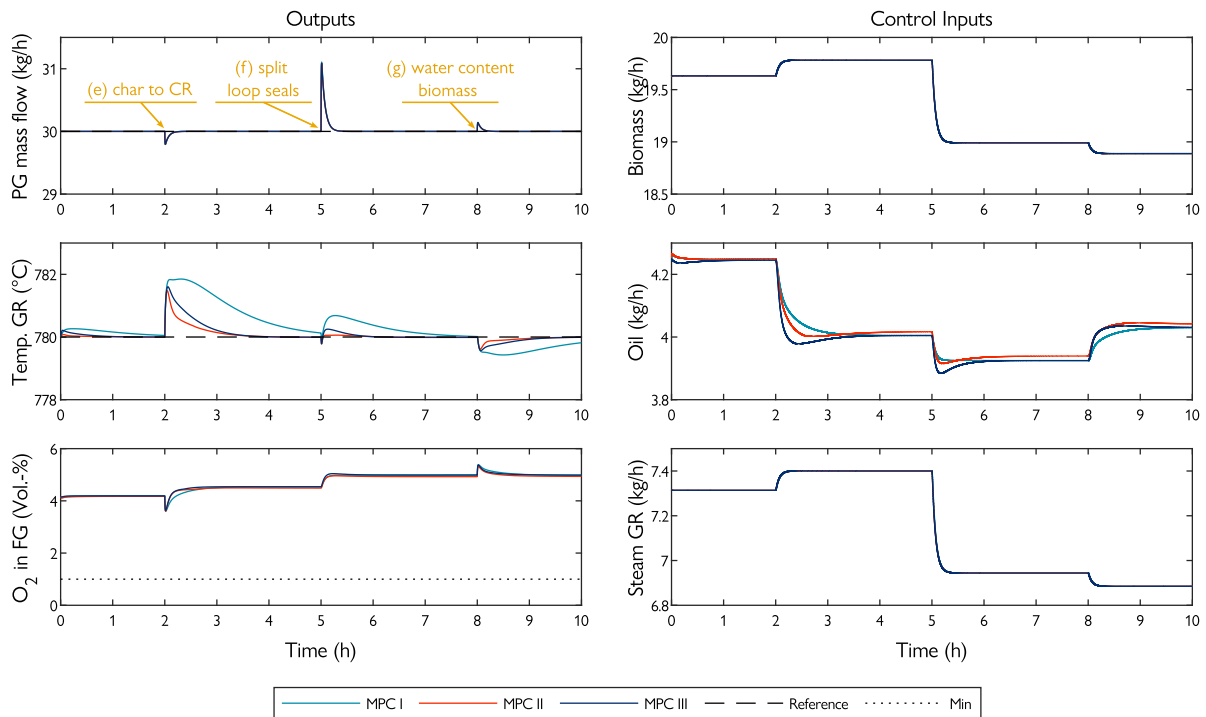


Fig. 6. Simulation results to show the influence of parameter deviations between the MPC model and the nonlinear simulation model.

- (e): The controller must increase both the biomass and the steam feed to bring the product gas mass flow back to its reference. More char is combusted in the CR, consequently, the oil feed must be reduced by the controllers.
- (f): The increased amount of steam to the GR results temporarily in a higher product gas mass flow. To compensate, the controller must reduce the feed to the GR. Since the steam-to-fuel ratio is fixed at a certain value, both the biomass and the steam feed are reduced. Due to the reduced biomass feed, less heat is required for the gasification reactions. As a result, the gasification temperature increases, which the controllers compensate for by reducing the oil feed.
- (g): Higher biomass moisture requires more heat to evaporate the water. Thus, the gasification temperature decreases temporarily, which is compensated by an increased oil feed. The model also assumes that a constant fraction of the dry and ash-free biomass is transported to the CR. As the dry and ash-free biomass feed decreases, the char flow to the CR decreases, resulting in a higher product gas mass flow. This is compensated for by the decrease in biomass and steam feed.

The controllers can compensate for the plant model mismatch using the disturbance model, but it takes a while. This is because in the observer design, it is assumed that the disturbances change slowly over time. In this simulation, parameters were changed instantaneously for easier interpretability of the closed-loop results. However, in the real process, parameters will change more slowly, for example, the fraction of biomass transported to the CR may depend on the gasification temperature, which changes slowly over time.

5.2. Experimental closed-loop validation on the pilot plant

The implementation and testing of the controller at the pilot plant were conducted in two stages: initially, the circulation MPC was tested independently to ensure its ability to correctly control the bed material circulation. In the second stage, the overall DFB controller, comprising the high-level DFB MPC and the circulation MPC, was tested as a complete system.

Table 4

Measurement equipment at the TU Wien pilot plant.

Source: Adapted from [23].

Process variable	Device
Temperature	Type K thermocouple
Pressure	Kalinsky pressure sensor
Steam and air flows	Variable area flowmeter
Product gas and flue gas flows	Barthel orifice meter
Main gas compositions	Rosemount NGA 2000
Fuel feed	Rot. speed of dosing screws ^a

^a The dosing screws are calibrated before every test run.

5.2.1. Experimental setup

For the experimental results presented in this work, softwood pellets were used as feedstock. The bed material inventory initially consisted of 70 kg and was composed of a mixture of 80% olivine and 20% limestone.

Table 4 provides an overview of the equipment utilized for measurement purposes. The thermocouples are mounted so that the tip protrudes a few millimeters into the reactor [34]. Detailed information regarding the measurement devices and actuators used at the pilot plant can be found in [35]. The measurement data collected by the plant's process control system is processed at a separate computer running MATLAB every 5 s. Further information regarding the data communication can be found in [36]. The MPC optimization problems are formulated using YALMIP [37] and solved with quadprog from the MATLAB optimization toolbox [38].

5.2.2. Circulation MPC tests

Fig. 7 shows the experimental results of the circulation MPC. Reference values were provided for two variables: the bed material circulation, represented by the pressure difference Δp in the upper CR, and the total amount of airflow to the CR. These reference values were changed stepwise during the test run. At around $t = 10$ min, for example, the reference for Δp is increased while keeping the reference for the

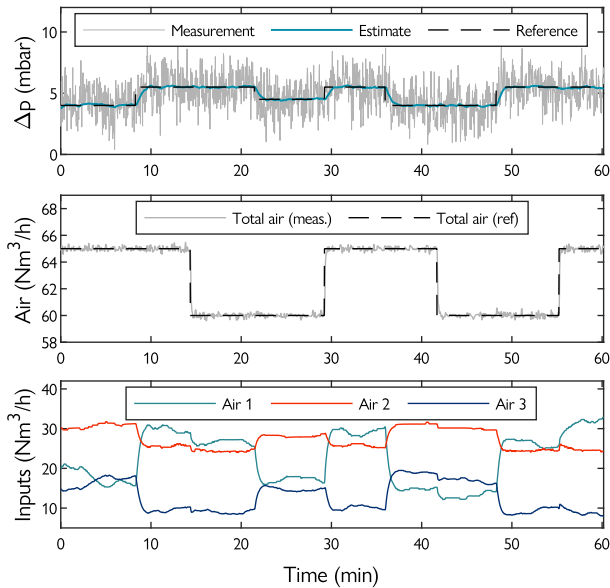


Fig. 7. Experimental results from the circulation MPC controlling the bed material circulation at the TU Wien pilot plant.

total airflow constant. The pressure difference can be increased by the circulation controller by increasing air 1 while reducing air 2 and air 3. It can be seen that the bed material circulation reacts quite fast to changes in the air staging.

5.2.3. DFB controller tests

The results obtained from the pilot plant controlled by the overall DFB controller, which comprises the high-level DFB MPC (MPC I from Section 5.1) and the circulation MPC, are presented in Fig. 8. Similar to the simulation in Section 5.1.1, the same changes in references were applied. The experimental results show effective control of the DFB gasification pilot plant. The tracking of the reference for the product gas quantity was rapid and efficient. Reference changes for the gasification temperature could be tracked successfully as well. The circulation MPC successfully achieved rapid control of the bed material circulation as required by the high-level DFB MPC, due to the fast dynamics of the circulation. The increase in the reference for the gasification temperature was initially conducted slightly before $t = 3$ h. However, due to the necessity of maintenance of the gas analysis system, the reference value was set back to 780°C . Manual operation of the plant was required as the maintenance caused wrong measurements in the product gas mass flow. The period during which the plant was operated manually is highlighted in the graph with a gray background. In addition to the raw measurement data, a smoothed signal of the pressure difference Δp is shown. The signal has been smoothed by calculating a centered moving average with a window size of 21 samples.

The orifice plates measuring the product gas and flue gas flow rates are flushed every 15 min using nitrogen. This results in peaks in their measurements. Due to the measurement limits of the variable area flowmeter, it was not possible to achieve small flow rates ($< 5 \text{ Nm}^3/\text{h}$ for air 1 and air 2, $< 3 \text{ Nm}^3/\text{h}$ for air 3). This issue affected air 3 between hours 2 and 4. During the test run, there was a calibration error in the dosing screws for the biomass. This resulted in an actual biomass feed that was 20% lower than the values calculated by the MPC. However, this was compensated by the controller by considering the estimated disturbance states. In Fig. 8, the corrected measurements are shown.

Setting the value for the desired oil feed to zero (b), decreased the oil consumption temporarily. However, the oil consumption increased

again. A more pronounced impact could be achieved by increasing the corresponding entry in the weighting matrix R_{ss} .

For changes in the reference of the gasification temperature, it took some time for the system to follow the new reference. MPC I was implemented as it is less aggressive than MPC II and MPC III. The simulation results match very well with the experimental results. This shows a high model accuracy. In future experiments, the MPC II or MPC III settings will be tested, which are expected to result in shorter rise times for setpoint changes in the gasification temperature.

6. Conclusion and outlook

Within the present work, model predictive control of a DFB gasification plant is investigated. The proposed control concept utilizes two MPCs. Firstly, a high-level DFB MPC is used to control the quantity of PG and the gasification temperature while ensuring a specific minimum oxygen content in the flue gas. Secondly, a circulation MPC controls the circulation of bed material according to the desired settings from the high-level DFB MPC by adjusting the air staging in the CR. This modular control structure is expected to enhance the transferability of the controller to other DFB gasification plants.

In our control strategy, the plant operator specifies the desired values for the gasification temperature and the steam-to-fuel ratio, in addition to other operation targets. These process variables have been identified with respect to their significant influence on the product gas composition. The desired values need to be specified in a way, that the product gas quality meets the expectations of the plant operator regarding product gas quality. The expectations with respect to the product gas quality can differ from case to case depending on the gas utilization pathway as well as local regulations.

The proposed DFB control concept was implemented and successfully tested for over eight hours at the DFB pilot plant in TU Wien. Different setpoints for the PG quantity as well as for the gasification temperature could be tracked successfully. The MPC operates based on physical models, which simplifies the application of the control concept to different fuels and other plants. When applying the controller to different plants, it is necessary to re-estimate the plant-specific model parameters, such as reactor heat capacities or parameters that describe the heat transferred by the bed material.

In industrial-sized plants, PG recirculation is typically employed, and the amount of PG is measured after H_2O separation, while in the considered pilot plant the wet flow of PG was measured and controlled. Controlling the dry quantity of PG that remains after recirculation should be investigated, as the dry PG is the desired product.

Finally, it can be summarized, that the present work was able to demonstrate a control strategy for a DFB gasification plant. Future work will concentrate on the implementation in an operational environment at a larger scale.

CRedit authorship contribution statement

Lukas Stanger: Writing – original draft, Visualization, Validation, Software, Methodology, Conceptualization. **Alexander Bartik:** Writing – review & editing, Resources, Investigation. **Martin Hammerschmid:** Writing – review & editing, Resources, Investigation. **Stefan Jankovic:** Writing – review & editing, Investigation. **Florian Benedikt:** Writing – review & editing, Resources, Investigation. **Stefan Müller:** Writing – review & editing, Resources. **Alexander Schirrer:** Writing – review & editing, Methodology, Conceptualization. **Stefan Jakubek:** Writing – review & editing. **Martin Kozek:** Writing – review & editing, Supervision, Conceptualization.

Declaration of competing interest

The authors declare that they have no known competing financial interests or personal relationships that could have appeared to influence the work reported in this paper.

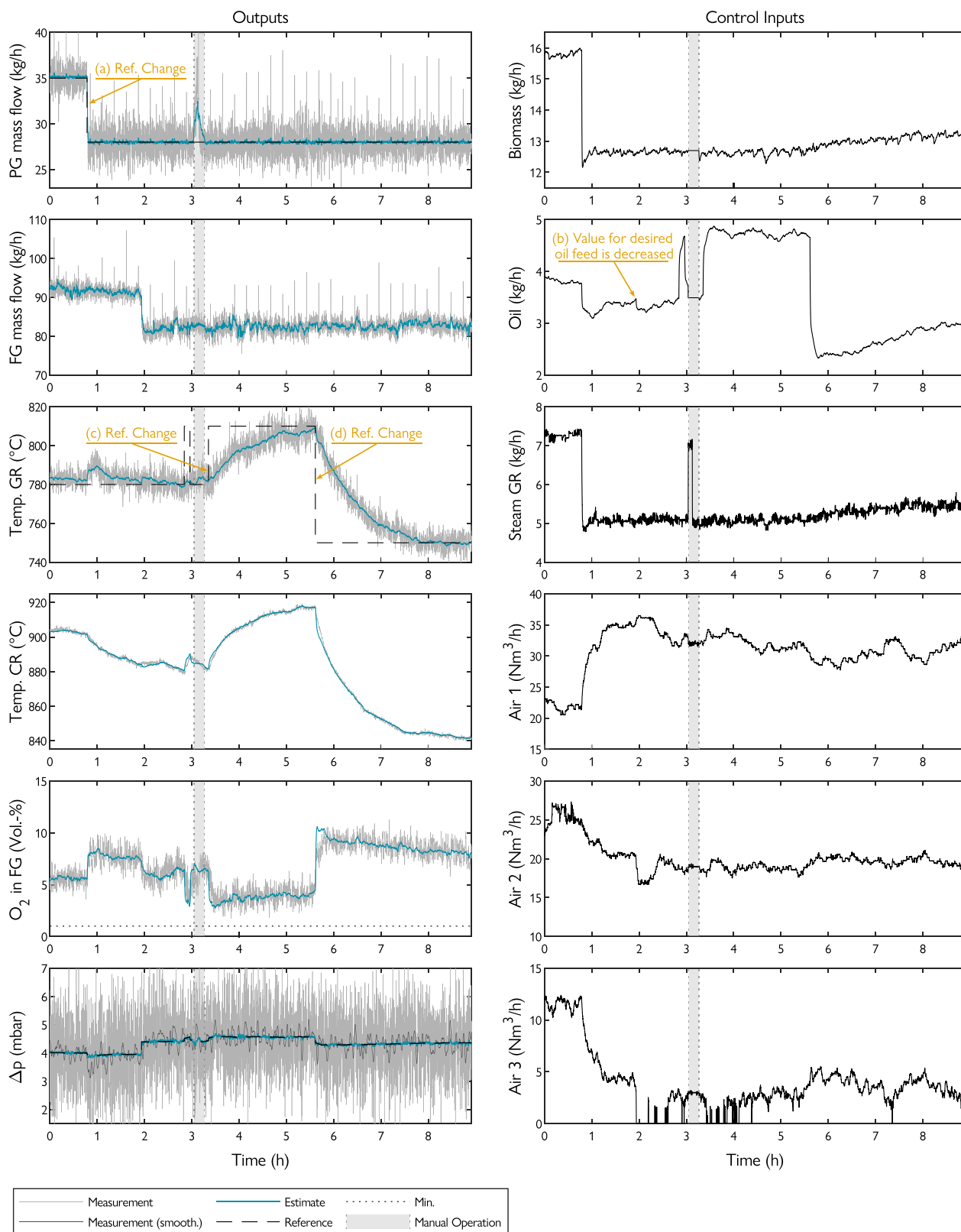


Fig. 8. Experimental results from the TU Wien DFB pilot plant controlled by the proposed DFB MPC.

Data availability

Data will be made available on request.

Acknowledgments

This work was supported by the project ADORe-SNG, which is funded by the Austrian Climate and Energy Fund (FFG, No. 881135).

The authors acknowledge TU Wien Bibliothek, Austria for financial support through its Open Access Funding Programme.

Appendix A

A.1. High-level DFB MPC

All state weighting matrices \mathbf{Q} involve a scaling with a state \mathbf{x}_0

$$\mathbf{Q} = \text{diag}(\mathbf{x}_0)^{-2} \tilde{\mathbf{Q}},$$

where $\tilde{\mathbf{Q}}$ is a design matrix that is always diagonal and specified below for the individual MPC configurations. The same applies for the control input weighting matrices

$$\mathbf{R} = \text{diag}(\mathbf{u}_0)^{-2} \tilde{\mathbf{R}},$$

$$\mathbf{R}_\Delta = \text{diag}(\mathbf{u}_0)^{-2} \tilde{\mathbf{R}}_\Delta,$$

$$\mathbf{R}_\infty = \text{diag}(\mathbf{u}_0)^{-2} \tilde{\mathbf{R}}_\infty.$$

The scaling vectors correspond to a state and control input, which represent the typical operating point of the plant and are specified as

$$\mathbf{u}_0 = [20, 4.386, 7.526, 64, 3.5]^T,$$

$$\mathbf{x}_0 = [29.563, 96.236, 782.97, 736.17, 932.44, 925.18, 3.561]^T.$$

The design matrices for the high-level DFB MPC are selected as follows: for MPC I,

$$\tilde{\mathbf{Q}} = \mathbf{I}, \quad w_\eta = 10^8,$$

$$\tilde{\mathbf{R}} = \mathbf{I}, \quad \tilde{\mathbf{R}}_\Delta = 20 \cdot \mathbf{I}, \quad \tilde{\mathbf{R}}_\infty = \mathbf{I},$$

for MPC II,

$$\tilde{\mathbf{Q}} = \text{diag}(10^4, 1, 10^4, 1, 1, 1, 1), \quad w_\eta = 10^8,$$

$$\tilde{\mathbf{R}} = 10 \cdot \mathbf{I}, \quad \tilde{\mathbf{R}}_\Delta = 10^3 \cdot \mathbf{I}, \quad \tilde{\mathbf{R}}_\infty = \mathbf{I},$$

and for MPC III,

$$\tilde{\mathbf{Q}} = \text{diag}(10^4, 1, 10^4, 1, 1, 1, 1), \quad w_\eta = 10^8$$

$$\tilde{\mathbf{R}} = \text{diag}(10, 10, 10, 10, 10^6), \quad \tilde{\mathbf{R}}_\Delta = 10^3 \cdot \mathbf{I}$$

$$\tilde{\mathbf{R}}_\infty = \text{diag}(1, 1, 1, 1, 10^4)$$

A.1.1. Kalman filter design

The steady-state Kalman gain is computed by

$$\mathbf{L} = -\Sigma \mathbf{C}^T (\mathbf{C} \Sigma \mathbf{C}^T + \mathbf{R}_{\text{KF}})^{-1},$$

where Σ is the solution of the discrete-time algebraic Riccati equation

$$\Sigma = \mathbf{A} \Sigma \mathbf{A}^T + \mathbf{Q}_{\text{KF}} - \mathbf{A} \Sigma \mathbf{C}^T (\mathbf{C} \Sigma \mathbf{C}^T + \mathbf{R}_{\text{KF}})^{-1} \mathbf{C} \Sigma \mathbf{A}^T.$$

\mathbf{A} and \mathbf{C} denote the system and the output matrix of the augmented system. The process noise covariance matrix \mathbf{Q}_{KF} and the measurement noise covariance matrix \mathbf{R}_{KF} are specified as

$$\mathbf{Q}_{\text{KF}} = \text{diag}(10, 10, 10, 10, 10, 10, 10, 1, 1, 1, 1, 1),$$

$$\mathbf{R}_{\text{KF}} = 10^3 \cdot \text{diag}(2, 2, 20, 10, 10).$$

A.2. Circulation MPC

The MPC weighting matrices are defined as

$$q_c = 10^4, \quad \mathbf{R}_c = 1.2 \cdot \mathbf{I}, \quad \mathbf{R}_{c|\Delta} = 1.2 \cdot 10^3 \cdot \mathbf{I}.$$

For the calculation of the steady-state Kalman gain, the covariance matrix of the process noise as well as the covariance of the measurement noise are specified as

$$\mathbf{Q}_{c|\text{KF}} = \mathbf{I}, \quad r_{c|\text{KF}} = 10^4.$$

Appendix B. Supplementary data

Supplementary material related to this article can be found online at <https://doi.org/10.1016/j.apenergy.2024.122917>.

References

- [1] IPCC. *Climate Change 2023: Synthesis Report*. Geneva, Switzerland: IPCC; 2023.
- [2] Hanchate N, Ramani S, Mathpati CS, Dalvi VH. Biomass gasification using dual fluidized bed gasification systems: A review. *J Clean Prod* 2021;280:123148. <http://dx.doi.org/10.1016/J.JCLEPRO.2020.123148>.
- [3] Bartik A, Benedikt F, Fuchs J, Hofbauer H, Müller S. Experimental investigation of hydrogen-intensified synthetic natural gas production via biomass gasification: a technical comparison of different production pathways. *Biomass Convers Biorefinery* 2023. <http://dx.doi.org/10.1007/s13399-023-04341-3>.
- [4] Hammerschmid M, Bartik A, Benedikt F, Veress M, Pratschner S, Müller S, et al. Economic and ecological impacts on the integration of biomass-based SNG and FT diesel in the Austrian energy system. *Energies* 2023;16(16). <http://dx.doi.org/10.3390/en16166097>.
- [5] Chiodini A, Bua L, Carnelli L, Zwart R, Vreugdenhil B, Vociante M. Enhancements in Biomass-to-Liquid processes: Gasification aiming at high hydrogen/carbon monoxide ratios for direct Fischer-Tropsch synthesis applications. *Biomass Bioenergy* 2017;106:104–14. <http://dx.doi.org/10.1016/J.BIOMBIOE.2017.08.022>.
- [6] Müller S, Groß P, Rauch R, Zweiler R, Aichernig C, Fuchs M, et al. Production of diesel from biomass and wind power – Energy storage by the use of the Fischer-Tropsch process. *Biomass Convers Biorefinery* 2018;8(2):275–82. <http://dx.doi.org/10.1007/s13399-017-0287-1>.
- [7] Kraussler M, Binder M, Schindler P, Hofbauer H. Hydrogen production within a polygeneration concept based on dual fluidized bed biomass steam gasification. *Biomass Bioenergy* 2018;111:320–9. <http://dx.doi.org/10.1016/J.BIOMBIOE.2016.12.008>.
- [8] Loipersböck J, Luisser M, Müller S, Hofbauer H, Rauch R. Experimental demonstration and validation of hydrogen production based on gasification of lignocellulosic feedstock. *ChemEngineering* 2018;2(4). <http://dx.doi.org/10.3390/chemengineering2040061>.
- [9] Kirnbauer F, Hofbauer H. Investigations on bed material changes in a dual fluidized bed steam gasification plant in güssing, Austria. *Energy Fuels* 2011;25(8):3793–8. <http://dx.doi.org/10.1021/ef200746c>.
- [10] Kuba M, Kraft S, Kirnbauer F, Maierhans F, Hofbauer H. Influence of controlled handling of solid inorganic materials and design changes on the product gas quality in dual fluid bed gasification of woody biomass. *Appl Energy* 2018;210:230–40. <http://dx.doi.org/10.1016/J.APENERGY.2017.11.028>.
- [11] Thunman H, Seemann M, Berdugo Vilches T, Maric J, Pallares D, Ström H, et al. Advanced biofuel production via gasification – lessons learned from 200 man-years of research activity with Chalmers' research gasifier and the GoBiGas demonstration plant. *Energy Sci Eng* 2018;6(1):6–34. <http://dx.doi.org/10.1002/ese3.188>.
- [12] Heyne S, Thunman H, Harvey S. Exergy-based comparison of indirect and direct biomass gasification technologies within the framework of bio-SNG production. *Biomass Convers Biorefinery* 2013;3(4):337–52. <http://dx.doi.org/10.1007/s13399-013-0079-1>.
- [13] Pröll T, Hofbauer H. Process and device for providing a constant product gas rate from a fluidized bed gas generation plant. 2010, WO201006353A3.
- [14] Nigitz T, Göllés M, Aichernig C, Schneider S, Hofbauer H, Horn M. Increased efficiency of dual fluidized bed plants via a novel control strategy. *Biomass Bioenergy* 2020;141:105688. <http://dx.doi.org/10.1016/J.BIOMBIOE.2020.105688>.
- [15] Stanger L, Schirrer A, Bartik A, Kozek M. Minimum-variance model predictive control for dual fluidized bed circulation control. *IFAC-PapersOnLine* 2023;56(2):2701–6. <http://dx.doi.org/10.1016/j.ifacol.2023.10.1364>.
- [16] Glad T, Ljung L. *Control theory*. CRC Press; 2000. <http://dx.doi.org/10.1201/9781315274737>.
- [17] Schwenzler M, Ay M, Bergs T, Abel D. Review on model predictive control: an engineering perspective. *Int J Adv Manuf Technol* 2021;117(5):1327–49. <http://dx.doi.org/10.1007/s00170-021-07682-3>.

- [18] Karl J, Pröll T. Steam gasification of biomass in dual fluidized bed gasifiers: A review. *Renew Sustain Energy Rev* 2018;98:64–78. <http://dx.doi.org/10.1016/j.RSER.2018.09.010>.
- [19] Mauerhofer AM, Schmid JC, Benedikt F, Fuchs J, Müller S, Hofbauer H. Dual fluidized bed steam gasification: Change of product gas quality along the reactor height. *Energy* 2019;173:1256–72. <http://dx.doi.org/10.1016/j.ENERGY.2019.02.025>.
- [20] Fuchs J, Schmid J, Benedikt F, Mauerhofer A, Müller S, Hofbauer H. A general method for the determination of the entrainment in fluidized beds. *Int J Multiphys* 2018;12(4):359–72. <http://dx.doi.org/10.21152/1750-9548.12.4.359>.
- [21] Schmid JC, Benedikt F, Fuchs J, Mauerhofer AM, Müller S, Hofbauer H. Syngas for biorefineries from thermochemical gasification of lignocellulosic fuels and residues—5 years' experience with an advanced dual fluidized bed gasifier design. *Biomass Convers Biorefinery* 2021;11(6):2405–42. <http://dx.doi.org/10.1007/s13399-019-00486-2>.
- [22] Benedikt F. Fuel flexible advanced dual fluidized bed steam gasification [Ph.D. thesis], TU Wien; 2020. <http://dx.doi.org/10.34726/hss.2020.39988>.
- [23] Stanger L, Schirrer A, Benedikt F, Bartik A, Jankovic S, Müller S, et al. Dynamic modeling of dual fluidized bed steam gasification for control design. *Energy* 2023;265:126378. <http://dx.doi.org/10.1016/j.ENERGY.2022.126378>.
- [24] Sun H, Bao G, Yang S, Hu J, Wang H. Numerical study of the biomass gasification process in an industrial-scale dual fluidized bed gasifier with 8MWth input. *Renew Energy* 2023;211:681–96. <http://dx.doi.org/10.1016/j.RENENE.2023.04.118>.
- [25] Liu H, Cattolica RJ, Seiser R, Liao Ch. Three-dimensional full-loop simulation of a dual fluidized-bed biomass gasifier. *Appl Energy* 2015;160:489–501. <http://dx.doi.org/10.1016/j.APENERGY.2015.09.065>.
- [26] Abdelouahed L, Authier O, Mauviel G, Corriou JP, Verdier G, Dufour A. Detailed modeling of biomass gasification in dual fluidized bed reactors under aspen plus. *Energy Fuels* 2012;26(6):3840–55. <http://dx.doi.org/10.1021/ef300411k>.
- [27] Wang L. A Tutorial on Model Predictive Control: Using a Linear Velocity-Form Model. *Dev Chem Eng Miner Process* 2004;12(5–6):573–614. <http://dx.doi.org/10.1002/apj.5500120511>.
- [28] Pannocchia G, Rawlings JB. Disturbance models for offset-free model-predictive control. *AIChE J* 2003;49(2):426–37. <http://dx.doi.org/10.1002/aic.690490213>.
- [29] Maeder U, Borrelli F, Morari M. Linear offset-free model predictive control. *Automatica* 2009;45(10):2214–22. <http://dx.doi.org/10.1016/j.automatica.2009.06.005>.
- [30] Muske KR, Rawlings JB. Model predictive control with linear models. *AIChE J* 1993;39(2):262–87. <http://dx.doi.org/10.1002/aic.690390208>.
- [31] Tippet MJ, Tan CK, Bao J. Non-constant prediction-step MPC for processes with multi-scale dynamics. *IFAC Proc Vol* 2014;47(3):3068–73. <http://dx.doi.org/10.3182/20140824-6-ZA-1003.01093>.
- [32] Mayne DQ, Rawlings JB, Rao CV, Scolaert PO. Constrained model predictive control: Stability and optimality. *Automatica* 2000;36(6):789–814. [http://dx.doi.org/10.1016/S0005-1098\(99\)00214-9](http://dx.doi.org/10.1016/S0005-1098(99)00214-9).
- [33] Schmid JC. Development of a novel dual fluidized bed gasification system for increased fuel flexibility [Ph.D. thesis], TU Wien; 2014. <http://dx.doi.org/10.34726/hss.2014.25397>.
- [34] Diem R. Design, construction and startup of an advanced 100 kW dual fluidized bed system for thermal gasification [Ph.D. thesis], TU Wien; 2015.
- [35] Schmalzl M. Implementierung der MSR-Technik einer 100 kW dual fluid versuchsanlage zur vergasung von festbrennstoffen [Master Thesis], TU Wien; 2014. <http://dx.doi.org/10.34726/hss.2014.23536>.
- [36] Hammerschmid M, Rosenfeld DC, Bartik A, Benedikt F, Fuchs J, Müller S. Methodology for the development of virtual representations within the process development framework of energy plants: From digital model to digital predictive twin—a review. *Energies* 2023;16(6). <http://dx.doi.org/10.3390/en16062641>.
- [37] Lofberg J. YALMIP : a toolbox for modeling and optimization in MATLAB. In: 2004 IEEE international conference on robotics and automation (IEEE cat. no.04CH37508). 2004, p. 284–9. <http://dx.doi.org/10.1109/CACSD.2004.1393890>.
- [38] The Mathworks Inc. MATLAB Optimization Toolbox. 2022, URL <https://www.mathworks.com/products/optimization.html>.

Publication C

Minimum-Variance Model Predictive Control for Dual Fluidized Bed Circulation Control

Lukas Stanger, Alexander Schirrer, Alexander Bartik, and Martin Kozek

IFAC-PapersOnLine 56 (2023) pp. 2701–2706

DOI: [10.1016/j.ifacol.2023.10.1364](https://doi.org/10.1016/j.ifacol.2023.10.1364)

Own Contribution: Conceptualization, Methodology, Validation, Software, Visualization, Writing - original draft



Minimum-Variance Model Predictive Control for Dual Fluidized Bed Circulation Control

Lukas Stanger* Alexander Schirrer* Alexander Bartik**
 Martin Kozek*

* TU Wien, Institute of Mechanics and Mechatronics, Getreidemarkt
 9, 1060 Vienna, Austria (e-mail:

{lukas.stanger,alexander.schirrer,martin.kozek}@tuwien.ac.at)

** TU Wien, Institute of Chemical, Environmental and Bioscience
 Engineering, Getreidemarkt 9, 1060 Vienna, Austria (e-mail:
 alexander.bartik@tuwien.ac.at)

Abstract: Dual fluidized bed steam gasification enables the production of gaseous energy carriers from woody biomass or biogenic residues. The circulation of bed material in dual fluidized bed gasifiers strongly affects the process behavior. Therefore, precise control of the bed material circulation is desired. This paper presents a control algorithm addressing two aspects of the given problem setting: On the one hand, redundant control actuators are available. Typically, there are several air streams to the reactors influencing the bed material circulation. On the other hand, only black box models with uncertainties in their model parameters are available for model-based control design. The presented control algorithm uses a model predictive controller considering known uncertainties in the model parameters and drives the process in a region with the lowest model uncertainties. This results in an improvement of the closed-loop performance when the actual plant deviates from the internal model used for the model predictive control predictions. Simulations show 66 % less offset from the design trajectory with the presented algorithm when compared to a standard model predictive controller.

Copyright © 2023 The Authors. This is an open access article under the CC BY-NC-ND license (<https://creativecommons.org/licenses/by-nc-nd/4.0/>)

Keywords: Model predictive and optimization-based control, Process control applications, Model uncertainties, Control allocation, Dual fluidized bed gasification

1. INTRODUCTION

Dual Fluidized Bed (DFB) steam gasification can be used to produce high-quality product gas from woody biomass or biogenic residues (Benedikt et al. (2018)). For an efficient operation of DFB plants, process variables such as reactor temperatures, product gas mass flow or product gas quality have to be controlled. Typically, a combination of single-input single-output controllers is used to control these process variables, as presented in Nigitz et al. (2020) and Pröll and Hofbauer (2010). Multiple-input multiple-output control concepts cannot be found in the literature for DFB plants, yet offer the chance to increase process efficiency (Stanger et al. (2023)). To control the reactor temperatures or the product gas quality, effective control of the bed material circulating between the two reactors is required since the bed material is transporting both heat and char between the reactors. The bed material circulation in DFB gasifiers is modeled mostly based on computational fluid dynamics and is shown in Liu et al. (2016) or Kraft et al. (2017). Estimating the mass of bed material circulating in fluidized beds is a challenging task and discussed for example in Medrano et al. (2016) and Matsuda (2008). In Stollhof et al. (2018) and Fuchs

et al. (2018) it is shown, that the pressure gradient in the upper part of the combustion reactor (CR) is a reliable indicator for the bed material circulation. The bed material circulation is mainly manipulated by the air streams to the CR: There are air inlets at different reactor heights. Thus, by changes in the air staging, the circulation can be influenced. At the advanced 100 kW DFB pilot plant at TU Wien, three air stages are available at the CR. Therefore, more control actuators are available than variables that need to be controlled.

In process control, split range control is often applied when redundant control actuators are available, as presented in Fonseca et al. (2013) and Reyes-Lúa and Skogestad (2020). In motion control for vehicles and aircrafts, control allocation is applied for over-actuated systems. In Johansen and Fossen (2013) a survey of control allocation algorithms is given and different applications are discussed. A method for control allocation incorporating the information on model uncertainties is presented in Grauer and Pei (2021).

The scope of this work is to present a method on how to handle the availability of redundant control actuators by using the knowledge about model uncertainties. The algorithm leads to the usage of the control actuators in a way that the process is driven within a region of low model uncertainties. The control algorithm is presented

* This work was supported by the project ADORe-SNG, which is funded by the Austrian Climate and Energy Fund (FFG, No.881135).

within a model predictive control (MPC) framework which allows the explicit consideration of input constraints, since constraints often occur in process control problems. Simulations are shown for the cold flow model (CFM) of the advanced 100 kW DFB pilot plant at TU Wien and demonstrate the effectiveness of the proposed algorithm.

2. PROCESS DESCRIPTION

The main components of a DFB gasifier are the gasification reactor (GR) and the combustion reactor (CR). Both reactors are operated as fluidized bed reactors, the GR as a bubbling fluidized bed reactor and the CR as a fast fluidized bed reactor. These two reactors are connected by loop seals. Bed material is constantly circulating between the GR and the CR transporting ungasified fuel from the GR to the CR and heat from the CR to the GR. The amount of heat and ungasified fuel transported between the two reactors depends on the bed material circulation rate (Stollhof et al. (2018)).

2.1 Cold Flow Model of a Dual Fluidized Bed Gasifier

CFMs have been widely used to investigate the fluid dynamical behavior of DFB gasifiers (Shrestha et al. (2016)). In this paper, modeling and control design are based on the CFM at TU Wien, since experiments can be easier carried out at the CFM. Fig. 1 shows the design of the CFM. A detailed description of the experimental setup can be found in Lunzer et al. (2021) and Fuchs (2013).

The CFM at TU Wien is designed in a way that the dimensionless similarity is given to the hot 100 kW pilot plant, which means that dimensionless quantities such as Reynolds number or Archimedes number are similar. Therefore, it behaves similarly in terms of fluid dynamics. The reactors and the loop seals of the CFM are fluidized with air, and bronze particles are used as bed material. Whereas the 100 kW pilot plant has three air inlets to the CR, there are only two air stages available at CFM: Primary air and secondary air. Those are the most significant inputs to manipulate the bed material circulation. The pressure is measured at various positions in both reactors and in the loop seals. For this work, the pressure measurements in the upper part of the CR are relevant and used for control, whereby the pressure difference is denoted as Δp .

2.2 Plant Model

In steady state, the pressure difference Δp in the upper part of the combustion reactor is modeled by the linear relationship

$$\Delta p = b_0 + b_1 \dot{V}_p + b_2 \dot{V}_s, \quad (1)$$

where \dot{V}_p and \dot{V}_s are the primary and secondary air flows, respectively. With the input vector

$$\mathbf{u} = [1 \ \dot{V}_p \ \dot{V}_s]^T = [1 \ u_1 \ u_2]^T, \quad (2)$$

and the parameter vector

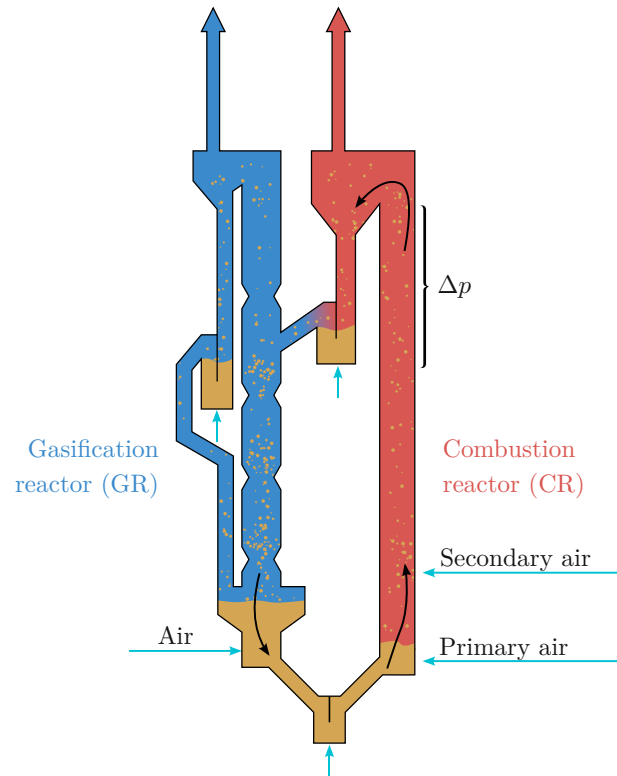


Fig. 1. Cold Flow Model to investigate the fluid dynamical behavior of the advanced 100 kW DFB pilot plant at TU Wien.

$$\boldsymbol{\theta} = [b_0 \ b_1 \ b_2]^T \quad (3)$$

we can write (1) compact to

$$\Delta p = \mathbf{u}^T \boldsymbol{\theta}. \quad (4)$$

The pressure difference Δp corresponds to the system state x . The parameter vector $\boldsymbol{\theta}$ is estimated from measurement data. Moreover, the parameter covariance matrix $\boldsymbol{\Sigma}$ is estimated from measurement data and is later used for control design.

If an input variable is changed step-wise, a PT1-like response can be observed in the pressure difference. This dynamic behavior is modeled by the first order differential equation

$$\dot{x} = \frac{1}{\tau} (-x + b_0 + b_1 u_1 + b_2 u_2) \quad (5)$$

with the time constant τ .

3. METHODS

In this section, first, the procedure of the control algorithm is described. Then, the disturbance model and the observer design are presented, followed by the minimum-variance MPC (MV-MPC) approach proposed as the main contribution.

3.1 Algorithmic Procedure

At each time step k , the following steps are carried out

- (1) *Observer*: Both the model state and a disturbance state are estimated by a Kalman filter.
- (2) *Target Calculation*: An operating point is calculated considering the disturbance state. This operating point is then tracked by the MPC.
- (3) *Solution of the MPC optimization problem*: The optimal sequence of control inputs is calculated by solving the MPC optimization problem.

3.2 Observer Design

In order to capture the plant-model mismatch and unmeasured disturbances the plant model is augmented by a disturbance model as follows:

$$\begin{cases} \dot{x} = \frac{1}{\tau}(-x + b_0 + b_1 u_1 + b_2 u_2 + d) \\ \dot{d} = 0 \\ y = x, \end{cases} \quad (6)$$

with the disturbance state d . This disturbance state models process variables that are influencing the bed material circulation and are slowly changing over time, such as the total amount of bed material in the system. A discretization of the model leads to the state-space system

$$\begin{bmatrix} x_{k+1} \\ d_{k+1} \end{bmatrix} = \begin{bmatrix} a & b_d \\ 0 & 1 \end{bmatrix} \begin{bmatrix} x_k \\ d_k \end{bmatrix} + \begin{bmatrix} \mathbf{b} \\ \mathbf{0} \end{bmatrix} \mathbf{u}_k, \quad (7)$$

$y_k = x_k,$

where the entries a , b_d , and \mathbf{b} in the system matrices are both a function of the continuous-time parameters and the sampling time.

A Kalman filter is designed to estimate both the original state x and the disturbance state d :

$$\begin{bmatrix} \hat{x}_{k+1} \\ \hat{d}_{k+1} \end{bmatrix} = \begin{bmatrix} a & b_d \\ 0 & 1 \end{bmatrix} \begin{bmatrix} \hat{x}_k \\ \hat{d}_k \end{bmatrix} + \begin{bmatrix} \mathbf{b} \\ \mathbf{0} \end{bmatrix} \mathbf{u}_k + \begin{bmatrix} l_x \\ l_d \end{bmatrix} (-y_{m|k} + \hat{x}_k), \quad (8)$$

$\hat{y}_k = \hat{x}_k,$

with the Kalman gain matrix $\mathbf{L} = [l_x \ l_d]^T$ and the measured output variable y_m .

3.3 MPC Cost Function

The MPC is designed to track a constant reference for the output y . A quadratic cost function is formulated and is minimized at every time step k :

$$\min_{\mathbf{U}} J_{\text{MPC}} = \sum_{i=0}^{N-1} (x_{k+i} - \bar{x}_k)^T q (x_{k+i} - \bar{x}_k) + (\mathbf{u}_{k+i} - \bar{\mathbf{u}}_k)^T \Sigma (\mathbf{u}_{k+i} - \bar{\mathbf{u}}_k),$$

$$\begin{aligned} \text{subj. to } & x_{k+i+1} = ax_{k+i} + \mathbf{b}\mathbf{u}_{k+i} + b_d d_k, \\ & x_k = \hat{x}_k, \\ & d_k = \hat{d}_k, \\ & u_{k+1}(1) = 1, \\ & \mathbf{u}_{\min} \leq \mathbf{u}_{k+i} \leq \mathbf{u}_{\max}, \end{aligned} \quad (9)$$

where \mathbf{U} is the input sequence $\mathbf{U} = [\mathbf{u}_k, \dots, \mathbf{u}_{k+N-1}]$ within the prediction horizon N , q is a weighting factor and \bar{x} and $\bar{\mathbf{u}}$ are the target state and target input vector, respectively. The MPC is designed to track these steady-state target values. The calculation of these target variables is discussed in the next section.

3.4 Target Calculation - The Minimum-Variance Approach

The aim of the target calculation is to find an input vector $\bar{\mathbf{u}}_k = [\bar{u}_{1|k}, \bar{u}_{2|k}]^T$ at time step k so that the target output $\bar{y}_k = \bar{x}_k$ meets the reference r_k in a steady state with minimized variance:

$$r_k = b_0 + b_1 \bar{u}_{1|k} + b_2 \bar{u}_{2|k} + d_k. \quad (10)$$

It can be seen that there is no unique solution for $\bar{u}_{1|k}$ and $\bar{u}_{2|k}$ so that (10) is fulfilled.

In this paper, we suggest incorporating knowledge about the model uncertainty to find a solution for the target inputs. The estimate for the parameter vector is given by

$$\hat{\boldsymbol{\theta}} = [\hat{b}_0 \ \hat{b}_1 \ \hat{b}_2]^T. \quad (11)$$

Moreover, the estimate for the parameter covariance matrix $\hat{\Sigma}$ is assumed to be known. The undisturbed model output in a steady state can be written as

$$\hat{y} = \mathbf{u}^T \hat{\boldsymbol{\theta}}. \quad (12)$$

The output variance can be computed by

$$\begin{aligned} \text{Var}(\hat{y}) &= \text{E}\{(\hat{y} - y)^2\} \\ &= \text{E}\{(\mathbf{u}^T \hat{\boldsymbol{\theta}} - \mathbf{u}^T \boldsymbol{\theta})^2\} \\ &= \mathbf{u}^T \text{E}\{(\hat{\boldsymbol{\theta}} - \boldsymbol{\theta})(\hat{\boldsymbol{\theta}} - \boldsymbol{\theta})^T\} \mathbf{u} \\ &= \mathbf{u}^T \hat{\Sigma} \mathbf{u}. \end{aligned} \quad (13)$$

This output variance is taken as the cost function and is minimized to find the target input vector $\bar{\mathbf{u}}_k$ at time step k :

$$\begin{aligned} \min_{\mathbf{u}_k} J_{\text{target}} &= \mathbf{u}_k^T \hat{\Sigma} \mathbf{u}_k, \\ \text{subj. to } & \mathbf{u}_k(1) = 1, \\ & r_k = \hat{b}_0 + \hat{b}_1 \bar{u}_{1|k} + \hat{b}_2 \bar{u}_{2|k} + \hat{d}_k, \\ & \mathbf{u}_{\min} \leq \bar{\mathbf{u}}_k \leq \mathbf{u}_{\max}. \end{aligned} \quad (14)$$

The input constraints in the optimization problem (14) can cause infeasibility. This means that no input vector within the constraints exists so that the model output meets the reference in a steady state. In this case instead the squared steady-state difference between the output and its reference

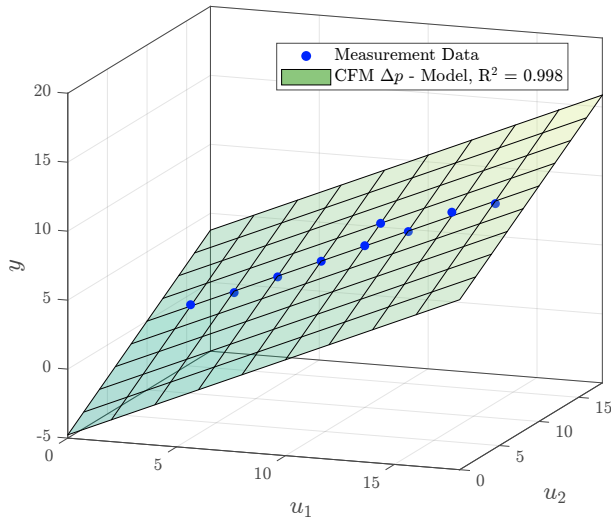


Fig. 2. Measurement points and model for Δp (model output y) as a function of the inputs \hat{V}_p and \hat{V}_s .

$$(r_k - \mathbf{u}_k^T \hat{\boldsymbol{\theta}} + \hat{d}_k)^2 \quad (15)$$

is minimized by solving the quadratic program

$$\begin{aligned} \min_{\mathbf{u}_k} J_{\text{target}} &= \mathbf{u}_k^T \hat{\boldsymbol{\theta}} \hat{\boldsymbol{\theta}}^T \mathbf{u}_k - 2(r_k + \hat{d}_k) \mathbf{u}_k \boldsymbol{\theta} \\ \text{subj. to } \mathbf{u}_k(1) &= 1 \\ \mathbf{u}_{\min} &\leq \mathbf{u}_k \leq \mathbf{u}_{\max}. \end{aligned} \quad (16)$$

4. RESULTS AND DISCUSSION

An identification experiment to find a mathematical model describing the input-output relationships has been carried out at the CFM at TU Wien. The minimum variance MPC approach is tested in simulations and compared to an MPC which does not consider model uncertainties in its design, hereinafter referred to as *Standard MPC*. For this Standard MPC, the identity matrix is used instead of the covariance matrix $\boldsymbol{\Sigma}$ in the cost functions (9) and (14). Thus, the Standard MPC aims to minimize the norm of the input vector.

4.1 Plant Model

Carrying out identification experiments at DFB gasifiers is usually an expensive task. Although industrial plants are running continuously, they are typically operated at the same operating points. Thus, only for a small region of the input space measurement data is available. Our control concept is presented for the CFM, however, the aim is to apply it to a DFB gasifier. Therefore, we assume that only a small data set for system identification is available. Furthermore, we investigate the case that the quality of data is different for different input variables. Fig. 2 shows the data points as well as the identified steady-state model

$$y = -4.7660 + 0.67158u_1 + 0.47462u_2, \quad (17)$$

describing the bed material circulation. The estimated coefficients in (17) show that the first input u_1 , the

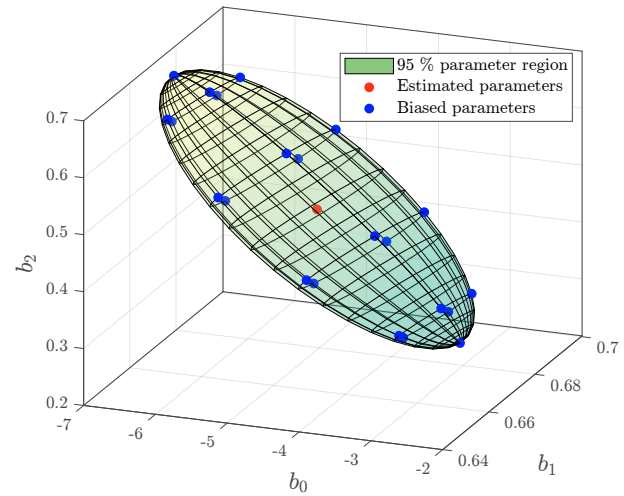


Fig. 3. The ellipsoid gives the region, where the parameters are located with a probability of 95 %. The red point shows the least squares estimate of the model parameters. The blue points are located on the ellipsoid and are used for closed-loop simulations.

primary air, locally has a higher influence on the bed material circulation. Moreover, it can be seen in Fig. 2 that 8 operating points are available with different values in the first input u_1 , the primary air volume flow. For the second input u_2 , however, only 2 different data points are available. This leads to higher uncertainties for the parameter b_2 describing the influence of u_2 on the output. The ellipsoid in Fig. 3 shows the region in which the parameters are located with a probability of 95 %, described by the estimate of the parameter covariance matrix

$$\hat{\boldsymbol{\Sigma}} = \begin{bmatrix} 0.6974 & -5.611e-04 & -0.0675 \\ -5.611e-04 & 1.403e-04 & -7.013e-05 \\ -0.0675 & -7.013e-05 & 0.0067 \end{bmatrix}. \quad (18)$$

The center of the ellipsoid corresponds to the parameter estimate. The closed-loop simulations are done with different plant models, where the parameters are biased to simulate modeling inaccuracies. The blue points in Fig. 3 show the different parameter sets used for the plant models in the closed-loop simulations.

4.2 Circulation Control Without Input Constraints

As a first step, the MPC algorithm is tested without any input constraints. The MV-MPC requires only one parameter, the state weighting q in (9). This parameter is chosen to be $q = 10^{-2}$. No input weighting is necessary, since the estimated parameter covariance matrix $\hat{\boldsymbol{\Sigma}}$ is chosen as the input weighting in the MPC cost function. For the Standard MPC, the state weighting $q = 20$ and the input weighting matrix $\mathbf{R} = \mathbf{I}$ is chosen in the MPC cost function. With these weightings, both MPC algorithms cause the same response to a step in the reference, as long as there are no model inaccuracies considered in the simulation. For the Standard MPC, the computation of the target values is done by minimizing the norm of the input vector. The disturbance model and the observer design are

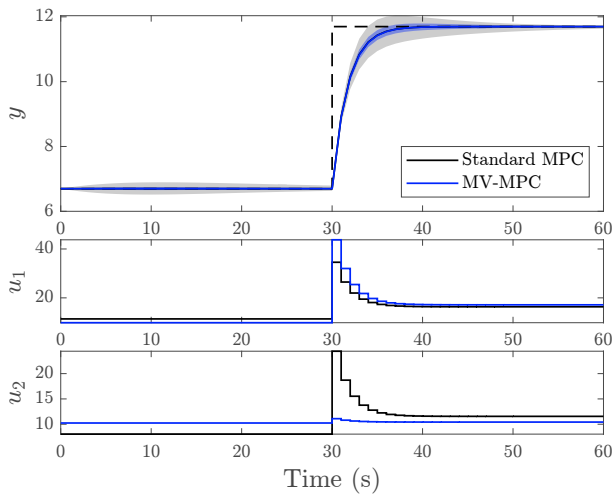


Fig. 4. Simulation of a step in the reference without input constraints.

the same for both MPCs. The Kalman gain matrix \mathbf{L} is computed by solving the discrete-time algebraic Riccati equation, with the process noise covariance matrix $\mathbf{Q} = \mathbf{I}$, and the measurement noise variance $\mathbf{R} = 10^2$.

The closed-loop simulation is carried out with the original plant model and with 22 different plant models that are biased in their parameters. The upper part of Fig. 4 shows the response to a step in the reference. The solid lines show the simulation with an unbiased plant model, which results in the same response for the MV-MPC and the Standard MPC. The areas around the solid lines indicate where the output trajectories are located for the simulations with the biased plant models. It can be seen that for the MV-MPC approach the deviation from the design trajectory can be reduced. For the biased plant models, also before the step in the reference, a deviation from the reference can be observed since the necessary control input needs to be corrected using the disturbance model. However, for the MV-MPC the maximum deviation from the design trajectory before the step in the reference is around 0.05 mbar, therefore it can hardly be seen in the plot. Due to the disturbance model, offset-free reference tracking can be achieved with both MPCs in steady-state (Maeder et al. (2009)). In the lower part of the figure, the input trajectories are shown for the simulation with the unbiased plant models. It can be seen that the MV-MPC avoids the usage of the input u_2 , since changes in this input would lead to a higher variance in the model output. The input trajectories are also shown in Fig. 5. In this figure, also the variance of the steady-state model output according to (13) is shown as a function of the input. As expected, the MV-MPC algorithm keeps the inputs in an area leading to low uncertainties in the model output.

4.3 Circulation Control With Input Constraints

For the second simulation scenario, input constraints are applied and a maximum value of $25 \text{ Nm}^3/\text{h}$ is set as a constraint for both inputs. Simulations are again performed for the original and for biased plant models. Fig. 6 shows the closed-loop step response plot for the MV-MPC and the Standard MPC. Here, the output trajectories with the

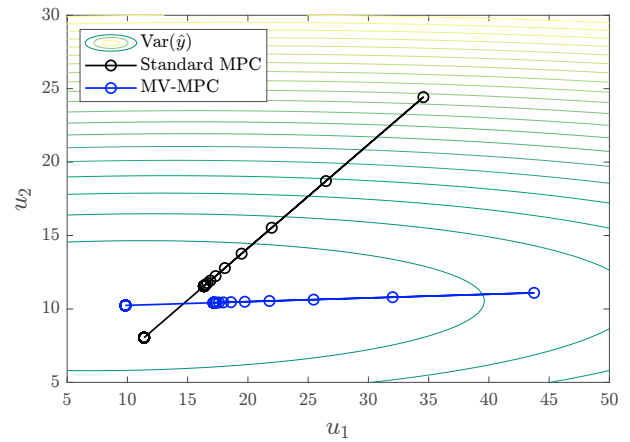


Fig. 5. MPC trajectories in the input space. The contour lines show the model output variance: brighter colors indicate a higher output variance and therefore a higher model uncertainty.

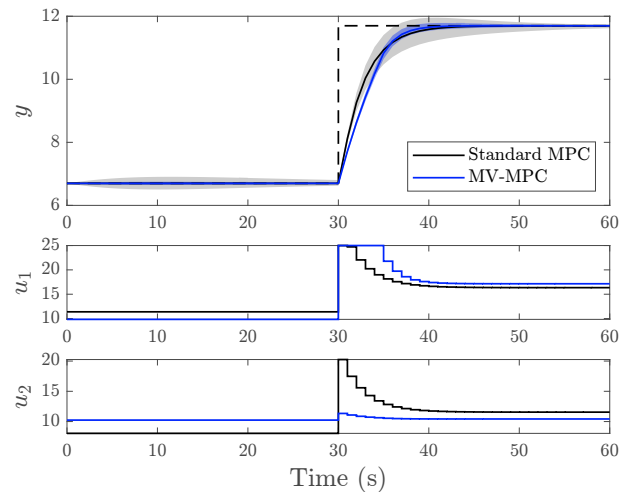


Fig. 6. Simulation of a step in the reference with input constraints. Both inputs are constrained to a maximum of $25 \text{ Nm}^3/\text{h}$.

unbiased plant model deviate for both MPCs, because the constraints are active for different time spans. Moreover, it can be seen that also with input constraints the MV-MPC reduces the deviation from the design trajectory if there are inaccurate parameters in the simulation model. Fig. 7 shows the input trajectories and the model output variance. Again, the MV-MPC keeps the inputs in an area with low model uncertainties.

Table 1 shows the maximum deviations from the design trajectory with the MV-MPC and the Standard MPC, both for the simulation without constraints and with constraints. With the MV-MPC the deviation can be reduced by up to 65.9 %.

5. CONCLUSION

In this paper, an MPC algorithm has been presented, which is beneficial for the case that there are known model uncertainties and redundant inputs for process control. In this case, the proposed MPC algorithm can improve

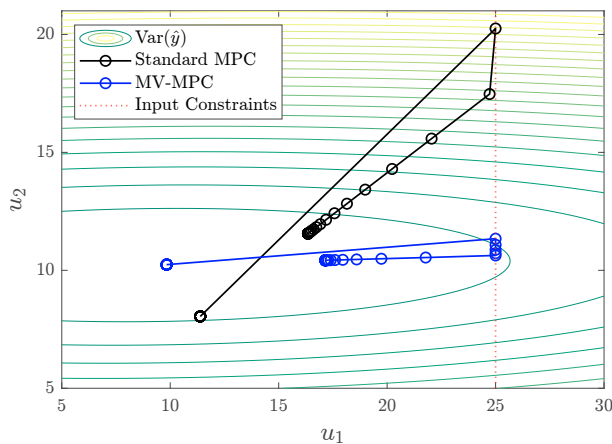


Fig. 7. Input Trajectory.

Table 1. Maximum deviation from the design trajectory.

	Standard MPC	MV-MPC	Δ
without constraints	0.5005 mbar	0.1705 mbar	-65.94 %
with constraints	0.4756 mbar	0.1868 mbar	-60.72 %

the closed-loop performance. This can be advantageous when system identification is expensive and there are high inaccuracies in the parameter estimates, which is often the case for DFB plants. The deviation from the reference can then be reduced and the bed material circulation demanded by the plant operator can be achieved more rapidly. Input constraints can be explicitly considered by the algorithm. An implementation of the proposed algorithm to the 100 kW pilot plant is envisaged.

REFERENCES

- Benedikt, F., Schmid, J.C., Fuchs, J., Mauerhofer, A.M., Müller, S., and Hofbauer, H. (2018). Fuel flexible gasification with an advanced 100 kW dual fluidized bed steam gasification pilot plant. *Energy*, 164, 329–343. doi:10.1016/j.energy.2018.08.146.
- Fonseca, R.R., Schmitz, J.E., Fileti, A.M.F., and Da Silva, F.V. (2013). A fuzzy-split range control system applied to a fermentation process. *Bioresource Technology*, 142, 475–482. doi:10.1016/J.BIORTECH.2013.05.083.
- Fuchs, J., Schmid, J., Benedikt, F., Mauerhofer, A., Müller, S., and Hofbauer, H. (2018). A general method for the determination of the entrainment in fluidized beds. *The International Journal of Multiphysics*, 12(4), 359–372. doi:10.21152/1750-9548.12.4.359.
- Fuchs, J. (2013). *Ermittlung des Betriebskennfeldes einer innovativen Zweibett-wirbelschicht anhand von Kaltmodelluntersuchungen*. University of Leoben.
- Grauer, J.A. and Pei, J. (2021). Minimum-Variance Control Allocation Considering Parametric Model Uncertainty. In *AIAA SCITECH 2022 Forum*, AIAA SciTech Forum. American Institute of Aeronautics and Astronautics. doi:10.2514/6.2022-0749.
- Johansen, T.A. and Fossen, T.I. (2013). Control allocation—A survey. *Automatica*, 49(5), 1087–1103. doi:10.1016/J.AUTOMATICA.2013.01.035.
- Kraft, S., Kirnbauer, F., and Hofbauer, H. (2017). CPFDD simulations of an industrial-sized dual fluidized bed steam gasification system of biomass with 8 MW fuel input. *Applied Energy*, 190, 408–420. doi:10.1016/J.APENERGY.2016.12.113.
- Liu, H., Cattolica, R.J., and Seiser, R. (2016). CFD studies on biomass gasification in a pilot-scale dual fluidized-bed system. *International Journal of Hydrogen Energy*, 41(28), 11974–11989. doi:10.1016/J.IJHYDENE.2016.04.205.
- Lunzer, A., Kraft, S., Müller, S., and Hofbauer, H. (2021). CPFDD simulation of a dual fluidized bed cold flow model. *Biomass Conversion and Biorefinery*, 11(1), 189–203. doi:10.1007/s13399-020-01229-4.
- Maeder, U., Borrelli, F., and Morari, M. (2009). Linear offset-free Model Predictive Control. *Automatica*, 45(10), 2214–2222. doi:10.1016/j.automatica.2009.06.005.
- Matsuda, S. (2008). Measurement of solid circulation rate in a circulating fluidized bed. *Powder Technology*, 187(2), 200–204. doi:10.1016/J.POWTECH.2008.02.004.
- Medrano, J.A., Nordio, M., Manzolini, G., van Sint Annaland, M., and Gallucci, F. (2016). On the measurement of solids circulation rates in interconnected fluidized beds: Comparison of different experimental techniques. *Powder Technology*, 302, 81–89. doi:10.1016/J.POWTECH.2016.08.035.
- Nitz, T., Göllies, M., Aichernig, C., Schneider, S., Hofbauer, H., and Horn, M. (2020). Increased efficiency of dual fluidized bed plants via a novel control strategy. *Biomass and Bioenergy*, 141, 105688. doi:10.1016/J.BIOMBIOE.2020.105688.
- Pröll, T. and Hofbauer, H. (2010). Process and device for providing a constant product gas rate from a fluidized bed gas generation plant.
- Reyes-Lúa, A. and Skogestad, S. (2020). Multi-input single-output control for extending the operating range: Generalized split range control using the baton strategy. *Journal of Process Control*, 91, 1–11. doi:10.1016/J.JPROCONT.2020.05.001.
- Shrestha, S., Ali, B.S., and Binti Hamid, M.D. (2016). Cold flow model of dual fluidized bed: A review. *Renewable and Sustainable Energy Reviews*, 53, 1529–1548. doi:10.1016/J.RSER.2015.09.034.
- Stanger, L., Schirrer, A., Benedikt, F., Bartik, A., Jankovic, S., Müller, S., and Kozek, M. (2023). Dynamic modeling of dual fluidized bed steam gasification for control design. *Energy*, 265, 126378. doi:10.1016/J.ENERGY.2022.126378.
- Stollhof, M., Penthor, S., Mayer, K., and Hofbauer, H. (2018). Estimation of the solid circulation rate in circulating fluidized bed systems. *Powder Technology*, 336, 1–11. doi:10.1016/J.POWTECH.2018.05.033.

Publication D

Gaussian Process Regression-Based Control of Solids Circulation Rate in Dual Fluidized Bed Gasification

Lukas Stanger, Alexander Bartik, Matthias Binder, Alexander Schirrer, Stefan Jakubek, and Martin Kozek

IEEE Access 12 (2024) pp. 138535–138546

DOI: [10.1109/ACCESS.2024.3466394](https://doi.org/10.1109/ACCESS.2024.3466394)

Own Contribution: Conceptualization, Methodology, Validation, Software, Visualization, Writing - original draft

Received 16 August 2024, accepted 15 September 2024, date of publication 23 September 2024, date of current version 3 October 2024.

Digital Object Identifier 10.1109/ACCESS.2024.3466394



Gaussian Process Regression-Based Control of Solids Circulation Rate in Dual Fluidized Bed Gasification

LUKAS STANGER¹, ALEXANDER BARTIK², MATTHIAS BINDER^{2,3}, ALEXANDER SCHIRNER¹, STEFAN JAKUBEK¹, AND MARTIN KOZEK¹

¹Institute of Mechanics and Mechatronics, TU Wien, 1060 Vienna, Austria

²Institute of Chemical, Environmental, and Bioscience Engineering, TU Wien, 1060 Vienna, Austria

³BEST-Bioenergy and Sustainable Technologies GmbH, 8010 Graz, Austria

Corresponding author: Lukas Stanger (lukas.stanger@tuwien.ac.at)

This work was supported in part by the Project Comprehensive Automation, Digitalisation and Optimization of Renewable and Sustainable SNG-production (ADORE-SNG), which is funded by the Austrian Research Promotion Agency (FFG) under Grant 881135; and in part by Technische Universität Wien (TU Wien) Bibliothek, Austria for financial support through its Open Access Funding Program.

ABSTRACT In dual fluidized bed (DFB) gasification, the solids circulation rate is critical as it determines the amount of char and heat transported between the interconnected reactors. In DFB plants, multiple control inputs are typically available to control the solids circulation rate, resulting in an over-actuated system. We propose a modeling and control method based on Gaussian process regression, a technique that provides a measure of confidence in the model prediction. The availability of redundant control inputs is resolved by explicitly incorporating the prediction confidence information into the control algorithm to drive the process in regions of low model uncertainty. To address plant-model mismatches, a disturbance model is employed, and an extended Kalman filter is used to estimate both system and disturbance states, enabling offset-free tracking of constant references. Modeling and closed-loop simulation results for both a 100 kW and a 1 MW DFB gasification plant demonstrate the applicability of the method to different plants. Experimental results are presented for the 100 kW plant, demonstrating the successful control of the circulation rate by the proposed algorithm.

INDEX TERMS Control, dual fluidized bed gasification, extended Kalman filter, Gaussian process regression, solids circulation rate.

I. INTRODUCTION

As the global energy demand continues to rise and greenhouse gas emissions have to be reduced, sustainable energy solutions are needed [1]. Gasification of biomass or residues can be employed to produce sustainable energy carriers. Dual fluidized bed (DFB) steam gasification represents a promising pathway to produce a product gas that is primarily composed of hydrogen, carbon monoxide, carbon dioxide, and methane [2]. This product gas can further be upgraded for example to synthetic natural gas [3], [4], Fischer-Tropsch liquids [5], [6], or pure hydrogen [7], [8]. These conversions

have substantial potential for both the energy sector and chemical manufacturing, providing a versatile platform for generating clean fuels from renewable resources.

A DFB gasification plant essentially consists of two interconnected reactors, a gasification reactor (GR) and a combustion reactor (CR). Both reactors are operated as fluidized bed reactors. Bed material continuously circulates between those two reactors and transports heat from the CR to the GR and ungasified feedstock from the GR to the CR. The solids circulation rate is thus crucial for the process since it influences reactor temperatures as well as product gas composition and tar content [9]. Therefore, its efficient control is desired. Typically, multiple air inlets to the CR are available to control the circulation rate, resulting in redundant

The associate editor coordinating the review of this manuscript and approving it for publication was Ángel F. García-Fernández .

actuators for control. The mass of circulating bed material is difficult to measure. However, the pressure drop in the upper CR is a reliable indicator of the solids circulation rate [10].

To implement model-based control, a mathematical process model is needed. Studies on modeling the solids circulation in DFB gasification plants mainly rely on computational fluid dynamics (CFD), such as [11], [12]. Process simulation based on CFD requires high computational effort and is thus less practical for real-time control applications. An alternative approach is to use data-driven modeling approaches such as artificial neural networks as presented in [13]. A major challenge, thereby, is the limited availability of training data.

The application of Gaussian processes (GP) to regression problems has been presented in [14]. GP regression includes a measure of the prediction uncertainty in the model prediction. An application in control has been proposed in [15] for nonlinear systems that are linear in their input. For general nonlinear systems, an internal model controller has been presented in [16] and a model predictive control approach in [17].

Linear methods for controlling the solids circulation rate in DFB gasification plants have been proposed in [18] and [19]. However, these approaches are plant-specific and lack general applicability. To the best of the authors' knowledge, no nonlinear methods have been published in this context. This work addresses this gap by presenting an approach based on GP regression, as it can be used to map nonlinearities. Additionally, the method incorporates an explicit measure of uncertainty in its predictions. The presented control approach considers this uncertainty measure as well as the availability of redundant control actuators to drive the system into a region of low model uncertainty. In contrast to linear methods for solids circulation control, the method proposed in this work offers more flexibility and improved transferability to other plants. The method is applied to two different plants to demonstrate the ease of implementation across plants without extensive modeling efforts.

II. PROCESS DESCRIPTION

This section gives a concise overview of the DFB process, highlighting key information essential for controlling the solids circulation rate. In addition, the two plants considered in this paper are described: a pilot plant with 100 kW thermal fuel input and a demonstration plant with 1 MW thermal fuel input. Fig. 1 illustrates the design of the DFB gasification plants. Comprehensive descriptions of the DFB process can be found in [2] and [20]. Detailed information on the 100 kW pilot plant are given in [21] and [22], while more details on the 1 MW demonstration plant can be found in [23] and [24].

A. DUAL FLUIDIZED BED STEAM GASIFICATION

DFB steam gasification converts a feedstock, which can be biomass or biogenic residues, into a product gas by separating the gasification process taking place in the GR from the combustion process in the CR. These two interconnected

reactors are both operated as fluidized bed reactors. The GR is operated as a bubbling fluidized bed reactor using steam as the gasification agent. The CR is operated as a fast fluidized bed reactor using air for fluidization. The bed material is constantly circulated between these two reactors. The feedstock is fed into the GR, where drying, devolatilization, and gasification take place. A portion of the feedstock remains ungasified and is transported as char by the bed material to the CR via a loop seal or chute at the bottom of the system. In the CR, the char is combusted, which heats the bed material. The hot bed material is returned to the GR through a loop seal at the top of the unit. The heat is required for the overall endothermic gasification reactions in the GR. The loop seals and chute, if present, are also fluidized by steam.

For better gas-solid interaction in the GR, a reactor design has been proposed in [25] that includes a countercurrent column above the freeboard in the GR. This design is intended to enhance the gas-solid contact and thus reduce the tar content in the product gas and increase the fuel flexibility of the process, allowing the gasification of low-cost feedstocks such as plastic waste. Both the 100 kW pilot plant and the 1 MW demonstration plant use this new design.

B. THE SOLIDS CIRCULATION RATE IN DFB GASIFICATION PLANTS

To adjust the solids circulation rate, the CR typically has multiple air inlets at different heights within the reactor. This design allows the solids circulation rate to be adjusted while maintaining the total amount of air required for complete combustion in the CR. Air introduced at lower levels of the reactor tends to lift the bed material upward, thereby increasing circulation. In contrast, air introduced at higher levels has less of an effect on circulation or may even reduce it.

Measurement of the solids circulation rate in circulating fluidized bed systems is challenging, and different approaches have been proposed. Several methods are reviewed in [26]. Some of them are based on interrupting the particle flow and measuring the accumulation of bed material as used in [27] and [28]. Other methods use optical measurements [29] or placing an obstacle in the flow and measuring the impact [30]. Other methods are based on measuring the pressure drop in the CR [10], [31], [32]. This method can be applied to industrial plants and is also applicable to hot plant operations. In this work, we directly interpret the pressure drop at the top of the CR as an indicator of the solids circulation rate and present a method to control it by adjusting the air staging in the CR.

C. DIFFERENCES IN THE DESIGN OF THE 100 KW PILOT PLANT AND THE 1 MW DEMONSTRATION PLANT

The design of the two DFB plants considered in this work is visualized in Fig. 1. The main differences are described below.

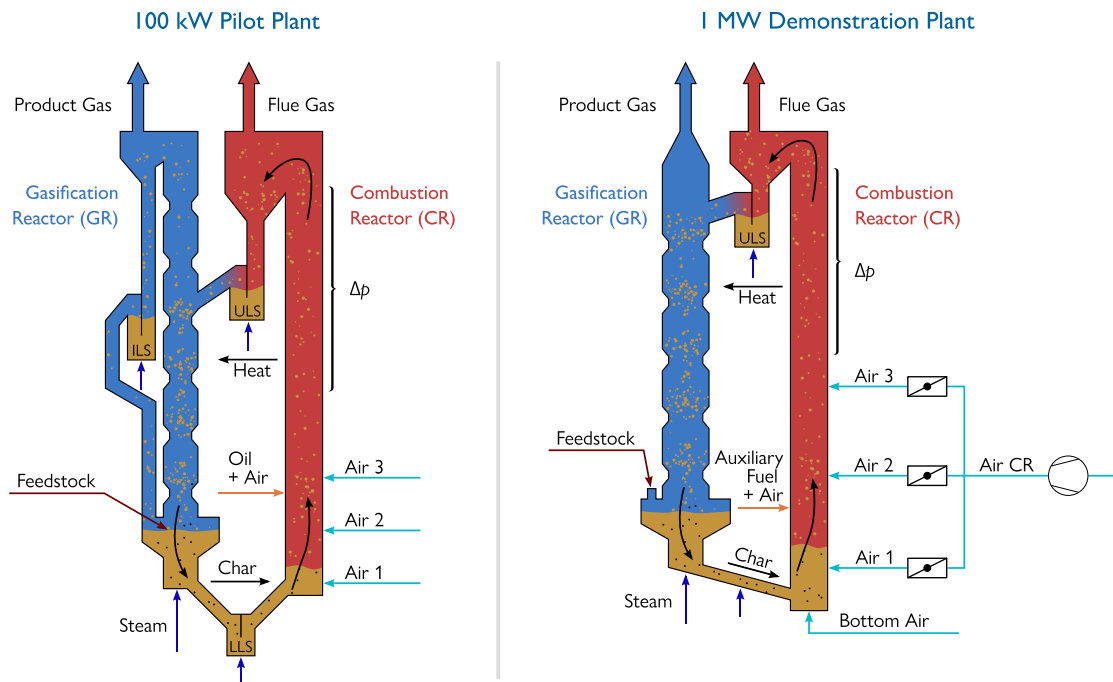


FIGURE 1. Design of the 100 kW pilot plant and the 1 MW demonstration plant, adopted from [13].

1) AIR SUPPLY TO THE CR

The most relevant process input variable for controlling the solids circulation rate is the air supply to the CR. In the 100 kW pilot plant, air can be supplied to the CR through three different air stages. The airflow is measured separately at each stage, and low-level controllers have been implemented to adjust the individual air streams as set by the plant operator or a high-level controller. For the 1 MW demonstration plant, in addition to the three air stages, there is a bottom air stage. The airflow through the bottom air stage to the CR is measured separately. For the other three air stages, only the total airflow is measured. This total airflow can be adjusted by changing the power of the compressor. The air can be distributed to the three air stages by adjusting the positions of the butterfly valves on the three stages. The valve for air 1 remains open during operation, and air is distributed by adjusting the valves for air 2 and air 3.

For both plants, additional air is supplied to the CR along with the auxiliary fuel. For the 100 kW pilot plant, a constant flow of 4 Nm³/h is fed to the CR, while for the 1 MW demonstration plant, 40 Nm³/h is provided.

2) LOWER LOOP SEAL AND CHUTE

For the 1 MW demonstration plant, a chute is used instead of a loop seal to connect the GR and the CR at the bottom. This is to allow the use of heterogeneous feedstocks, some of which also contain larger particles that could clog a loop seal.

3) AUXILIARY FUEL

To provide sufficient heat for the gasification reactions and for temperature control, auxiliary fuel is fed to the CR.

For the 100 kW plant, heating oil is used. Auxiliary fuel is particularly necessary to compensate for the relatively high heat losses that occur at the pilot plant scale. Industrial plants typically do not use heating oil as an auxiliary fuel, but product gas can be recirculated to the CR. In the 1 MW plant, both fuel supply options are implemented. In addition, emulsion fluid from the product gas cleaning can be fed to the CR.

4) INTERNAL LOOP SEAL

For the 100 kW pilot plant, a gravity separator is used, and the separated particles are returned to the gasifier reactor (GR) via an internal loop seal. In the 1 MW demonstration plant, the product gas passes through a radiation cooler after exiting the GR, where the separated particles are then fed back to the GR (not shown in Fig. 1).

D. EXPERIMENTAL SETUP

Both plants are equipped with various measurement and actuation devices. The measurement and actuation equipment for the process variables presented in this work are listed in Table 1.

The experiments at the 100 kW pilot plant were conducted using softwood pellets as feedstock. The bed material consisted of a mixture of 80 % olivine and 20 % limestone.

Experiments at the 1 MW demonstration plant were conducted using olivine as the bed material, with the occasional addition of limestone to enhance catalytic activity. The test runs utilized various feedstocks, including wood

TABLE 1. Instrumentation for both the 100 kW pilot plant and the 1 MW demonstration plant.

	Process variable	Measurement	Actuator
100 kW	Pressure	Kalinsky pressure transmitter type DS1	-
	Air flows	Krohne H250	Bürkert electromotive 2 way globe proportional valve 3280
	Fuel feed	Rot. speed of dosing screws*	Motor with ABB ACS355 drive
1 MW	Pressure	Endress+Hauser PMC21	-
	Total air flow	Endress+Hauser Prowirl F 200	Elmo Rietschle (Gardner Denver) type DLR 301
	Bottom air	Endress+Hauser Prowirl F 200	Bürkert globe control valve 8802 GD with positioner 8692
	Fuel feed	Rot. speed of dosing screws*	SEW Eurodrive type KF77 DRN100LS4/V/PK gearmotor
	Valve positions	AGS butterfly valve RDB-L, pneumatic actuator PAG-E92-S10, limit switch ELR.ER, Siemens SIPART PS2 valve positioner	

* The dosing screws are calibrated before every test run.

chips, softwood pellets, bark, forest residues, and a mixture of plastic residues and wood chips.

III. MODELING

This section describes the modeling approach used to model the pressure difference Δp in the upper CR, which represents the solids circulation rate. Given the nonlinearities present in the static input-output relationship, combined with the fact that the system dynamics can be adequately represented by a linear time-invariant (LTI) model, we employ a Hammerstein model. Fig. 2 visualizes the structure of the Hammerstein model and the model inputs used for the two different plants considered in this work. Preliminary studies have identified these model inputs as the process variables that most significantly affect the solids circulation rate. The model consists of a nonlinear static part and a linear dynamic part. We use GP regression for the static part to describe the input-output relationship at steady state, using steady-state process data as training data. The linear dynamic model captures the system dynamics and includes a disturbance model to account for plant model mismatch and unmeasured disturbances.

Additionally, artificial neural networks (ANNs) are utilized as simulation models for conducting closed-loop tests of the control algorithms, as described in the last part of this section. The use of ANNs allows the validation of the

controller's performance against a model that is unknown to the controller. Furthermore, ANNs are chosen for their ability to model nonlinearities in the process.

A. GAUSSIAN PROCESS REGRESSION

This section gives a brief introduction to GP regression. More detailed explanations can be found in [33] and [34].

Assuming a training dataset consisting of input measurements $\bar{\mathbf{U}} = [\bar{\mathbf{u}}_1, \dots, \bar{\mathbf{u}}_N]$ and the corresponding output measurements $\bar{\mathbf{y}} = [\bar{y}_1, \dots, \bar{y}_N]$. The goal is to predict a new output \bar{y}_* given a new input vector $\bar{\mathbf{u}}_*$.

The outputs $\bar{\mathbf{y}} = [\bar{y}_1(\bar{\mathbf{u}}_1), \dots, \bar{y}_N(\bar{\mathbf{u}}_N)]$ are assumed to be random variables with a joint normal distribution, thus

$$\bar{\mathbf{y}} \sim \mathcal{N}(\boldsymbol{\mu}, \mathbf{C}), \quad (1)$$

where $\boldsymbol{\mu}$ is the mean vector and \mathbf{C} is the covariance matrix. In many applications, the mean vector is assumed to be the zero vector after the data has been appropriately scaled. The entries of the covariance matrix \mathbf{C} are calculated using a covariance function $c(\cdot, \cdot)$, defined as

$$C_{ij} = c(\bar{\mathbf{u}}_i, \bar{\mathbf{u}}_j). \quad (2)$$

A popular choice for the covariance function is the squared exponential covariance function

$$c(\bar{\mathbf{u}}_i, \bar{\mathbf{u}}_j) = \sigma_f^2 \exp\left(-\frac{1}{2} \frac{\|\bar{\mathbf{u}}_i - \bar{\mathbf{u}}_j\|^2}{\sigma_l^2}\right) + \delta_{ij} \sigma_n^2, \quad (3)$$

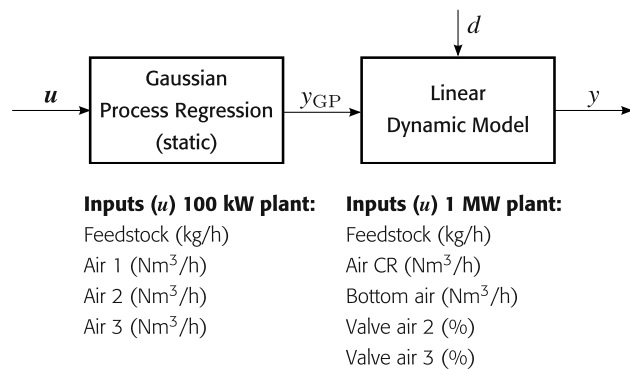
where the hyperparameters $\boldsymbol{\theta} = [\sigma_f, \sigma_l, \sigma_n]^T$ are governing the function's amplitude, length-scale, and noise level, respectively. The Kronecker delta δ_{ij} is defined as

$$\delta_{ij} = \begin{cases} 1 & \text{if } i = j, \\ 0 & \text{if } i \neq j. \end{cases} \quad (4)$$

This covariance function ensures that outputs \bar{y}_i and \bar{y}_j will have higher covariance if their corresponding inputs $\bar{\mathbf{u}}_i$ and $\bar{\mathbf{u}}_j$ are closer in the input space.

To predict a new output \bar{y}_* , a joint normal distribution is assumed for both the training points and the new data point, leading to

$$\begin{bmatrix} \bar{\mathbf{y}} \\ \bar{y}_* \end{bmatrix} \sim \mathcal{N}\left(\mathbf{0}, \begin{bmatrix} \mathbf{C} & \mathbf{c}_* \\ \mathbf{c}_*^T & c_{**} \end{bmatrix}\right), \quad (5)$$

**FIGURE 2.** Hammerstein model structure and model inputs used for the two different DFB plants.

where \mathbf{c}_* is the covariance of the training outputs and the new output, given by

$$\mathbf{c}_* = c(\bar{\mathbf{U}}, \bar{\mathbf{u}}_*), \quad (6)$$

and c_{**} is the variance of the new input $\bar{\mathbf{u}}_*$, calculated as

$$c_{**} = c(\bar{\mathbf{u}}_*, \bar{\mathbf{u}}_*). \quad (7)$$

Given the observed training outputs $\bar{\mathbf{y}}$, the prediction for \bar{y}_* is derived by computing the conditional normal distribution

$$\mu_* = \mathbf{c}_*^T \mathbf{C}^{-1} \bar{\mathbf{y}}, \quad (8a)$$

$$\sigma_*^2 = c_{**} - \mathbf{c}_*^T \mathbf{C}^{-1} \mathbf{c}_*, \quad (8b)$$

with the mean μ_* and the variance σ_* of the predicted output.

A common approach to training the hyperparameters θ , which is also used in this work, is to maximize the logarithmic marginal likelihood,

$$\log p(\bar{\mathbf{y}} | \mathbf{U}, \theta) = -\frac{1}{2} \bar{\mathbf{y}}^T \mathbf{C}^{-1} \bar{\mathbf{y}} - \frac{1}{2} \log |\mathbf{C}| - \frac{N}{2} \log 2\pi, \quad (9)$$

where $p(\bar{\mathbf{y}} | \mathbf{U}, \theta)$ is the probability that the training data was generated by the model given the input data and the hyperparameters.

Note that for each prediction, all the training data points are used, which can lead to a high computational effort for a large number of training data points. In [35], approximation methods are given to reduce this computational effort. In this work, the full data set is used to make predictions.

B. HAMMERSTEIN MODEL

GP regression is used to predict the output at steady state, hereinafter referred to as y_{GP} . In the real process, changes in input variables do not immediately affect the output. However, dynamic behavior can be observed. To incorporate these dynamics into the model, a linear dynamic model is used in series with the GP regression. In addition, a disturbance state is added to the model to account for plant model mismatch and unmeasured disturbances acting on the process. This disturbance state adds an integrator to the plant model, which later enables offset-free tracking of constant references. The resulting model is described by the differential equations

$$\begin{cases} \dot{x}(t) = \frac{1}{\tau}(-x(t) + y_{\text{GP}}(\mathbf{u}(t)) + d(t)), \\ \dot{d}(t) = 0, \\ y(t) = x(t), \end{cases} \quad (10)$$

where $x(t)$ and $d(t)$ are the system state and the disturbance state, respectively.

Both the state estimator and the controller are implemented in discrete time. Therefore, the model is discretized assuming zero-order hold for the GP prediction y_{GP} and the disturbance

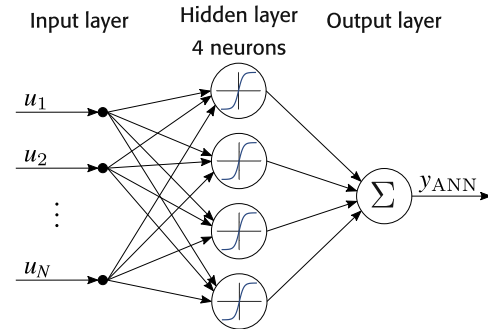


FIGURE 3. Structure of the artificial neural network (ANN) used as a simulation model in closed-loop simulations, where y_{ANN} represents the ANN's prediction.

state d , which leads to

$$\begin{cases} x_{k+1} = ax_k + by_{\text{GP}}(\mathbf{u}_k) + bd_k, \\ d_{k+1} = d_k, \\ y_k = x_k, \end{cases} \quad (11)$$

where

$$a = e^{-T_s/\tau}, \quad b = 1 - e^{-T_s/\tau}, \quad (12)$$

with the sampling time T_s . The GP prediction is a normally distributed random variable

$$y_{\text{GP}} \sim \mathcal{N}(\mu_{\text{GP}}, \sigma_{\text{GP}}^2). \quad (13)$$

This can be decomposed to

$$y_{\text{GP}} = \mu_{\text{GP}} + \eta_{\text{GP}}, \quad (14)$$

where

$$\eta_{\text{GP}} \sim \mathcal{N}(0, \sigma_{\text{GP}}^2). \quad (15)$$

C. ARTIFICIAL NEURAL NETWORKS AS SIMULATION MODELS

An ANN is trained for each plant using the same model inputs as those used for GP regression. Unlike GP regression, the ANNs are trained on time series data. Each ANN consists of a single hidden layer with four neurons and an output layer, as shown in Fig. 3. The neurons in the hidden layer use tangent sigmoid activation functions, while the output layer establishes a linear relationship between the outputs of the hidden layer neurons and the ANN's final output. Quasi-Newton backpropagation is used to train the networks using the MATLAB Deep Learning Toolbox [36].

IV. STATE ESTIMATION AND NONLINEAR CONTROL

A. EXTENDED KALMAN FILTER FOR STATE ESTIMATION

An extended Kalman filter (EKF) [37] is used to estimate both the system state x and the disturbance state d . It is assumed that zero mean white noise drives the disturbance state d and acts on the measured output y . For the system state x , it is assumed that the uncertainty originates solely from the

GP prediction, which is normally distributed with a known variance. This leads to the following model for the EKF:

$$\begin{cases} x_{k+1} = ax_k + b\mu_{\text{GP}}(\mathbf{u}_k) + bd_k + b\eta_{\text{GP}}(\mathbf{u}_k), \\ d_{k+1} = d_k + w_k, \\ y_k = x_k + v_k, \end{cases} \quad (16)$$

with

$$w_k \sim \mathcal{N}(0, \sigma_w^2), \quad v_k \sim \mathcal{N}(0, \sigma_v^2). \quad (17)$$

To estimate the states, first, a prediction step is carried out

$$\begin{aligned} \hat{x}_{k+1}^- &= a\hat{x}_k + b\mu_{\text{GP}}(\mathbf{u}_k) + b\hat{d}_k, \\ \hat{d}_{k+1}^- &= \hat{d}_k, \\ \mathbf{P}_k^- &= \mathbf{F}\mathbf{P}_{k-1}\mathbf{F}^T + \mathbf{Q}_k, \end{aligned} \quad (18)$$

with the prediction of the state covariance matrix \mathbf{P}_k^- , the system matrix of the augmented system \mathbf{F} , and the covariance matrix of the process noise \mathbf{Q}_k , which are

$$\mathbf{F} = \begin{bmatrix} a & b \\ 1 & 0 \end{bmatrix}, \quad \mathbf{Q}_k = \begin{bmatrix} b^2\sigma_{\text{GP}}^2 & 0 \\ 0 & \sigma_w^2 \end{bmatrix}. \quad (19)$$

The prediction step is followed by a correction step

$$\begin{aligned} \mathbf{k}_k &= \mathbf{P}_k^- \mathbf{h}^T (\mathbf{h}\mathbf{P}_k^- \mathbf{h}^T + r)^{-1} \\ \begin{bmatrix} \hat{x}_k \\ \hat{d}_k \end{bmatrix} &= \begin{bmatrix} \hat{x}_k^- \\ \hat{d}_k^- \end{bmatrix} + \mathbf{k}_k (y_k - \hat{x}_k^-) \\ \mathbf{P}_k &= (\mathbf{I} - \mathbf{k}_k \mathbf{h}) \mathbf{P}_k^- \end{aligned} \quad (20)$$

with

$$r = \sigma_v^2, \quad \mathbf{h} = [1 \quad 0]. \quad (21)$$

Note that no approximation by model linearization is necessary because the state equation is nonlinear only in the input, not in the state.

B. NONLINEAR CONTROLLER DESIGN

For the process under consideration, multiple control inputs are available to control a single output. In addition, the GP prediction includes information about the confidence of the prediction. These two aspects are considered in the control design: A steady-state input vector $\bar{\mathbf{u}}_k$ should be found so that the output meets the reference r_k at steady state. Since there is no unique solution to this problem, $\bar{\mathbf{u}}_k$ is computed by solving the optimization problem

$$\min_{\bar{\mathbf{u}}_k} J = \sigma_{\text{GP}}^2(\bar{\mathbf{u}}_k) + \lambda \|\bar{\mathbf{u}}_k - \mathbf{u}_{k-1}\|, \quad (22a)$$

$$\text{subject to } \mu_{\text{GP}}(\bar{\mathbf{u}}_k) = r_k - \hat{d}_k, \quad (22b)$$

$$\bar{\mathbf{u}}_k \in \mathbb{U}, \quad (22c)$$

at each time step k , assuming that there are regions in the input space with higher and regions with lower uncertainty in the GP prediction. The first term in the cost function (22a) represents the uncertainty of the GP prediction, which is, generally a non-convex function. To avoid large steps in the input space for small improvements in uncertainty, the second

term is added to the cost function, with a weighting factor $\lambda \geq 0$. Constraint (22b) ensures that an input vector is found such that the GP prediction matches the reference corrected by the estimated disturbance state \hat{d}_k . This correction by the disturbance state enables offset-free tracking of a constant reference, despite plant model mismatch or unmeasured disturbances acting on the process, and incorporates the feedback in the closed-loop system. By restricting the input space with (22c), some inputs that should not be used by the controller to control the output, such as the feedstock feed rate, can be fixed. In addition, upper and lower bounds can be implemented for the control inputs.

Since the cost function is generally non-convex, we solve the optimization problem (22) multiple times with different initial conditions, where the different initial conditions are generated by Latin hypercube sampling [38]. The solution with the lowest value of the cost function is then selected from the feasible solutions. The cost function is minimized using `fmincon` from the MATLAB Optimization Toolbox [39].

The optimization problem (22) may be infeasible, e.g. if a reference is set to a value that can not be reached according to GP regression. In this case, an alternative optimization problem is solved as a fallback that minimizes the squared difference between the GP prediction and the reference, corrected by the estimated disturbance state, which is

$$\min_{\bar{\mathbf{u}}_k} J = (\mu_{\text{GP}}(\bar{\mathbf{u}}_k) - r_k + \hat{d}_k)^2, \quad (23a)$$

$$\text{subject to } \sigma_{\xi}^2(\bar{\mathbf{u}}_k) \leq \sigma_{\text{GP,max}} \quad (23b)$$

$$\bar{\mathbf{u}}_k \in \mathbb{U}. \quad (23c)$$

With (23b), an upper bound for the uncertainty of the model prediction $\sigma_{\text{GP,max}}$ is established to prevent finding a solution in regions of the input space where limited model information is available. Constraint (23b) may still lead to infeasibility, which can be avoided by omitting it.

Up to this point, the control input has been selected to ensure that the output will match the reference at steady state. However, this approach can result in abrupt, step-like changes in the control input, e.g. if the reference is changed stepwise. Such rapid changes in the control input may not be desired by the operator and the excitation of higher modes, which are not represented in the model, can be avoided. This can be avoided by not applying $\bar{\mathbf{u}}_k$ directly, but by applying a first-order delayed input \mathbf{u}_k to the process, calculated as

$$\mathbf{u}_k = (\mathbf{I} + \mathbf{R}_c)^{-1} (\mathbf{I}\bar{\mathbf{u}}_k + \mathbf{R}_c \mathbf{u}_{k-1}), \quad (24)$$

where \mathbf{R}_c is a weighting matrix. For $\mathbf{R}_c = \mathbf{0}$, $\bar{\mathbf{u}}_k$ is applied to the process immediately, while higher values in \mathbf{R}_c result in smoother control inputs.

V. RESULTS AND DISCUSSION

This section presents modeling and controller simulation results for both the 100 kW and the 1 MW plant. In addition, experimental closed-loop results are shown for the 100 kW plant. All of the algorithms are implemented in MATLAB.

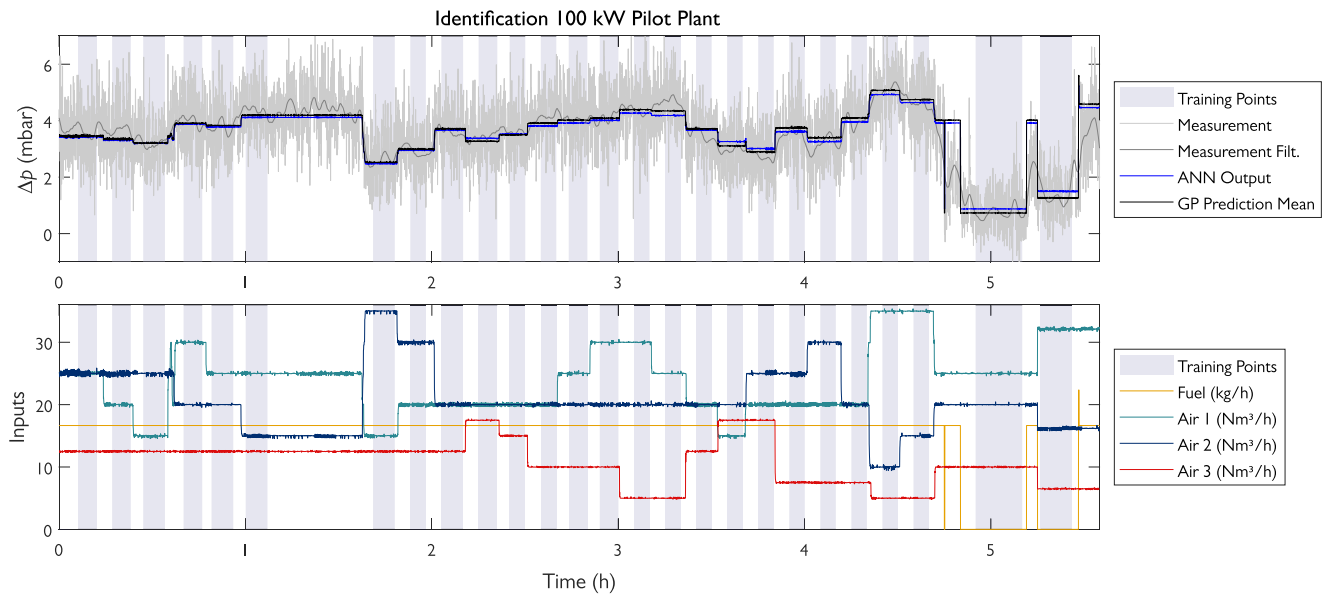


FIGURE 4. Identification data for the 100 kW demonstration plant with simulated output from GP regression and ANN.

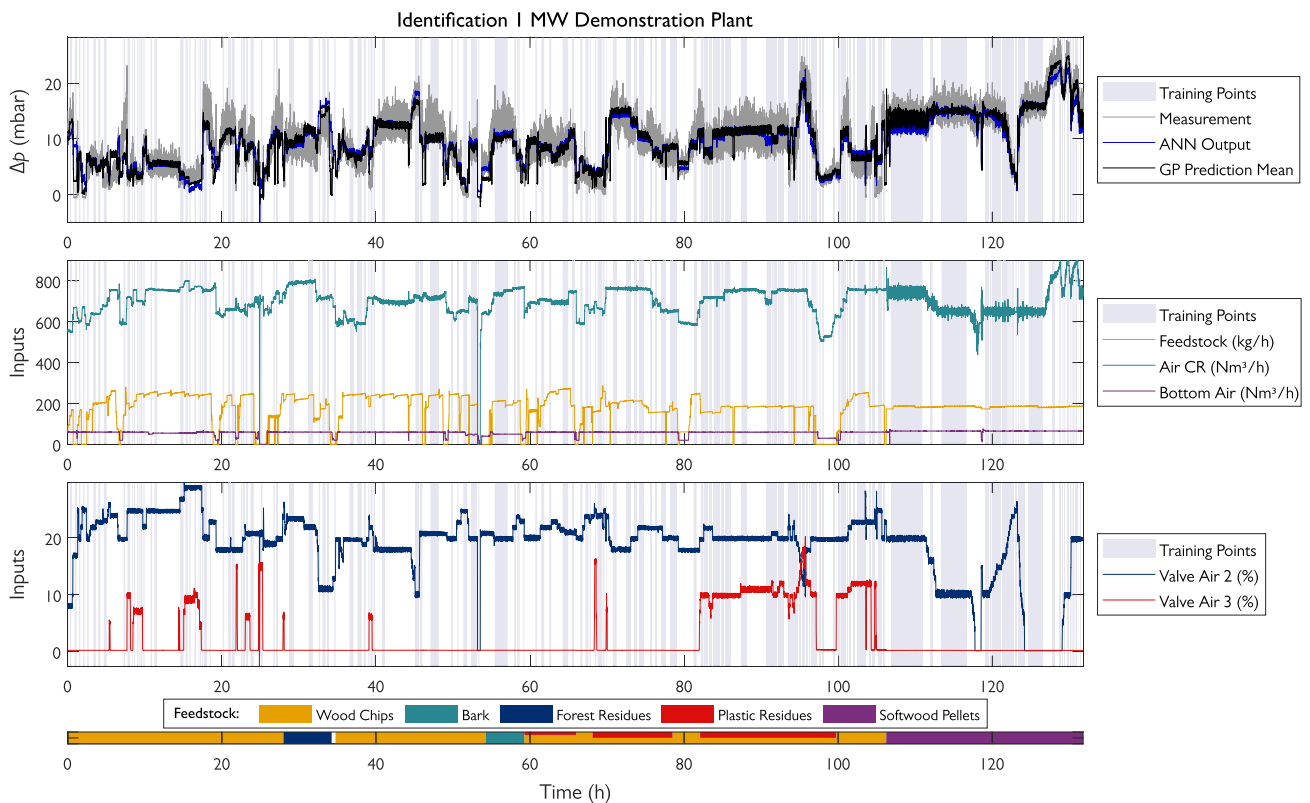


FIGURE 5. Identification data for the 1 MW demonstration plant with simulated output from GP regression and ANN.

The GP regression is implemented using the Statistics and Machine Learning Toolbox [40].

A. MODELING RESULTS

For both plants, data points from steady-state operation, represented as \bar{U} and \bar{y} , are used as training points for the GP

regression. These training points were manually selected by averaging the time series data over periods when the process was at steady state.

At the 100 kW pilot plant, an identification experiment was conducted to generate training data for the GP regression. Fig. 4 shows the time series data from this experiment.

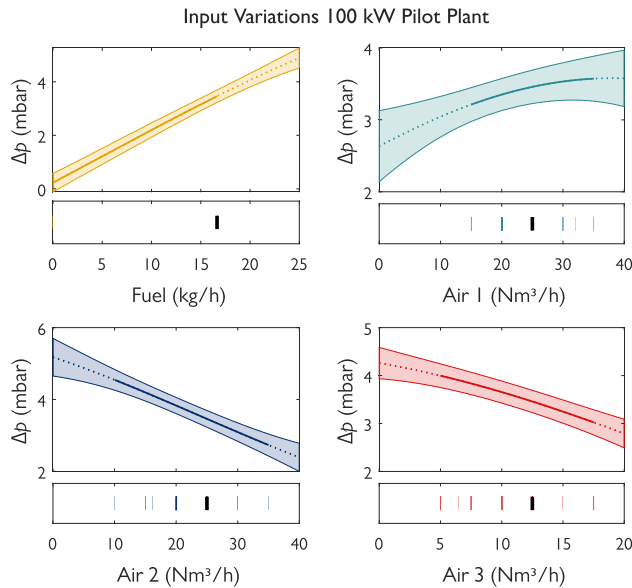


FIGURE 6. Variation of the inputs used by GP regression. The 4 inputs are varied individually from a starting point indicated by the black bars. The dotted lines indicate regions outside of where there are training data points.

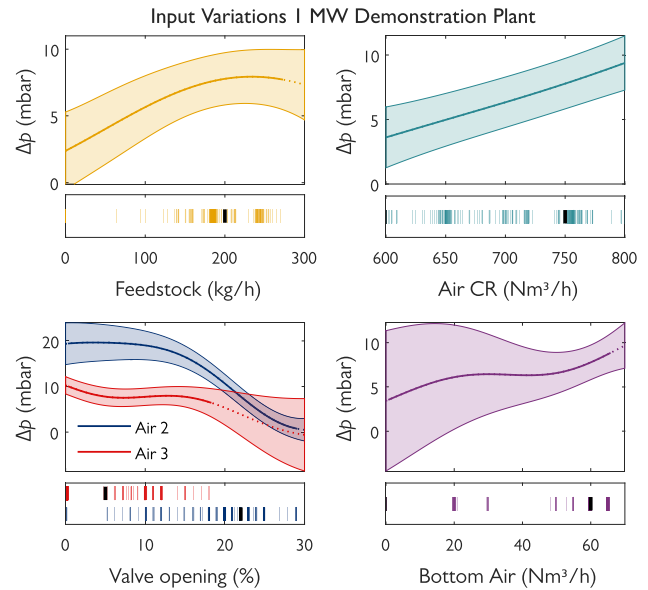


FIGURE 7. Variation of the inputs used by GP regression. The 5 inputs are varied individually from a starting point indicated by the black bars. The dotted lines indicate regions outside of where there are training data points.

TABLE 2. Computation times required for each time step in the closed-loop simulations.

	Calculation time	
	Mean	Max.
100 kW Pilot Plant	0.194 s	0.457 s
1 MW Demonstration Plant	0.277 s	0.528 s

The highlighted time periods indicate the steady-state points used as training points. The upper plot shows the pressure difference in the upper part of the CR, which represents the solids circulation rate. Both the raw measurement data and a filtered version are visualized. The filtering was performed using a 50-sample centered moving average. In addition, the predictions from both the GP regression and the ANN model are shown, generated by applying the respective models to the time series input data. The hyperparameters were identified as

$$\sigma_{l,100\text{kW}} = 11.58, \quad \sigma_{f,100\text{kW}} = 4.962, \quad \sigma_{n,100\text{kW}} = 0.2151.$$

Note that $\sigma_{n,100\text{kW}}^2$ is not the variance of the noise present in the time series data, since the data was averaged over measurement periods. However, noise can still be present due to disturbances that affect the output but are not accounted for in the model, such as variations in reactor temperature.

For the 1 MW demonstration plant, no specific identification experiments were conducted. Instead, measurement data from two different test runs, totaling approximately 136 hours of plant operation, was utilized. From these data, 201 points corresponding to steady-state operation were selected as training points for GP regression. Fig. 5 displays the measurement data, the selected training points,

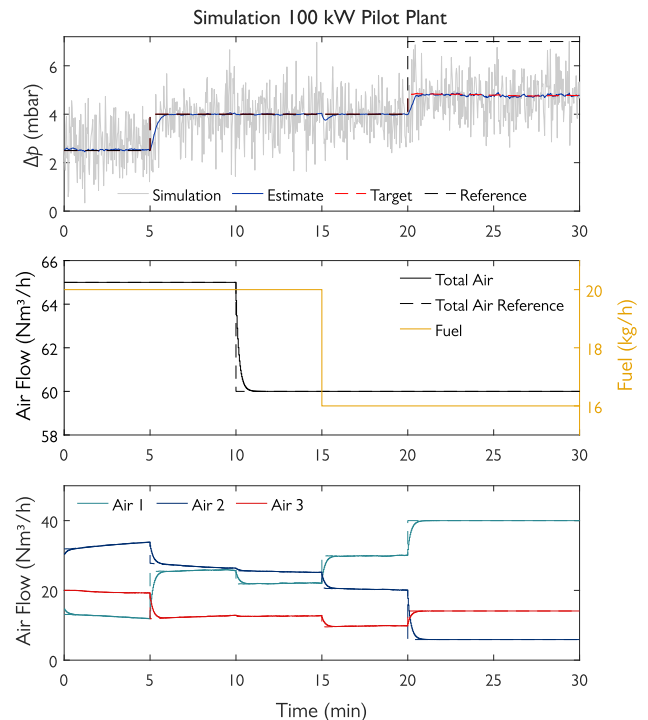


FIGURE 8. Closed-loop simulation results for the 100 kW pilot plant.

and predictions from both GP regression and the ANN. Additionally, the feedstock used is displayed at the bottom of the figure. When a mixture of plastic residues and wood chips was used, the height of the bar indicates the ratio, either 50:50 or 25:75. The hyperparameters were identified to be

$$\sigma_{l,1\text{MW}} = 1.998, \quad \sigma_{f,1\text{MW}} = 8.844, \quad \sigma_{n,1\text{MW}} = 1.828.$$

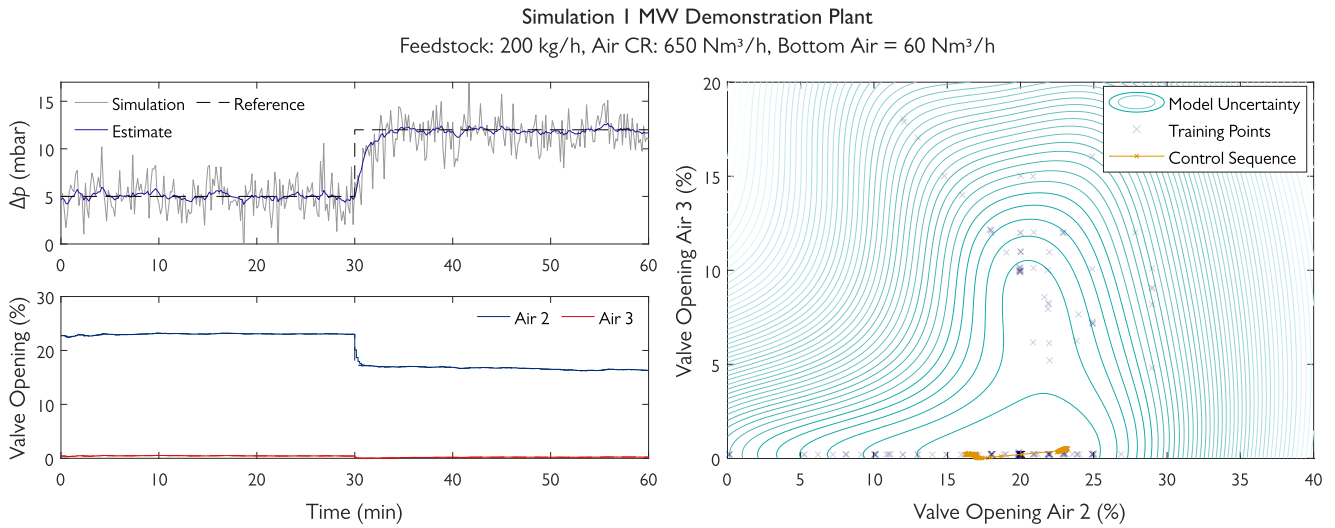


FIGURE 9. Closed-loop simulation for the 1 MW demonstration plant. The plots on the left show the controlled variable (top) and the control inputs (bottom). The plot on the right visualizes the GP uncertainty.

To gain insight into GP regression and to understand how individual inputs affect GP prediction, input variations are performed. The results are shown in Fig. 6 and Fig. 7 for the 100 kW pilot plant and the 1 MW demonstration plant, respectively. In these figures, the horizontal axes represent the varied inputs, while the vertical axes show the GP predictions. The line represents the mean, with dashed lines indicating regions where no training data is available. The shaded area around it represents the standard deviation of the prediction. The smaller plots below show the starting point from which the inputs are varied (shown in black) and the locations of the training data points (shown as colored bars).

According to the model, the circulation rate for both plants increases with higher feedstock feed rates. For the 100 kW plant, increasing the volume flow of air 1 results in increased circulation, which is expected as this air blows up the bed material. Conversely, increasing the volume flow of air 2 and air 3 decreases the circulation, probably because these air inlets are mounted facing downwards, opposing the circulation.

For the 1 MW plant, circulation increases with higher total airflow or, to a limited extent, increased bottom air volume flow. Opening the valves for air 2 or air 3 decreases circulation, as these actions increase the air fed to the reactor at higher positions, thus reducing the volume flow of air 1. Air 2 has a greater effect than air 3, possibly because the pipe diameter for air 3 is smaller, resulting in less air being diverted from air 1 when the air 3 valve is opened compared to when the air 2 valve is opened.

The dynamic components of the models incorporate time constants of $\tau_{100\text{kW}} = 10$ s and $\tau_{1\text{MW}} = 50$ s, respectively.

B. CLOSED-LOOP SIMULATIONS

The control algorithm is validated in closed-loop simulations for both the 100 kW pilot plant and the 1 MW demonstration plant. The ANNs are used as simulation models.

1) 100 KW PILOT PLANT

For the 100 kW pilot plant, the controller parameters are chosen to be

$$\lambda = 10^{-2}, \mathbf{R}_c = 5\mathbf{I}, \sigma_{\text{GP,max}} = 0.5,$$

and the EKF parameters

$$\sigma_w^2 = 10^{-5}, \sigma_v^2 = 0.85.$$

The controller was executed with a sampling time of $T_s = 2$ s. The results of the closed-loop simulation for the 100 kW pilot plant are presented in Fig. 8. The upper plot depicts the solids circulation rate, indicated by the pressure difference in the upper CR. The gray line represents the simulated output, with noise introduced by adding a normally distributed random number with zero mean and variance σ_v^2 . Reference changes occur at 5 min and 20 min. The second reference change is set to an unattainable level to demonstrate how infeasibility is handled using (23). The middle subplot shows the total airflow to the CR with its reference and the fuel input. The lower plot illustrates the three air volume flows, which are the control inputs. The dashed lines represent the steady-state inputs $\bar{\mathbf{u}}$, while the solid lines represent the control inputs \mathbf{u} applied to the process.

2) 1 MW DEMONSTRATION PLANT

For the 1 MW demonstration plant, the controller parameters are chosen to be

$$\lambda = 10^{-2}, \mathbf{R}_c = \mathbf{I}, \sigma_{\text{GP,max}} = 3,$$

and the EKF parameters

$$\sigma_w^2 = 10^{-3}, \sigma_v^2 = 3.3.$$

The controller operates with a sampling time of $T_s = 10$ s.

Fig. 9 and 10 show the corresponding closed-loop simulation results. For this plant, which has two control inputs, the

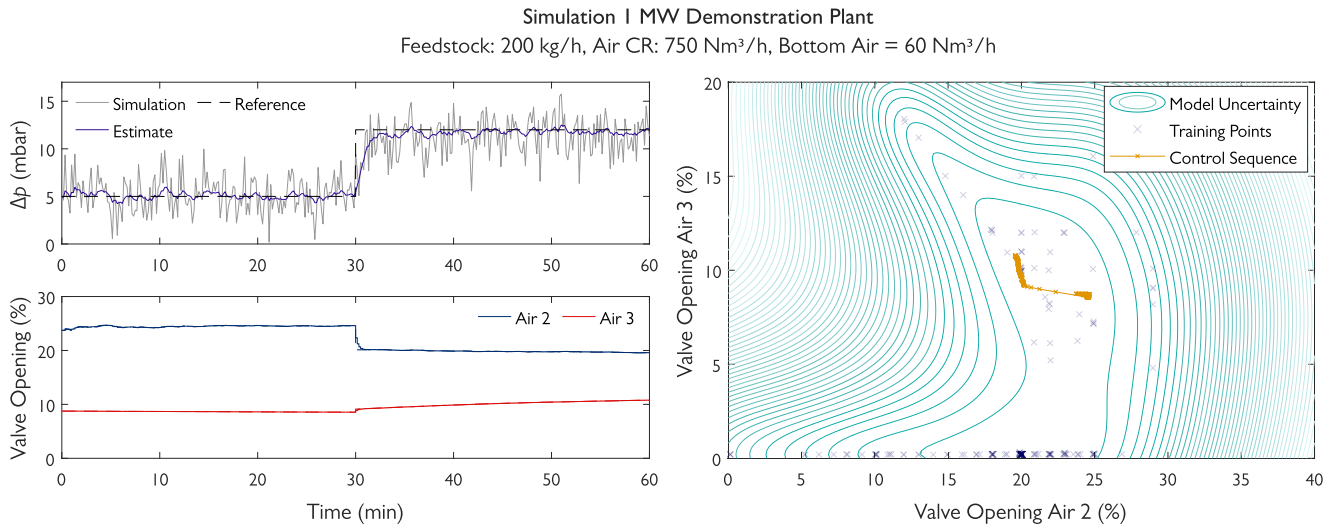


FIGURE 10. Closed-loop simulation for the 1 MW demonstration plant. Second simulation scenario with a different airflow to the CR.

model uncertainty can be visualized over the control input space, as shown in the contour plots in the right subplots. The training data points are also shown in these plots. This model uncertainty is affected by other model inputs - feed rate, airflow to the CR, and bottom airflow - which are not control inputs. Therefore, two separate simulations were conducted holding these three variables constant so that the model uncertainties over the control input space remain unchanged within each simulation. In the first simulation scenario, the lowest model uncertainty occurs when the air 3 valve is nearly closed and the air 2 valve is used to track changes in the reference. In contrast, in the second scenario, the model uncertainty is minimized when both valves are used for control.

The calculation times required for the closed-loop simulations are given in Table 2.

C. EXPERIMENTAL VALIDATION

The results of the experimental closed-loop validation for the 100 kW pilot plant are shown in Fig. 11. The controller parameters are identical to those used in the 100 kW pilot plant simulation. The controller was implemented in MATLAB, running on a separate computer, and receives measurement data from the process control system every 2 seconds. For clarity, a smoothed version of the solids circulation rate, represented by the pressure difference in the CR, is also shown in the plot. This was smoothed using a centered moving average with a window length of 20 samples. During the test run, the references for the solids circulation rate, the total airflow to the CR, and the feedstock feed rate were varied multiple times. Around 40 min into the run, the reference for the solids circulation rate was set to an unattainable level. In this case, the controller applied the maximum possible circulation rate while maintaining a maximum model uncertainty as specified by (23b).

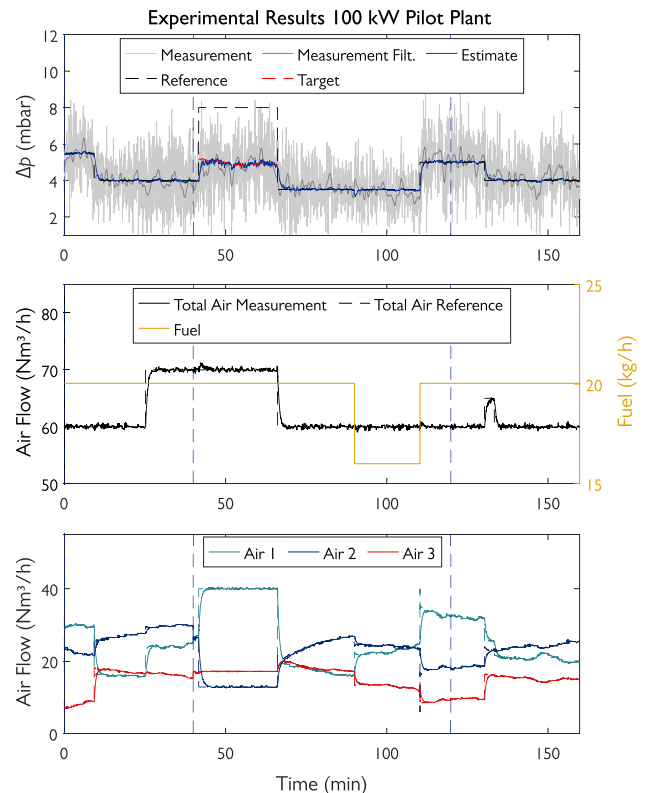


FIGURE 11. Experimental results of the GP regression-based controller applied to the DFB process at the 100 kW pilot plant at TU Wien.

The experiment was interrupted twice, as indicated by the vertical dashed lines.

The controller performed very well, effectively managing the variations and maintaining stable operation throughout the test run. This demonstrates the robustness and reliability of the control strategy under different operating conditions.

VI. CONCLUSION AND OUTLOOK

This study presents a method for modeling and controlling the solids circulation rate in DFB gasification using GP regression. By exploiting the uncertainty in the GP predictions, the process was driven toward regions of low model uncertainty, thereby improving the reliability and accuracy of control actions. Simulation results for both a 100 kW pilot plant and a 1 MW demonstration plant demonstrated the applicability of the method to different plants without extensive modeling efforts. The controller was successfully implemented in the 100 kW pilot plant and achieved offset-free tracking of constant references. This was achieved by incorporating a disturbance state into the model to compensate for plant model mismatch and unmeasured disturbances.

The controller presented can also be used as a subordinate controller, whereby the desired circulation is not specified directly by the plant operator, but by a higher-level controller that regulates temperatures or gas compositions.

In addition, the GP regression method employed in this study has potential for other applications. First, it could be used to identify regions of low data availability and high model uncertainty, facilitating the design of targeted identification experiments to improve model accuracy. Second, the control approach demonstrated here could be extended to similar processes, such as chemical looping combustion, where precise control of the solids circulation rate is critical.

REFERENCES

- [1] H. Lee and J. Romero, Eds., 2023: *Climate Change 2023: Synthesis Report. Contribution of Working Groups I, II and III to the Sixth Assessment Report of the Intergovernmental Panel on Climate Change*. Geneva, Switzerland: IPCC, pp. 35–115, doi: 10.59327/IPCC/AR6-9789291691647. [Online]. Available: <https://www.ipcc.ch/report/ar6/syr/>
- [2] J. Karl and T. Pröll, “Steam gasification of biomass in dual fluidized bed gasifiers: A review,” *Renew. Sustain. Energy Rev.*, vol. 98, pp. 64–78, Dec. 2018.
- [3] A. Bartik, F. Benedikt, J. Fuchs, H. Hofbauer, and S. Müller, “Experimental investigation of hydrogen-intensified synthetic natural gas production via biomass gasification: A technical comparison of different production pathways,” *Biomass Convers. Biorefinery*, vol. 14, no. 18, pp. 23091–23110, Sep. 2024.
- [4] M. Hammerschmid, A. Bartik, F. Benedikt, M. Veress, S. Pratschner, S. Müller, and H. Hofbauer, “Economic and ecological impacts on the integration of biomass-based SNG and FT diesel in the Austrian energy system,” *Energies*, vol. 16, no. 16, p. 6097, Aug. 2023.
- [5] A. Chiodini, L. Bua, L. Carnelli, R. Zwart, B. Vreugdenhil, and M. Voccianta, “Enhancements in biomass-to-liquid processes: Gasification aiming at high hydrogen/carbon monoxide ratios for direct Fischer-Tropsch synthesis applications,” *Biomass Bioenergy*, vol. 106, pp. 104–114, Nov. 2017.
- [6] S. Müller, P. Groß, R. Rauch, R. Zweiler, C. Aichernig, M. Fuchs, and H. Hofbauer, “Production of diesel from biomass and wind power—Energy storage by the use of the Fischer-Tropsch process,” *Biomass Convers. Biorefinery*, vol. 8, no. 2, pp. 275–282, Jun. 2018.
- [7] M. Kraussler, M. Binder, P. Schindler, and H. Hofbauer, “Hydrogen production within a polygeneration concept based on dual fluidized bed biomass steam gasification,” *Biomass Bioenergy*, vol. 111, pp. 320–329, Apr. 2018.
- [8] J. Loipersböck, M. Luisser, S. Müller, H. Hofbauer, and R. Rauch, “Experimental demonstration and validation of hydrogen production based on gasification of lignocellulosic feedstock,” *ChemEngineering*, vol. 2, no. 4, p. 61, Dec. 2018.
- [9] K. Göransson, U. Söderlind, and W. Zhang, “Experimental test on a novel dual fluidised bed biomass gasifier for synthetic fuel production,” *Fuel*, vol. 90, no. 4, pp. 1340–1349, Apr. 2011.
- [10] J. Fuchs, J. Schmid, F. Benedikt, A. Mauerhofer, S. Müller, and H. Hofbauer, “A general method for the determination of the entrainment in fluidized beds,” *Int. J. Multiphys.*, vol. 12, pp. 359–372, Nov. 2018.
- [11] H. Liu, R. J. Cattolica, and R. Seiser, “Operating parameter effects on the solids circulation rate in the CFD simulation of a dual fluidized-bed gasification system,” *Chem. Eng. Sci.*, vol. 169, pp. 235–245, Sep. 2017.
- [12] J. Gu, Y. Shao, X. Liu, W. Zhong, and A. Yu, “Modelling of particle flow in a dual circulation fluidized bed by a Eulerian-Lagrangian approach,” *Chem. Eng. Sci.*, vol. 192, pp. 619–633, Dec. 2018.
- [13] L. Stanger, A. Schirrer, F. Benedikt, A. Bartik, S. Jankovic, S. Müller, and M. Kozek, “Dynamic modeling of dual fluidized bed steam gasification for control design,” *Energy*, vol. 265, Feb. 2023, Art. no. 126378.
- [14] C. Williams and C. Rasmussen, “Gaussian processes for regression,” in *Advances in Neural Information Processing Systems*, vol. 8. Cambridge, MA, USA: MIT Press, 1995.
- [15] R. Murray-Smith and D. Sbarbaro, “Nonlinear adaptive control using nonparametric Gaussian process prior models,” *IFAC Proc. Volumes*, vol. 35, pp. 325–330, Dec. 2002.
- [16] G. Gregoric and G. Lightbody, “Internal model control based on a Gaussian process prior model,” in *Proc. Amer. Control Conf.*, vol. 6, 2003, pp. 4981–4986.
- [17] J. Kocijan, R. Murray-Smith, C. E. Rasmussen, and A. Girard, “Gaussian process model based predictive control,” in *Proc. Amer. Control Conf.*, 2004, pp. 2214–2219.
- [18] L. Stanger, A. Schirrer, A. Bartik, and M. Kozek, “Minimum-variance model predictive control for dual fluidized bed circulation control,” *IFAC-PapersOnLine*, vol. 56, no. 2, pp. 2701–2706, 2023.
- [19] L. Stanger, A. Bartik, M. Hammerschmid, S. Jankovic, F. Benedikt, S. Müller, A. Schirrer, S. Jakubek, and M. Kozek, “Model predictive control of a dual fluidized bed gasification plant,” *Appl. Energy*, vol. 361, May 2024, Art. no. 122917.
- [20] N. Hanchate, S. Ramani, C. S. Mathpati, and V. H. Dalvi, “Biomass gasification using dual fluidized bed gasification systems: A review,” *J. Cleaner Prod.*, vol. 280, Jan. 2021, Art. no. 123148.
- [21] J. C. Schmid, “Development of a novel dual fluidized bed gasification system for increased fuel flexibility,” Ph.D. dissertation, Inst. Chem., Environ. Biosci. Eng., TU Wien, Vienna, Austria, 2014.
- [22] F. Benedikt, “Fuel flexible advanced dual fluidized bed steam gasification,” Ph.D. dissertation, Inst. Chem., Environ. Biosci. Eng., TU Wien, Vienna, Austria, 2020.
- [23] D. Kadlez, F. Benedikt, M. Huber, K. Fürsatz, J. Schmid, H. Hofbauer, and S. Müller, *Technology Development of Advanced Dual Fluidized Bed Steam Gasification From Pilot To Demonstration Scale First Results From a 1 Mw Demonstration Plant*, document SSRN 4763693, 2024.
- [24] D. Hochstöger, “Performance evaluation of DFB gas generation based on a comparison of two research plants with 100 kW and 1 MW,” M.S. thesis, Inst. Chem., Environ. Biosci. Eng., TU Wien, Vienna, Austria, 2023.
- [25] J. Schmid, C. Pfeifer, H. Kitzler, T. Pröll, and H. Hofbauer, “A new dual fluidized bed gasifier design for improved in situ conversion of hydrocarbons,” in *Proc. Int. Conf. Polygeneration Strateg.*, 2011, pp. 1–18.
- [26] X. Liu, M. Zhang, S. Zhang, Y. Ding, Z. Huang, T. Zhou, H. Yang, and G. Yue, “Measuring technologies for CFB solid circulation rate: A review and future perspectives,” *Energies*, vol. 15, no. 2, p. 417, Jan. 2022.
- [27] A. Kreuzeder, C. Pfeifer, and H. Hofbauer, “Fluid-dynamic investigations in a scaled cold model for a dual fluidized bed biomass steam gasification process: Solid flux measurements and optimization of the cyclone,” *Int. J. Chem. React. Eng.*, vol. 5, no. 1, pp. 1–8, Aug. 2007.
- [28] T. Karlsson, X. Liu, D. Pallarès, and F. Johnsson, “Solids circulation in circulating fluidized beds with low riser aspect ratio and varying total solids inventory,” *Powder Technol.*, vol. 316, pp. 670–676, Jul. 2017.
- [29] S. Matsuda, “Measurement of solid circulation rate in a circulating fluidized bed,” *Powder Technol.*, vol. 187, no. 2, pp. 200–204, Oct. 2008.
- [30] X. Liu, Y. Zhang, H. Yang, X. Liu, Y. Zhang, and G. Yue, “A method for measuring the solid circulation rates of CFB boilers based on the particle flow-around principle,” *Chem. Eng. J.*, vol. 481, Feb. 2024, Art. no. 148424.
- [31] Y. Alghamdi, Z. Peng, K. Shah, B. Moghtaderi, and E. Doroodchi, “Predicting the solid circulation rate in chemical looping combustion systems using pressure drop measurements,” *Powder Technol.*, vol. 286, pp. 572–581, Dec. 2015.
- [32] M. Stollhof, S. Penthor, K. Mayer, and H. Hofbauer, “Estimation of the solid circulation rate in circulating fluidized bed systems,” *Powder Technol.*, vol. 336, pp. 1–11, Aug. 2018.

- [33] C. E. Rasmussen and C. K. I. Williams, *Gaussian Processes for Machine Learning*. Cambridge, MA, USA: MIT Press, 2006.
- [34] M. N. Gibbs, "Bayesian Gaussian processes for regression classification," Ph.D. dissertation, Univ. Cambridge, Cambridge, England, 1997.
- [35] C. E. Rasmussen and C. K. I. Williams, *Gaussian Processes for Machine Learning*. Cambridge, MA, USA: MIT Press, 2005.
- [36] Mathworks Inc. (2023). *MATLAB Deep Learning Toolbox*. [Online]. Available: <https://www.mathworks.com/products/deep-learning.html>
- [37] M. Grewal and A. Andrews, *Kalman Filtering: Theory and Practice Using MATLAB*. Hoboken, NJ, USA: Wiley, 2008.
- [38] M. D. McKay, R. J. Beckman, and W. J. Conover, "A comparison of three methods for selecting values of input variables in the analysis of output from a computer code," *Technometrics*, vol. 42, no. 1, p. 55, Feb. 2000.
- [39] Mathworks Inc. (2023). *MATLAB Optimization Toolbox*. [Online]. Available: <https://www.mathworks.com/products/optimization.html>
- [40] MathWorks Inc. (2023). *MATLAB Statistics and Machine Learning Toolbox*. [Online]. Available: <https://www.mathworks.com/products/statistics.html>



LUKAS STANGER received the master's degree in mechanical engineering-management from TU Wien, Vienna, Austria, in 2021, where he is currently pursuing the Ph.D. degree. Since 2021, he has been a member of the Project Team with the Institute of Mechanics and Mechatronics, TU Wien. His research interests include modeling, control, and optimization, with a recent focus on energy systems.



ALEXANDER BARTIK received the Ph.D. degree in chemical engineering from TU Wien, in 2024. He is currently a Postdoctoral Researcher with the Institute of Chemical, Environmental, and Bioscience Engineering. His research interests include biomass gasification technologies and downstream synthesis processes employing experimental and simulation-based methods.



MATTHIAS BINDER received the M.Sc. degree in process and chemical engineering from TU Wien. Since 2015, he has been with the BEST-Bioenergy and Sustainable Technologies in the field of syngas platform technologies, including gasification, gas cleaning, and downstream synthesis applications. His dissertation is dedicated to mixed alcohol synthesis based on biomass steam gasification with TU Wien.



ALEXANDER SCHIRRER received the M.S., Ph.D., and Habilitation degrees in mechanical engineering from TU Wien, Vienna, Austria, in 2007, 2011, and 2018, respectively. Since 2023, he has been a Senior Scientist with the Institute of Mechanics and Mechatronics, TU Wien. His research interests include modeling, simulation, optimization, and control of complex and distributed-parameter systems.



STEFAN JAKUBEK received the M.Sc. degree in mechanical engineering, the Ph.D. degree in technical sciences, and the Habilitation (professorial qualification) degree in control theory and system dynamics from TU Wien, Vienna, Austria, in 1997, 2000, and 2007, respectively. From 2006 to 2009, he was the Head of Development of the Hybrid Powertrain Calibration and Battery Testing Technology, Automotive Industry Company AVL List GmbH, Graz, Austria. He is currently a Professor and the Head of the Institute of Mechanics and Mechatronics, TU Wien. His research interests include fault diagnosis, nonlinear system identification, and simulation technology.



MARTIN KOZEK received the M.S. degree in mechanical engineering, and the Ph.D. and Habilitation degrees from TU Wien, Vienna, Austria, in 1994, 2000, and 2009, respectively. He is currently a Professor with the Institute of Mechanics and Mechatronics, TU Wien. His research interests include nonlinear systems modeling and identification, model predictive process control, and active control of structural vibrations.

...

About the author



Lukas Stanger was born in 1994 and grew up in Wartberg ob der Aist, Austria. He graduated from BHAK Perg before fulfilling his civilian service with the Austrian Red Cross. He earned his Bachelor's degree in Mechanical Engineering - Management from TU Wien, followed by a Master's degree, which he completed with distinction. During his studies, he spent an exchange semester at Lund University, broadening his academic experience. He also gained industrial experience during a six-month internship in the NVH department at BMW in Steyr. His passion for control engineering led him to pursue a PhD at the Institute of Mechanics and Mechatronics at TU Wien, where he started as a research associate in 2021. His research focused on the ADORe-SNG and Industry4Redispatch projects, as well as contributing to teaching activities. As part of the ADORe-SNG

research project, he developed models and control algorithms for dual fluidized bed gasification and fluidized bed methanation processes. This thesis is based on this research. An up-to-date list of the author's publications can be found at ORCID  (orcid.org/0000-0003-3846-732X). You can follow his professional career on LinkedIn  (linkedin.com/in/lukasstanger).